Dissertation
submitted to the
Combined Faculties of the Natural Sciences and Mathematics
of the Ruperto-Carola-University of Heidelberg, Germany
for the degree of
Doctor of Natural Sciences

Put forward by
Dipl.-Phys. Sven Augustin
born in Limburg, Germany
Oral examination: Thursday 24th July, 2014

Bethe–Heitler Pair Creation in a Bichromatic Laser Field

Referees: Professor Dr. Dr. Carsten Müller
Professor Dr. Jörg Jäckel

Zusammenfassung
Gegenstand dieser Arbeit ist die nichtlineare Erzeugung von Elektron-Positron-Paaren im Coulomb-Feld eines Kerns durch ein zweifarbiges Laserfeld hoher Intensität. Der Schwerpunkt liegt dabei auf zwei komplementären Szenarien:

Zum einen können für kommensurable Kombinationen der zwei Laserfelder Quanteninterferenzeffekte auftreten. Diese werden anhand totaler Paarerzeugungsraten und Emissionswinkelspektren im Ruhesystem des Kerns und im Laborsystem untersucht. Darüber hinaus zeigt sich, dass die relative Phase zwischen den zwei Lasermoden Kontrolle über die Stärke der Interferenzen gewährt. Entsprechend kann dieser Parameter dazu verwandt werden, die Ausbeute erzeugter Paare zu optimieren.

Zum anderen wird für inkommensurable Frequenzen ein Aufbau betrachtet, in dem diese stark voneinander abweichen. Dies beschreibt ein starkes Laserfeld im nicht-störungstheoretischen Regime, welchem von einem einzelnen hochenergetischen γ-Photon bei der Paarerzeugung assistiert wird. Dies führt zu einer starken Erhöhung der Paarerzeugungsrate für bestimmte Laserintensitätsbereiche. Außerdem zeigt sich der Einfluss des γ-Photons in Emissionswinkel- und Energiespektren, welche wiederum im Ruhesystem des Kerns und im Laborsystem untersucht werden.

Die Unterschiede zwischen diesen beiden Szenarien werden weiterhin über eine kontinuierliche Variation des Frequenzverhältnisses untersucht. Hier zeigt sich der starke Einfluss der Interferenzen für kommensurable Frequenzen im direkten Vergleich zum inkommensurablen Fall. Schließlich wird der Spezialfall zweier Moden mit gleicher Frequenz betrachtet. In der Variation der Elliptizität des kombinierten Laserfeldes wird die Abhängigkeit der totalen Paarerzeugungsrate von diesem Parameter im Vergleich zwischen konstanter totaler Feldintensität und konstanter maximaler Feldintensität untersucht.

Abstract
Within this thesis, the non-linear creation of electron-positron pairs in the superposition of a nuclear Coulomb field and a two-colour laser field of high intensity is studied. Primarily, two complementary scenarios are investigated:

On the one hand, if the two laser frequencies are commensurable, quantum interference may occur. This interference manifests in the total pair-creation rate and the angular distribution of the created particles, which are studied in the nuclear rest frame and the laboratory frame. Furthermore, the relative phase between the two laser modes allows to tune the strength of the terms arising from interference. Therefore, this parameter may be used to optimize the pair-creation yield.

On the other hand, for incommensurable frequencies, a set-up of largely differing frequencies is considered. This way, a strong laser field in the non-perturbative regime assisted by a single highly-energetic γ-photon is described. Due to the assistance of the latter, a strong enhancement of the total pair-creation rate can be found depending on the laser intensity. Additionally, the influence of the γ-photon on the angular and energetic distribution of the created particles is investigated, again in the nuclear rest frame and the laboratory frame.

Furthermore, the differences arising in the two former cases are directly compared by means of a continuous variation of the laser frequency ratio. This illustrates the strong modifications due to the interference in the commensurable case. Finally, for the special case of two modes with identical frequency, the total pair-creation rate is studied as a function of the ellipticity of the combined laser field. Here, the cases of a constant total field intensity and a constant maximum field intensity are compared.

Contents

Chapter 1.

Introduction

The subject matter of the presented thesis is a process of energy to mass conversion: electron-positron pair creation. In the following linear pair-creation processes induced by single γ-photons and non-linear pair-creation processes induced by intense laser light are put into context. Particular emphasis lies on laser fields composed of two modes. Furthermore, the objective of this study is discussed, as well as an overview of the subsequent chapters given.

1.1. Mass and Energy

One of the most ubiquitously applicable physical concepts is Newton's *lex secunda* [113]. It states that the same force $\mathbf{F}$ applied to an object with high mass m will lead to less acceleration $\mathbf{a}$ than it would if applied to a lighter object. It contains the *lex prima* in the sense that if no force is applied ($\mathbf{F} = 0$) an object is not accelerated ($\mathbf{a} = 0$). One can easily argue that it governs daily life more than any other idea. Therefore, it is surprising that Euler's mathematical representation [56],

$$\mathbf{F} = m\mathbf{a}, \tag{1.1}$$

is not the physical formula every non-physicist can instantly quote. This is by all means Einstein's *mass-energy equivalence* [53]:

$$E = mc^2, \tag{1.2}$$

with the speed of light c. In fact, the latter equation is often used to symbolize physics – or even science in general – in popular culture, even though it might not have an application to our usual interaction with our environment. However, its implication – the conversion of matter to energy, particularly to light, and vice versa – is intriguing to everyone. It contains physics that exalts the imagination, while its notation retains remarkable simplicity.

In the two Eqs. (1.1) and (1.2) an important distinction has to be made as far as the meaning of the symbol m is concerned. In the relativistic case it is usually used for the relativistic mass

$$m = \gamma m_0, \tag{1.3}$$

and the additional m_0 is introduced for the rest (or invariant) mass. The Lorentz factor

$$\gamma = \frac{1}{\sqrt{1-\beta^2}} \tag{1.4}$$

is defined by the velocity of the considered object in units of the speed of light $\beta = v/c$. In the classical case m is usually understood as the rest mass, as the concept of the relativistic mass is not applicable.[1]

While Eq. (1.2) refers to the relativistic energy, the rest energy

$$E_0 = m_0 c^2, \tag{1.5}$$

is analogously defined. Both energies are connected to the momentum $\mathbf{p} = m\mathbf{v}$ by the energy-momentum relation

$$E^2 = (\mathbf{p}c)^2 + E_0^2. \tag{1.6}$$

1.2. Pair Creation and Gamma Rays

A class of physical processes in which Eq. (1.2) is directly applicable is pair creation, wherein the energy provided by a photon is converted into a particle-antiparticle pair. The particles have to be created as pairs, in order to ensure that all quantum numbers are conserved. The pair that is most likely created is the lightest lepton, the electron (e^-), and its antiparticle, the positron (e^+). Therefore, the photon energy has to overcome the threshold of twice the rest mass of the electron m_e,

$$E \geq 2m_e c^2 \simeq 1.022\,\mathrm{MeV}, \tag{1.7}$$

which means that the photon must be a γ-ray[2] photon. While energy is conserved according to Eq. (1.2), momentum conservation leads to the requirement of a fourth constituent of the process. This can be verified by assuming that the pair is created from the photon in vacuum and choosing the pair's centre of

[1] An expression corresponding to Eq. (1.1) for the relativistic case can be extracted from the more general $\mathbf{F} = \dot{\mathbf{p}}$ with the momentum $\mathbf{p} = \gamma(\mathbf{v}) m_0 \mathbf{v}$.

[2] Here, γ-ray denotes only the energy of the photon, not its source.

mass as reference frame. Therein, the total momentum is zero. For momentum conservation to be fulfilled, this requires

$$\mathbf{p}_\gamma = \mathbf{p}_+ + \mathbf{p}_- \equiv 0. \tag{1.8}$$

However, a photon with vanishing momentum does not exist.

The additional constituent may be a nucleus with nuclear charge number Z. The respective process is called Bethe–Heitler effect [22]:

$$Z + \gamma \longrightarrow Z + e^- + e^+. \tag{1.9}$$

The nucleus absorbs a small recoil, and momentum conservation is fulfilled:

$$\mathbf{p}_Z + \mathbf{p}_\gamma = \mathbf{p}'_Z + \mathbf{p}_+ + \mathbf{p}_-. \tag{1.10}$$

Alternatively, in the so-called Breit–Wheeler effect, a second photon collides with the first one [29]:

$$\gamma_1 + \gamma_2 \longrightarrow e^- + e^+. \tag{1.11}$$

In the centre of mass of the created pair, the momenta of the two photons have to cancel, too. Thus, they must counterpropagate and have identical frequency in that frame of reference.

Both processes have first been studied theoretically in 1934 by the eponymous authors [22, 29]. In both cases, the obtained rates increase linearly with the beam intensity I. A few years earlier, the first effects that can be interpreted as pair creation had been found by Klein for electrons scattering from a rectangular potential barrier [81] and by Sauter from a linearly increasing potential barrier [137]. The latter corresponds to a constant electric field [65], and led already to the so-called *Schwinger limit* or *critical field strength*

$$\mathscr{E}_\mathrm{crit} = \frac{m_e^2 c^3}{e\hbar} \simeq 1.3 \times 10^{18}\,{}^\mathrm{V}\!/_\mathrm{m}, \tag{1.12}$$

i.e., the maximum electric field before the vacuum becomes unstable and emits e^-e^+ pairs spontaneously. Here, e is the positive elementary charge and $\hbar$ is the reduced Planck constant. Twenty years later, Schwinger applied the then still young methods of Quantum Electrodynamics (QED) to the same problem, leading to a pair-creation rate of the form [141]

$$R \sim \exp\left(-\pi \frac{\mathscr{E}_\mathrm{crit}}{\mathscr{E}}\right), \tag{1.13}$$

where $\mathscr{E} \sim \sqrt{I}$ is the applied field strength. The strongly non-perturbative dependence on $\mathscr{E}$ leads to the tunneling picture of pair creation: The electron

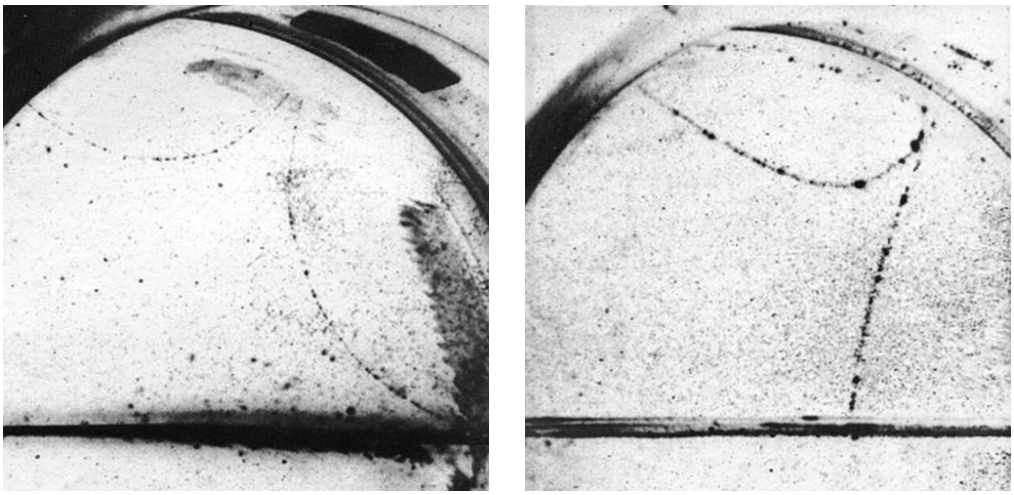

(a) Plate 3.: Fig. 5. [37] (b) Plate 3.: Fig. 6. [37]

Figure 1.1.: *Two e^-e^+ pairs traced in a cloud-chamber – Taken from Ref.* [37]*, colours inverted and figures cropped. In both figures the upper trace is due to an electron, the lower to a positron.*

tunnels through the gap of $2m_ec^2$ from the negative continuum, the so-called *Dirac Sea*, to the positive continuum (cf. also Figs. 1.2 and 2.2).

On the experimental side, two Nobel laureates are directly linked to e^-e^+ pair creation. In 1936, Anderson was awarded 'for his discovery of the positron' four years earlier [9]. The positron was found in cloud-chamber traces induced by cosmic radiation and the accompanying γ-rays. A year after the discovery, in 1933, Blackett could attribute the origin of these positrons to pair-creation processes of the Bethe–Heitler type [25, 37], eventually leading to his Nobel prize in 1948. Two examples of the recorded traces that lead to the hypotheses of electron and positron created as pairs can be seen in Fig. 1.1. Further early observations in the laboratory relied on γ-rays from nuclear decays or bremsstrahlung [3, 89, 152]. Nowadays, the process serves for applications such as the generation of polarized positron beams [5, 118], which are of relevance for experimental particle physics.

1.3. Non-Linear Pair Creation and Lasers

The demonstration of the first laser in 1960 [96] led to several theoretical investigations into its applicability to pair creation. Due to its monochromaticity,

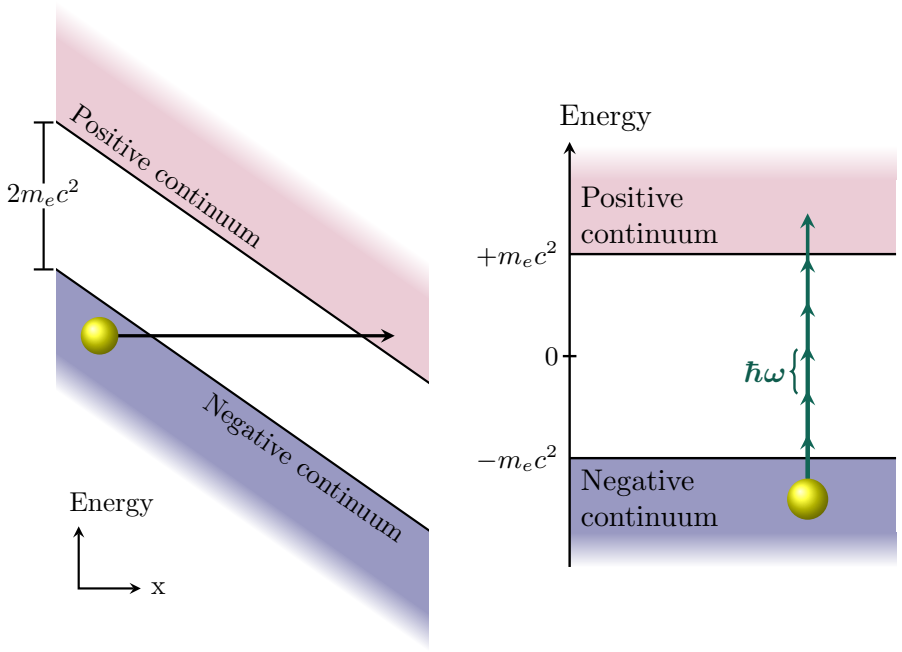

(a) Tunneling ($\xi \gg 1$) (b) Multiphoton ($\xi \ll 1$)

Figure 1.2.: *Illustrations of the two commonly used pictures of pair creation – In the tunneling regime the continua are tilted along the x-axis by the electric field $\mathscr{E}$ thereby forming a barrier. In the multiphoton regime an appropriate number of photons is "stacked" to overcome the gap of $2m_ec^2$. In both cases the pair-creation process is a transition from the negative continuum, the so-called* Dirac Sea*, to the positive continuum.*

coherence, and low divergence, where the latter means that all photons propagate in the same direction, a laser beam is well described by a unifrequent plane wave. However, Schwinger had already proven in 1951 that such a field alone can not produce a pair, regardless of how strong the field or how high its frequency [141]. This can be intuitively explained by the fact that if all photons propagate in the same direction (obviously with the same velocity) they cannot interact with each other.[3] Again, an additional constituent is necessary. Furthermore, the energy of a laser photon is usually not in the γ-ray range. Therefore, non-linear extensions of the Bethe–Heitler and the Breit–Wheeler process have been subject to many studies (recall Eqs. (1.9) and (1.11), respectively). Instead of a single γ-photon, the energy to overcome the pair-creation threshold is gained by absorbing $n \gg 1$

[3]However, the plane wave picture is an idealized assumption and an experimental laser has, e.g, an energetic bandwidth. Furthermore, under the assumption of a finite background temperature a single plane wave alone was recently found to produce pairs [76].

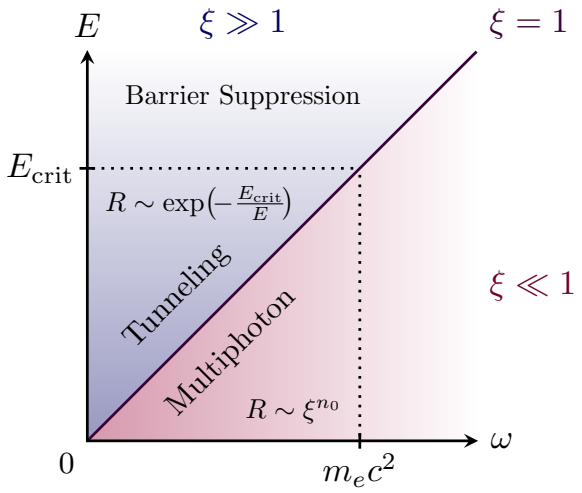

Figure 1.3.: *Regimes of pair creation – Distinction of the non-perturbative tunneling and perturbative multiphoton regime by means of the intensity parameter ξ in analogue to the* Keldysh parameter [74]. *A third regime, that of the* barrier suppression, *is also indicated. Once the critical field strength $\mathscr{E}_{\text{crit}}$ is overcome, the barrier is suppressed sufficiently to allow the electron to escape over the barrier rather than tunneling through it. This behaviour has first been found in laser-induced photo-ionization* [11].

photons from a laser beam, each with an energy $\hbar\omega \ll 2m_e c^2$, but a total energy $n\hbar\omega > 2m_e c^2$. The non-linear Bethe–Heitler effect,

$$Z + n\omega \longrightarrow Z + e^- + e^+, \tag{1.14}$$

has been studied in Ref. [154], just as the non-linear Breit–Wheeler effect,

$$\gamma + n\omega \longrightarrow e^- + e^+, \tag{1.15}$$

in Refs. [111, 115, 128]. Due to the large and still ongoing progress in high-intensity laser technology, interest in these two processes has been strongly revived in recent years (cf. the reviews in Refs. [43, 51] and references therein). A third alternative, the head-on collision of two laser beams, replacing each γ_i in Eq. (1.11) with n_i laser photons of frequency ω_i, has also been subject to several more recent studies [19, 34, 102, 135].

For the non-linear pair-creation processes it is commonly distinguished whether they occur in the *tunneling regime* (as illustrated in Fig. 1.2(a)) and thus exhibit a non-perturbative dependence on the applied electric field similar to the Schwinger case of Eq. (1.13) [35, 49, 64, 83, 132, 136], or in the *multiphoton regime* (as

illustrated in Fig. 1.2(b)). In the latter, the rate is a perturbative sum over the number of involved photons n [101, 105]:

$$R = \sum_{n=n_0}^{\infty} R_n, \tag{1.16}$$

$$R_n \sim \xi^{2n} \tag{1.17}$$

where n_0 is the minimal number of photons for which $n_0\hbar\omega \geq 2m_e c^2$, and the dimensionless intensity parameter $\xi \sim \mathscr{E}$ (cf. Eqs. (2.7) and (A.11)). As illustrated in Fig. 1.3, the distinction between the two regimes is usually made by means of the latter. This may be understood in analogue to the *Keldysh parameter* of non-linear photoionization [74]

$$\kappa_{\text{ion}} = \frac{\sqrt{2m_e B}\,\omega}{e\mathscr{E}}, \tag{1.18}$$

with the binding energy of the respective electron B. The corresponding parameter for non-linear pair-creation is gained if one associates $B = 2m_e c^2$ in the sense that the pair-creation threshold is the energy with which an electron is "bound" in the Dirac Sea [124]:

$$\kappa_{e^-e^+} = \frac{2m_e c\,\omega}{e\mathscr{E}} = \frac{\sqrt{2}}{\xi}. \tag{1.19}$$

Thus, the tunneling regime[4] is assumed for $\xi \gg 1$, and the multiphoton regime for $\xi \ll 1$. The latter means that Eq. (1.16) may be approximated by

$$R \approx R_{n_0} \sim \xi^{2n_0} \tag{1.20}$$

as orders in n higher than n_0 will be suppressed due to $\xi \ll 1$.

The only ever experimental realization of a *matter from laser light* reaction, has been the E-144 experiment at the Stanford Linear Accelerator Center (SLAC) [17, 36]. There, e^-e^+ pairs have been created by colliding a highly relativistic electron beam with a highly intense optical laser beam. Naïvely, one would

[4] It is important to stress that limitations of the traditional tunneling picture in strong-field physics exist [130, 131]. The picture is based on the concept that a laser field in the zero-frequency limit is quasi-static, i.e., a slowly oscillating field is almost constant. Moreover, this *tunneling limit* $\xi \to \infty$ (which is also reached for $I \to \infty$) is called the *classical limit* in the sense that the electron is generated after a *tunneling time* outside the barrier with a classical distribution and travels on a classical trajectory afterwards. However, in the aforementioned Refs. [130, 131] it is shown that for laser fields, due to their transversal nature, this limit is relativistic instead of classical. Furthermore, figures similar to Fig. 1.3 are shown therein with the limits of the tunneling picture indicated.

suspect a process of the Bethe–Heitler type from Eq. (1.14), the so-called *trident process*, to be the source of the occurring pairs:

$$e_{\text{projectile}} + n\omega \longrightarrow e_{\text{projectile}} + e^- + e^+, \tag{1.21}$$

with the projectile nucleus replaced by an electron from the beam. However, it turns out that due to the low mass of the projectile ($m_e \approx {}^{m}Z/_{(4000 \cdot Z)}$) this process is a few orders of magnitude weaker [33, 82] than an alternative two-step variation of the Breit–Wheeler process:

$$\omega + e_{\text{projectile}} \longrightarrow \gamma + e'_{\text{projectile}} \tag{1.22a}$$

$$\gamma + n\omega \longrightarrow e^+ + e^-. \tag{1.22b}$$

In the first step, a laser photon turns into a highly energetic γ-photon by Compton-scattering on a projectile electron. The projectile electron is thereby deflected. Then, in the second step, the γ collides with several ($n \gtrsim 4$) laser photons creating the e^-e^+ pair, analogously to Eq. (1.15). Even more than a decade after the measurement, the two processes of Eqs. (1.21) and (1.22) are still subject to theoretical analysis [68, 70, 77].

For an experimental realization of the non-linear Bethe–Heitler process given in Eq. (1.14) with a nucleus as projectile, the two-step process corresponding to Eqs. (1.22) would be strongly suppressed. For instance, the lightest nuclear projectile, an H^+ ion, i.e., a single proton, already has a 1836-times larger mass than the electron. As the cross section of Compton scattering is proportional to ${}^{1}/_{m^2_{\text{projectile}}}$ the first step in Eq. (1.22a) becomes very unlikely. Moreover, the non-linear Bethe–Heitler reaction is accessible by modern experimental techniques, e.g., by using the highly relativistic nuclear beam from the Large Hadron Collider (LHC) [32] at CERN (*Conseil Européen pour la Recherche Nucléaire*) in conjunction with a counterpropagating highly intense laser beam. In the nuclear rest frame, the laser frequency and intensity are subject to a strong amplification by a relativistic Doppler shift, reaching the levels required for pair creation.

The prospect of an experimental test naturally fuels further theoretical investigations: Production rates and emission spectra in various field parameter regimes have been calculated (e.g., [14, 60, 87, 105, 106, 145]), as well as more refined properties, such as nuclear recoil [84, 108], polarization [40] and spin effects [109]. However, in all mentioned studies the laser field was assumed to be a monochromatic plane wave with either linear or circular polarization.

1.4. Bichromatic Laser Fields

A propitious extension to these studies is the non-linear Bethe–Heitler effect employing a bichromatic laser field, i.e., a laser field comprised of two frequencies:

$$Z + n_1\omega_1 + n_2\omega_2 \to Z + e^- + e^+. \tag{1.23}$$

In an appropriate set-up, the addition of a second frequency mode to the laser field allows the study of quantum interference effects. Therefore, both modes have to propagate in the same direction and must have commensurable frequencies, i.e., frequencies with a rational ratio. Then, the total four-momentum of n_1 photons from the first mode may equal that of n_2 photons from the second mode. With this condition fulfilled, it is indistinguishable whether a pair was produced through photon absorption from the first or the second mode. Thus, these two quantum paths can interfere.

Recently, a process of this kind has been investigated with both modes linearly polarized along the same direction [85, 86]. In addition, both modes were assumed to have the same value for the intensity parameter (defined in Eq. (2.7) below). There, the relative phase between the modes was shown to exhibit a distinct influence on the angular distributions of the created particles. The non-linear Bethe–Heitler process was also considered for a bichromatic laser field of commensurable frequencies and circularly polarized modes [134]. A further study revealed interference effects in e^-e^+ pair creation by a highly energetic non-laser photon in the presence of a bichromatic laser field of commensurable frequencies [110]. Besides, it is worth mentioning that other types of interference effects in field-induced pair production have recently been subject to theoretical investigation as well [4, 38, 48, 73, 77].

Two-colour quantum interference effects are well known for photoinduced atomic processes [52] and chemical reactions [142], where they can be exploited for *coherent control* schemes. Furthermore, in the interaction of a single photon with a structured target, Bethe–Heitler pair creation may exhibit signatures of quantum interference. Particularly, coherently enhanced pair creation by a photon propagating through a crystal has been studied in detail [121, 149]. Similar interference effects occur in pair creation on molecules [126, 151]. In both cases, the pairs are produced at two or more Coulombic centres, with the corresponding process amplitudes adding up coherently and leading to interference. Finally, a study on entanglement in e^-e^+ production by two counter-propagating laser beams is worth mentioning [57].

For the incommensurable case of largely differing frequencies with $\omega_1/\omega_2 \gtrsim 100$, where no interference may occur, the influence of an assisting rapidly-oscillating

electric field on the strong-field Bethe–Heitler process has been studied [93], as well as the possibility of controlling the barrier in a tunneling pair-creation process [41, 42]. Similar studies on *dynamically assisted* variants of Schwinger [50, 140] and Breit–Wheeler pair creation [71] exist.

Two-colour laser fields have been successfully employed in several recent experiments on coherent control. By variation of the relative phase between the two laser modes, control over photo-ionization and -dissociation of various systems has been gained, such as hydrogen-deuteride molecular ions (HD^+) [143], the asymmetric non-polar molecule ethylene bromochloride ($Cl\,CH_2\,CH_2\,Br$) [117], deuterium molecules (D_2) [127], and several other molecules (e.g., N_2, O_2, CO, CO_2, and HBr) [23]. In particular, the emission direction of the ejected electrons and ionic fragments could be steered in these experiments. Note that, a frequency ratio of $\omega_1/\omega_2 = 2$ has been used in all given examples.

Light sources based on High-Harmonic Generation (HHG) [91] are ideal for the realization of asymmetric bichromatic laser fields because the two modes are intrinsically synchronized as they originate from the same pump laser. Therefore, they exhibit very high temporal resolution. Most commonly used are combinations of infrared (IR) and extreme ultraviolet (XUV) radiation [47, 75]. However, the intensities typically reached by HHG-based XUV lasers are not yet sufficient for inducing multiphoton processes.

Higher intensities are available at Free-Electron Lasers (FELs) [133] such as FLASH[5] in Hamburg, where XUV radiation in the multiphoton regime can be combined with IR laser pulses [139]. Furthermore, joint X-ray FEL radiation and IR laser beams are available at LCLS[6] in Stanford [98]. Additionally, the X-ray beam of the LCLS can be combined with high-power optical laser beams by means of the MEC (Matter in Extreme Conditions) instrument in order to achieve very asymmetric combinations of two frequencies [163]. In the context of bichromatic laser fields, the recent demonstration [95] of an intense two-colour X-ray FEL beam achieved by self-seeding [8] at LCLS is especially worth mentioning. However, FLASH and LCLS are both based on SASE (Self-Amplified Spontaneous Emission), which is a stochastic process [27]. Therefore, the generated pulses are only partially coherent [123]. They consist of stochastic spikes [2] whose width of a few femtoseconds corresponds to the temporal coherence length [104]. Furthermore, the phase changes randomly. Full control over all pulse parameters – including the phase – may be gained by laser-seeding both FEL beams, as has been demonstrated recently [7] at FERMI[7] in Trieste.

[5] Free-Electron Laser in Hamburg [58], since 2005, (28–295) eV [156]
[6] Linac Coherent Light Source [54], since 2009, (270–9500) eV [162]
[7] Free-Electron Laser for Multidisciplinary Investigations [6], since 2011, (12–124) eV [157]

1.5. Objective

In the present work, the non-linear Bethe–Heitler effect in a bichromatic laser field is studied for both, commensurable and incommensurable frequencies. Both field modes are assumed to be linearly polarized with mutually orthogonal polarization vectors. The presented theory relies on an $\mathscr{S}$-matrix formalism in the Furry picture using Volkov solutions to the Dirac equation as basis states. The nuclear Coulomb field is treated in the lowest order of perturbation theory.

For the commensurable case, the focus lies on signatures of two-colour quantum interference in the pair-creation process. Therefore, the intensity ratio of the frequency modes is chosen such that the contributions from interference in the square of the $\mathscr{S}$-matrix is maximized. It will be shown that, the two-colour interference manifests itself in a modified angular distribution of the created particles. In particular, shifts of the angular peak positions are found, as well as increases (or decreases) of the total pair-production rate. These modifications depend on the relative phase between the two field modes. Thus, the latter can be chosen to maximize the yield of produced pairs. The results are discussed in the nuclear rest frame and the laboratory frame. Additionally, an intuitive explanation for the phase dependence of the total pair production rate is developed. A special case, a monochromatic laser wave of arbitrary elliptical polarization, is also investigated by means of a transition from a single linearly polarized to a circularly polarized laser wave.

Regarding the chosen geometry of the bichromatic laser field, it is worth noting that the orthogonality of the field modes offers two advantages: On the one hand, the mathematical treatment of the process is simplified as certain cross terms will vanish. On the other hand, it is guaranteed that the laser intensity remains constant under variation of the relative phase between the modes. These two features facilitate gaining intuitive insights into the rather complex nature of two-colour quantum interferences in the non-linear Bethe–Heitler effect. Furthermore, in this context it is interesting to note that, orthogonally polarized two-colour laser fields have been employed to gain control on the laser-driven recollision dynamics of field-ionized electrons [31, 78].

The incommensurable case is compared to the commensurable one, in order to further emphasize the interference effects. In this comparison, it is discussed that the latter should particularly differ from the former for largely differing frequencies. Hence, this case is studied in form of the non-linear Bethe–Heitler process by a highly intense laser in the non-perturbative regime assisted by a highly energetic photon just below the pair-creation threshold. For this process, the total rates, just as rates differential in the emission angle, the energy, and the momentum of the created particles are compared to the unassisted counterpart.

This way, the laser intensity regime where the assisted photon leads to a strong enhancement of the total rate is identified, as well as that where its contribution is negligible. In the differential spectra, modifications to the width of the distribution and its peak position are found. Finally, the study is extended to the next-higher order process. The doubly-assisted pair-creation process is examined for the same properties as the singly-assisted before, leading to similar conclusions.

Parts of the results presented in the subsequent sections have been published in Refs. [12, 13]. A third publication based on the results shown in Sec. 4.2 is in preparation.

1.6. Outline

This thesis is organized as follows: In the subsequent Ch. 2, the theoretical framework is discussed. In Sec. 2.1, the laser field geometry is introduced and the Volkov solutions of the Dirac equation are adapted to it. From this, the transition amplitude, describing the non-linear Bethe–Heitler process in such a laser field, and the pair-creation rates are derived in Sec. 2.2. The latter contains a six-fold integral over the momenta of the created particles and a four-fold sum over photon numbers, which both can effectively be reduced by one due to energy constraints. The remaining integrations are performed numerically. The chapter concludes with remarks on the employed terminology and parameters.

The discussion of the results is divided into two parts: On the one hand, commensurable frequencies are treated in Ch. 3, with an emphasis on the effects of interference between the two laser modes. On the other hand, incommensurable frequencies are discussed in Ch. 4, starting with a comparison to the commensurable case, followed by the strongly differing frequencies of a γ-assisted tunneling pair-creation process. In both parts, pair-creation rates differential in the polar emission angle and in the radial momentum coordinate are shown for various frequency ratios and (total) photon energies. Furthermore, total pair-creation rates are compared for the different occurring processes.

A summary of the found results and the conclusions drawn from them is given in Ch. 5, as well as a brief discussion of the potential experimental realizations of the proposed pair-creation schemes. Additionally, in the Appendices an overview of the applied units (App. A) and notation (App. B) is given, as well as a derivation of the aforementioned Volkov solutions in App. C and various rules for the evaluation of products and traces of Dirac γ-matrices in App. D. Finally, an important caveat for the numerical integration is discussed in App. E.

Chapter 2.

Theoretical Framework

In the following, an expression for the fully differential pair-creation rate is developed by means of the amplitude of the transition from a negative- to a positive-continuum state. For the latter, Volkov wave functions adapted to the bichromatic field geometry are introduced. Furthermore, the employed terminology and parameters are discussed.

2.1. Volkov Solutions and Field Geometry

For an electron interacting with an electromagnetic plane wave in vacuum, the Dirac equation has an exact solution, the so-called Volkov wave functions. In the following, their application to pair creation in a bichromatic laser field will be discussed.

The Dirac equation [46] may be written in a conveniently compact form when Feynman slash notation $\not{A} = \gamma_\mu A^\mu$ and Einstein summation convention[8] is applied (see also App. B):

$$\left(\mathrm{i}\hbar\not{\partial} + \frac{e}{c}\not{A} - mc\right)\Psi = 0. \tag{2.1}$$

Here, e is the positive elementary charge, m the electronic rest mass, and c the speed of light in vacuum. The four-gradient $\partial = \left(\frac{1}{c}\frac{\partial}{\partial t}, -\nabla\right)$ is defined in terms of partial derivative operators with respect to the four dimensions of the space-time coordinate $x = (ct, \mathbf{r})$.

A plane-wave vector potential $A = A(\eta)$, i.e., a potential with constant frequency and amplitude whose wave fronts are infinite parallel planes perpendicular to

[8] Implied summation over indices appearing twice in a product (cf. App. B.1): $a_i b^i = \sum_i a_i b_i = \mathbf{a}\cdot\mathbf{b}$ and $a_\mu b^\mu = \sum_\mu a_\mu b^\mu = a_0 b_0 - \mathbf{a}\cdot\mathbf{b} = \langle ab\rangle$.

the wave vector $k = (\omega/c, \mathbf{k})$, depends only on a phase variable

$$\eta = k_\mu x^\mu = \omega t - \mathbf{k}\cdot\mathbf{r}. \tag{2.2}$$

Thus, Lorenz[9] gauge $\partial_\mu A^\mu = 0$ is fulfilled, which is equivalent to A being transversal: $k_\mu A^\mu = 0$.

From this ansatz, the Volkov solutions [153]

$$\Psi^{(\pm)}_{p_\pm,s_\pm} = N_\pm \left(\mathbb{1} \pm \frac{e\not{k}\not{A}}{2ck_\mu p^\mu_\pm}\right) \exp\!\left(\frac{\mathrm{i}}{\hbar} S^{(\pm)}\right) u^{(\pm)}_{p_\pm,s_\pm} \tag{2.3}$$

for electrons and positrons, as denoted by the superscripts $(-)$ and $(+)$, respectively, are obtained. The derivation is briefly outlined in App. C. Here, $u^{(\pm)}$ are free Dirac spinors with the spins $s_\pm$ and the momenta $p_\pm = (E_{p_\pm}/c, \mathbf{p}_\pm)$, where $p_\pm^2 = (mc)^2$. $N_\pm$ are normalizers, and $S^{(\pm)}$ is the respective action:

$$S^{(\pm)} = \pm x_\mu p^\mu_\pm + \frac{e}{ck_\mu p^\mu_\pm} \int^\eta \left[A_\mu(\tilde\eta)\, p^\mu_\pm \mp \frac{e}{2c} A^2(\tilde\eta)\right] \mathrm{d}\tilde\eta. \tag{2.4}$$

Using these wave functions, the interaction between electrons or positrons and the laser field are fully taken into account.

As depicted in Fig. 2.1, the laser field is defined as a superposition of two independent laser modes: $A = A_1 + A_2$. With each of them assumed to be a general plane wave

$$A_i = a_i \cos(\eta_i + \varphi_i) \quad (i = 1 \text{ or } 2), \tag{2.5}$$

with relative phases φ_i, phase coordinates $\eta_i = (\omega_i/c)\, \kappa_\mu x^\mu$, where the direction of propagation $\kappa = (1, 0, 0, 1)$ is shared among the wave vectors $k_i = (\omega_i/c)\kappa$. The field vectors a_i are chosen to be perpendicular, $\langle a_1 a_2 \rangle = 0$, and given by

$$a_1 = (0, 1, 0, 0)\, |\mathbf{a}_1| \quad \text{and} \quad a_2 = (0, 0, 1, 0)\, |\mathbf{a}_2|\,. \tag{2.6}$$

Their absolute amplitudes $|\mathbf{a}_i|$ are measured by the dimensionless intensity parameters

$$\xi_i = \frac{e}{mc^2} \frac{|\mathbf{a}_i|}{\sqrt{2}}. \tag{2.7}$$

In the superposition of these two fields, one can make use of an advantage of the considered geometry, namely $A^2 = A_1^2 + A_2^2$. Therefore, despite the squared laser

[9] Often erroneously attributed to H. A. Lorentz, however first published by L. Lorenz in Ref. [92] (cf. also Refs. [26, 112]). This confusion is particularly eminent in the so-called *Lorenz-Lorentz equation* of refractivity [146].

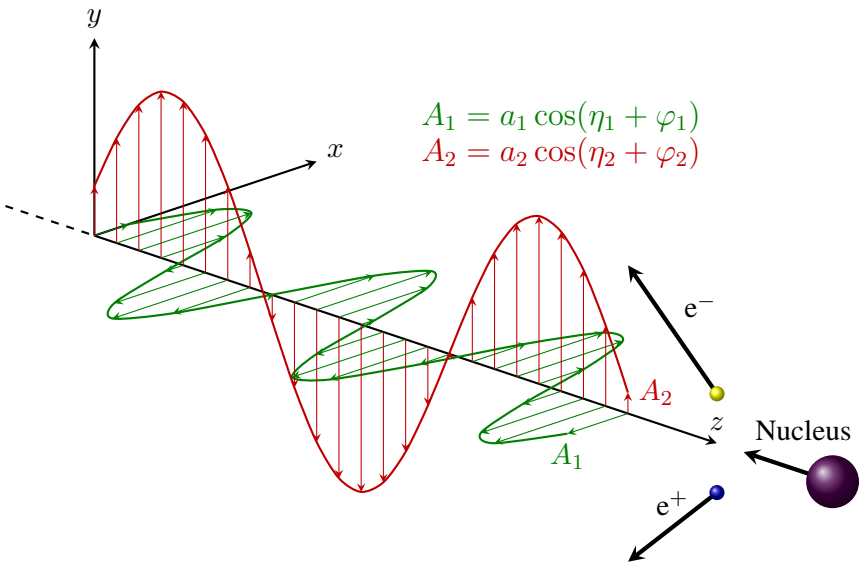

Figure 2.1.: *The employed laser geometry and pair creation scheme – Two linearly polarized plane waves with perpendicular field vectors propagating along the z-axis onto a counter-propagating nucleus, creating an electron-positron pair.*

amplitude in Eq. (2.4), functions of the two phase coordinates are separable:

$$S^{(\pm)} = \pm \langle x p_\pm \rangle + \sum_{i=1,2} S_i^{(\pm)}, \tag{2.8}$$

$$S_i^{(\pm)} = \frac{e}{c \langle k_i p_\pm \rangle} \int^{\eta_i} \left[\langle p_\pm A_i(\tilde{\eta}_i) \rangle \mp \frac{e}{2c} A_i^2(\tilde{\eta}_i) \right] \mathrm{d}\tilde{\eta}_i. \tag{2.9}$$

Note that, $\langle p_\pm A_i \rangle = -\mathbf{p}_\pm \cdot \mathbf{A}_i$ and $A_i^2 = -\mathbf{A}_i^2$. Upon insertion of the laser fields from Eq. (2.5), the integral in Eq. (2.9) can be performed:

$$S_i^{(\pm)} = \frac{e}{c \langle k_i p_\pm \rangle} \left[\langle p_\pm a_i \rangle \sin(\eta_i') \pm \frac{e}{4c} a_i^2 \left(\frac{\sin(2\eta_i')}{2} + \eta_i' \right) \right], \tag{2.10}$$

with the convenient abbreviation $\eta_i' = \eta_i + \varphi_i$. At this point it is useful to define the laser-dressed momenta [20]

$$q_\pm = p_\pm + \frac{e^2 \overline{\mathbf{A}^2}}{2c^2 \langle p_\pm \kappa \rangle} \kappa \tag{2.11}$$

$$= \left(\frac{E_{q_\pm}}{c}, \mathbf{q}_\pm \right), \tag{2.12}$$

via the mean square of the laser field amplitude

$$\overline{\mathbf{A}^2} = \frac{1}{2}\left(\mathbf{a}_1^2 + \mathbf{a}_2^2\right) = \frac{m^2c^4}{e^2}\left(\xi_1^2 + \xi_2^2\right). \tag{2.13}$$

These *effective* momenta contain the term linear in η_i from Eq. (2.10). However, the frequencies ω_i cancel and only the direction of propagation κ is of relevance. Furthermore, the term linear in the relative phases φ_i will eventually cancel in the following steps, particularly in the exponential of Eq. (2.22) as can be seen in Eq. (2.30), and will thus be dropped here. The average intensity of the total laser field is also independent of φ_i, due to the perpendicular field vectors.

The normalizers from Eq. (2.3),

$$N_\pm = \sqrt{\frac{mc}{q_\pm^0}}, \tag{2.14}$$

may be defined via the effective momenta, while its Lorentz-invariant square

$$q_\pm^2 = p_\pm^2 + \frac{e^2}{c^2}\overline{\mathbf{A}^2} \tag{2.15}$$

allows the definition of the effective or *laser dressed* electron mass [90]

$$m_* = m\sqrt{1 + \xi_1^2 + \xi_2^2} \tag{2.16}$$

such that $q_\pm^2 = (m_* c)^2$.

Finally, the so-called ponderomotive energy is defined by the difference

$$E_{q_\pm} - E_{p_\pm} = c\,(q_0 - p_0) = E_{\text{pond}} \tag{2.17}$$

$$= \frac{e^2\overline{\mathbf{A}^2}}{2c\,\langle p_\pm \kappa\rangle}\,\kappa_0 \tag{2.18}$$

$$\approx \frac{e^2\overline{\mathbf{A}^2}}{2mc^2} = \frac{mc^2}{2}\left(\xi_1^2 + \xi_2^2\right), \tag{2.19}$$

where the approximation holds for the non-relativistic limit. In the last step Eq. (2.13) has been inserted. The ponderomotive energy describes the cycle-averaged quiver motion of a free electron in an electric field.

2.2. Transition Amplitude and Pair-Creation Rates

The creation of an e^-e^+ pair may be modelled as a transition from a state in the negative continuum $\Psi^{(+)}$ to one of the positive continuum $\Psi^{(-)}$, as illustrated in

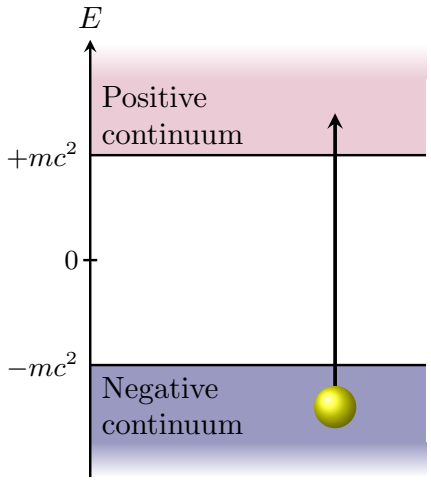

Figure 2.2.: *The employed model of e^-e^+ pair creation – The electron transitions from the negative continuum, the so-called* Dirac sea, *to the positive continuum. This leaves a hole in the former, which corresponds to the positron. The gap that has to be crossed along the energy axis is $2mc^2$ wide.*

Fig. 2.2. Throughout this study, these states are assumed to be Volkov states, while the transition is induced by a nuclear Coulomb potential A_N. In the rest frame of the nucleus, the potential consists only of a scalar part, which makes it convenient to introduce the four-vector $\epsilon = (1, 0, 0, 0)$ and write

$$A_{\mathrm{N}} = \frac{Ze}{|\mathbf{r}|}\epsilon. \tag{2.20}$$

Pair creation is then described by the transition amplitude[10]

$$\mathscr{S} = \frac{\mathrm{i}\,e}{\hbar c}\int \bar{\Psi}^{(-)}_{p_-,s_-}\, \not{A}_{\mathrm{N}}\, \Psi^{(+)}_{p_+,s_+}\, \mathrm{d}^4x, \tag{2.21}$$

treating the nuclear field in first-order perturbation theory. Upon insertion of the Volkov wave functions from Eq. (2.3), one obtains

$$\mathscr{S} = N_-N_+\frac{\mathrm{i}Ze^2}{\hbar c}\int\frac{\mathrm{d}^4x}{|\mathbf{r}|}\;\bar{u}^{(-)}_{p_-,s_-}\, G\, u^{(+)}_{p_+,s_+}\, \exp\!\left(\frac{\mathrm{i}}{\hbar}\left(-S^{(-)}+S^{(+)}\right)\right), \tag{2.22}$$

where all slashed quantities are collected in

$$G = \left(\mathbb{1} - \frac{e\not{A}\not{k}}{2c\,\langle \kappa p_-\rangle}\right)\not{\epsilon}\left(\mathbb{1} + \frac{e\not{k}\not{A}}{2c\,\langle \kappa p_+\rangle}\right). \tag{2.23}$$

[10]Here, the abbreviation $\bar{\psi} = \psi^\dagger\gamma_0$ for a spinor ψ is used.

This can be rewritten as

$$G = \not{\epsilon} + \frac{e}{2c}\left[\frac{\not{\epsilon}\not{k}}{\langle \kappa p_+\rangle} - \frac{\not{k}\not{\epsilon}}{\langle \kappa p_-\rangle}\right]\not{A} + \frac{e^2}{2c^2}\frac{\langle \epsilon\kappa\rangle\,\not{k}}{\langle \kappa p_-\rangle\,\langle \kappa p_+\rangle}A^2 \tag{2.24}$$

employing

$$\not{A}\not{k}\not{\epsilon}\not{k}\not{A} = -2\,\langle \epsilon\kappa\rangle\,A^2\not{k}, \tag{2.25}$$

$$\not{A}\not{k}\not{\epsilon} = \not{k}\not{\epsilon}\not{A}, \tag{2.26}$$

which may be verified using Eqs. (D.4).

Upon insertion of the laser fields from Eq. (2.5), G adopts the form

$$G = \not{\epsilon} + \sum_{i=1,2}\Big(\gamma_i \cos(\eta_i') + \delta_i \cos^2(\eta_i')\Big) \tag{2.27}$$

with

$$\gamma_i = \frac{e}{2c}\left[\frac{\not{\epsilon}\not{k}}{\langle \kappa p_+\rangle} - \frac{\not{k}\not{\epsilon}}{\langle \kappa p_-\rangle}\right]\not{a}_i, \tag{2.28}$$

$$\delta_i = \frac{e^2}{2c^2}\frac{\langle \epsilon\kappa\rangle\,\not{k}}{\langle \kappa p_-\rangle\,\langle \kappa p_+\rangle}a_i^2. \tag{2.29}$$

Due to Eq. (2.8) and Eq. (2.10), the exponential from Eq. (2.22) may be written as a product:

$$\exp\Big(\frac{\mathrm{i}}{\hbar}\left(S^{(+)} - S^{(-)}\right)\Big) = \exp\Big(\frac{\mathrm{i}}{\hbar}\left(\langle xp_-\rangle + \langle xp_+\rangle\right)\Big)\prod_{i=1,2}\exp\Big(\frac{\mathrm{i}}{\hbar}\left(S_i^{(+)} - S_i^{(-)}\right)\Big). \tag{2.30}$$

Wherein

$$\frac{\mathrm{i}}{\hbar}\left(S_i^{(+)} - S_i^{(-)}\right) = -\mathrm{i}\alpha_i \sin(\eta_i) - \mathrm{i}\beta_i \sin(2\eta_i), \tag{2.31}$$

with the definitions

$$\alpha_i = \frac{e}{\hbar\omega_i}\left(\frac{\langle a_i p_-\rangle}{\langle \kappa p_-\rangle} - \frac{\langle a_i p_+\rangle}{\langle \kappa p_+\rangle}\right), \tag{2.32}$$

$$\beta_i = \frac{e^2 a_i^2}{8c\hbar\omega_i}\left(\frac{1}{\langle \kappa p_-\rangle} + \frac{1}{\langle \kappa p_+\rangle}\right), \tag{2.33}$$

allows the identification of a set of three periodic functions $b(\eta_i)$, $c(\eta_i)$, and $d(\eta_i)$ for each laser mode i:

$$\begin{aligned} b(\eta_i) &= \exp(-\mathrm{i}\alpha_i \sin(\eta_i) - \mathrm{i}\beta_i \sin(2\eta_i)),\\ c(\eta_i) &= b(\eta_i)\cos(\eta_i),\\ d(\eta_i) &= b(\eta_i)\cos^2(\eta_i). \end{aligned} \tag{2.34}$$

A Fourier series expansion of the form

$$f(\eta_i) = \sum_{n_i} F_{n_i} \mathrm{e}^{-\mathrm{i}n_i\eta_i}, \tag{2.35}$$

where the function $f \in \{b, c, d\}$ as in Eq. (2.34) has the coefficients $F \in \{B, C, D\}$, yields six coefficients:

$$\begin{aligned} B_{n_i} &= \tilde{J}_{n_i}(\alpha_i, \beta_i), \\ C_{n_i} &= \frac{1}{2}\left[\tilde{J}_{n_i-1}(\alpha_i, \beta_i) + \tilde{J}_{n_i+1}(\alpha_i, \beta_i)\right], \\ D_{n_i} &= \frac{1}{4}\left[\tilde{J}_{n_i-2}(\alpha_i, \beta_i) + 2\tilde{J}_{n_i}(\alpha_i, \beta_i) + \tilde{J}_{n_i+2}(\alpha_i, \beta_i)\right], \end{aligned} \tag{2.36}$$

built from generalized Bessel functions $\tilde{J}_n(\alpha, \beta)$ [129], as defined via the ordinary Bessel function $J_n(x)$ by

$$\tilde{J}_n(\alpha, \beta) = \sum_{l=-\infty}^{\infty} J_{n-2l}(\alpha)\, J_l(\beta). \tag{2.37}$$

Note that, the relative phases φ_i have not been taken into account so far. This is because they may be treated in general instead of separately for each coefficient above. A Fourier series of the form

$$f(\eta_i') = \sum_{n_i} F_{n_i} \mathrm{e}^{-\mathrm{i}n_i\eta_i'} = \sum_{n_i} F_{n_i} \mathrm{e}^{-\mathrm{i}n_i\eta_i} \mathrm{e}^{-\mathrm{i}n_i\varphi_i} \tag{2.38}$$

leads to the same coefficient as Eq. (2.35), however for each addend an additional factor $\phi_{n_i} = \mathrm{e}^{-\mathrm{i}n_i\varphi_i}$, identical for all coefficients from Eq. (2.36), occurs.

The series expansion introduces two indices n_i, which can be interpreted as count for the number of photons taken from the respective mode i. Upon inserting the expansions into the transition amplitude, it can be rewritten as summation over the n_i:

$$\mathscr{S} = \frac{\mathrm{i}Ze^2mc}{\hbar c\sqrt{q_-^0 q_+^0}} \sum_{n_1,n_2} \phi_{(n_1,n_2)}\, M_{p_-p_+}^{(n_1,n_2)} \int \frac{\mathrm{d}^4x}{|\mathbf{r}|}\, \exp\!\left(\frac{\mathrm{i}}{\hbar} x_\mu Q_{(n_1,n_2)}^\mu\right), \tag{2.39}$$

where the normalizers from Eq. (2.14) have been inserted. Additionally, the momentum transfer to the nucleus

$$Q_{(n_1,n_2)} = q_+ + q_- - n_1\hbar k_1 - n_2\hbar k_2 \tag{2.40}$$

has been introduced, as well as the matrix element $M_{p_-p_+}^{(n_1,n_2)} = \bar{u}_{p_-,s_-}^{(-)} \Gamma_{n_1,n_2}\, u_{p_+,s_+}^{(+)}$. The latter contains all slashed quantities and the Fourier coefficients listed in Eq. (2.36):

$$\begin{aligned} \Gamma_{n_1,n_2} = {} & \not{B}_{n_1} B_{n_2} + (\gamma_1 C_{n_1} + \delta_1 D_{n_1})\, B_{n_2} \\ & + (\gamma_2 C_{n_2} + \delta_2 D_{n_2})\, B_{n_1} \end{aligned} \tag{2.41}$$

Note that, this form is reminiscent of Eq. (2.27) and the abbreviations from Eq. (2.28) and Eq. (2.29) have been used. Besides, each coefficient contributes a phase factor ϕ_{n_i}, which have been collected in $\phi_{(n_1,n_2)} = \mathrm{e}^{-\mathrm{i}n_1\varphi_1}\mathrm{e}^{-\mathrm{i}n_2\varphi_2}$.

The four-dimensional integral in Eq. (2.39) may be solved by treating the spatial and the temporal part separately [24]. For the integral in space, the Fourier transform of the Coulomb potential

$$\int \mathrm{d}^3r \, \frac{1}{|\mathbf{r}|} \, \mathrm{e}^{-\frac{\mathrm{i}}{\hbar}\mathbf{Q}\cdot\mathbf{r}} = \frac{4\pi\hbar^2}{|\mathbf{Q}|^2} \tag{2.42}$$

is used, while the integral in time ($x_0 = ct$) is a representation of the δ-function:

$$\int \mathrm{d}x_0 \, \mathrm{e}^{\frac{\mathrm{i}}{\hbar}Q_0\, x_0} = 2\pi\hbar\, \delta(Q_0). \tag{2.43}$$

By definition of $Q^0_{(n_1,n_2)}$, this δ-function ensures energy conservation.

In order to obtain the pair-creation rate R, the transition amplitude has to be squared. In particular, the fully differential rate is obtained by summing this square over the final spin states and dividing by a time interval τ:

$$\mathrm{d}^6R = \frac{1}{\tau} \sum_{s_+.s_-} |\mathscr{S}|^2 \, \frac{\mathrm{d}^3q_-}{(2\pi\hbar)^3} \frac{\mathrm{d}^3q_+}{(2\pi\hbar)^3}. \tag{2.44}$$

Throughout this work, total rates or spectra of rates differential in one coordinate are discussed, thus the six integrations have to be performed. Due to the δ-function introduced above, one integration can be performed analytically, while the remaining ones are performed numerically (cf. also App. E).

In $|\mathscr{S}|^2$, the two photon-counting indices n_i introduced by the Fourier series expansions in Eq. (2.35) have to be accounted for twice each. Thus one finds a sum over four indices:

$$|\mathscr{S}|^2 = \sum_{\substack{n_1',n_2'\\ n_1,n_2}} \mathscr{P}_{[n_1,n_2,n_1',n_2']}, \tag{2.45}$$

with the addends being the thereby defined *partial contributions*

$$\mathscr{P}_{[n_1,n_2,n_1',n_2']} = C\, \phi_{(n_1,n_2,n_1',n_2')}\, \bar{M}^{(n_1,n_2)}_{p_-p_+} M^{(n_1',n_2')}_{p_-p_+} \frac{c\tau}{Q^4_{(n_1n_2)}}\, \delta\Big(Q^0_{(n_1,n_2)}\Big), \tag{2.46}$$

with $C = \frac{Z^2e^4m^2}{\hbar^2 q^0_+ q^0_-}\, 32\pi^3\hbar^5$, $\bar{M} = \gamma_0 M^\dagger \gamma_0$, and the phase factor

$$\begin{aligned} \phi_{(n_1,n_2,n_1',n_2')} &= \phi^*_{(n_1,n_2)}\phi_{(n_1',n_2')} \\ &= \mathrm{e}^{\mathrm{i}n_1\varphi_1}\mathrm{e}^{\mathrm{i}n_2\varphi_2}\mathrm{e}^{-\mathrm{i}n_1'\varphi_1}\mathrm{e}^{-\mathrm{i}n_2'\varphi_2} = \mathrm{e}^{\mathrm{i}(n_1'-n_1)\varphi_1+\mathrm{i}(n_2'-n_2)\varphi_2}. \end{aligned} \tag{2.47}$$

Note that, the real part of the phase factor

$$\Re\Big(\phi_{(n_1,n_2,n_1',n_2')}\Big) = \cos((n_1' - n_1)\varphi_1 + (n_2' - n_2)\varphi_2) \tag{2.48}$$

yields the actual dependence on the relative phases once rates are considered. The imaginary part must vanish so that the rates are real quantities. This may be verified by studying the summation over the photon numbers: For every combination of the four indices with $n_i \neq n_i'$ another combination exists with the values of n_i and n_i' switched. For symmetry reasons, these two contributions are equal apart from the sign in the argument of the exponential from Eq. (2.47). As the imaginary part is an odd function, i.e., a sine with the same argument as above, the imaginary parts of the two contributions cancel. The cosine of the real part is an even function, thus the two contributions are indeed identical. Additionally, for combinations of the four indices with $n_i = n_i'$, the phase factor is simply unity as the argument of the exponential (or rather the cosine) vanishes.

The δ-function in Eq. (2.46) as introduced in Eq. (2.43) enforces

$$n_1 k_1 + n_2 k_2 = n_1' k_1 + n_2' k_2, \tag{2.49a}$$

$$Q_{(n_1,n_2)} = Q_{(n_1',n_2')}. \tag{2.49b}$$

Therefore, one may use Eq. (2.49a) to define

$$\varphi_1' = \varphi_1 + \frac{\omega_1}{\omega_2}\varphi_2 \quad \text{and} \quad \varphi_2' = 0. \tag{2.50}$$

Without loss of generality, it is thus justified to use only a single relative phase $\varphi = \varphi_1'$ instead of two.

Furthermore, using Eq. (2.49b) the squared δ-function has introduced the time interval τ into Eq. (2.46) according to [24]:

$$\Big[2\pi\hbar\,\delta\Big(Q^0_{(n_1,n_2)}\Big)\Big]^2 = 2\pi\hbar\,\delta\Big(Q^0_{(n_1,n_2)}\Big)\,c\tau. \tag{2.51}$$

As can be seen immediately, τ will cancel once $|\mathscr{S}|^2$ and consequently $\mathscr{P}$ are inserted into Eq. (2.44). However, it is of particular interest for the presented study to define an additional measure via the partial contributions, the differential partial rates

$$\mathrm{d}^6 R_{[n_1,n_1',n_2,n_2']} = \frac{1}{\tau}\sum_{s_+,s_-} \mathscr{P}_{[n_1,n_1',n_2,n_2']}\,\frac{\mathrm{d}^3 q_-}{(2\pi\hbar)^3}\,\frac{\mathrm{d}^3 q_+}{(2\pi\hbar)^3}. \tag{2.52}$$

With this, Eq. (2.44) may be written as

$$\mathrm{d}^6 R = \sum_{\substack{n_1',n_2'\\ n_1,n_2}} \mathrm{d}^6 R_{[n_1,n_1',n_2,n_2']}. \tag{2.53}$$

As will be discussed later, different combinations of indices will characterize and classify the different processes occurring for a given nuclear beam and laser geometry. However, it is important to note, that the partial rates are, in general, no experimental observables. Particularly, they may be negative and accordingly decrease the total rate.

Inserting $\mathscr{P}$ from Eq. (2.46) into Eq. (2.52) leads to

$$\mathrm{d}^6 R_{[n_1,n_1',n_2,n_2']} = C\,\phi_{(n_1,n_2,n_1',n_2')}\; T\;\frac{c}{Q^4_{(n_1 n_2)}}\;\delta\Big(Q^0_{(n_1,n_2)}\Big)\,\frac{\mathrm{d}^3 q_-}{(2\pi\hbar)^3}\frac{\mathrm{d}^3 q_+}{(2\pi\hbar)^3}, \tag{2.54}$$

wherein the occurring spin sum T may be expressed as a trace of products of γ-matrices (cf. App. D):

$$T = \sum_{s_+,s_-} \bar{M}^{(n_1,n_2)}_{p_- p_+} M^{(n_1',n_2')}_{p_- p_+} = \mathrm{tr}\left(\Gamma_{n_1,n_2}\frac{\not{p}_+ - c}{2c}\,\bar{\Gamma}_{n_1',n_2'}\frac{\not{p}_- + c}{2c}\right). \tag{2.55}$$

For the evaluation of the trace, $\bar{\Gamma} = \gamma_0\Gamma^\dagger\gamma_0$ with the complex conjugate

$$\begin{aligned}\Gamma^\dagger_{n_1',n_2'} = \not{\epsilon} B_{n_1'} B_{n_2'} &+ \left(\gamma_1^\dagger C_{n_1'} + \delta_1 D_{n_1'}\right) B_{n_2'} \\ &+ \left(\gamma_2^\dagger C_{n_2'} + \delta_2 D_{n_2'}\right) B_{n_1'}\end{aligned} \tag{2.56}$$

is needed, wherein the Fourier coefficients are real quantities and $\delta_i = \delta_i^\dagger$, as it contains only a single γ-matrix. However, for $\gamma_i^\dagger$ the order of the contained slashed quantities has to be reversed (cf. Eq. (D.5)):

$$\gamma_i^\dagger = \frac{e}{2c}\not{a}_i\left[\frac{\not{\kappa}\not{\epsilon}}{\langle\kappa p_+\rangle} - \frac{\not{\epsilon}\not{\kappa}}{\langle\kappa p_-\rangle}\right], \tag{2.57}$$

which is connected to γ_i via

$$\gamma_i^\dagger + \gamma_i = \frac{e}{c}\langle\epsilon\kappa\rangle\left[\frac{1}{\langle\kappa p_+\rangle} - \frac{1}{\langle\kappa p_-\rangle}\right]. \tag{2.58}$$

Applying the algebra presented in Eqs. (D.4) yields an expression for T of the form

$$T = U + V_{12} + V_{21} + W, \tag{2.60}$$

with the individual terms given in Eq. (2.59) on page 23. The result is expectedly symmetric in the laser amplitudes a_i and may be broken up into four parts. The first part, U, is independent of a_i. The second and third part have the same form, $V_{ij} = V_{ij}(a_i)$, and are a function of only one of the amplitudes. Therefore, the only occurring coefficients for mode j are B_{n_j} and $B_{n_j'}$. The fourth part,

$$U = \frac{1}{4c^2}\, 4 \left(2 \langle \epsilon p_+ \rangle \langle \epsilon p_- \rangle - \Big[\langle p_+ p_- \rangle + c^2 \Big] \right) \left(B_{n_1} B_{n_1'} B_{n_2} B_{n_2'} \right) \tag{2.59a}$$

$$\begin{aligned} V_{ij} = \frac{1}{4c^2} \frac{2}{\langle \kappa p_+ \rangle \langle \kappa p_- \rangle} \frac{e}{c} \\ \times \Bigg\{ & \Bigg(2 \langle \epsilon \kappa \rangle \Big[\langle \kappa p_- \rangle \langle \epsilon p_- \rangle \langle a_i p_+ \rangle - \langle \kappa p_+ \rangle \langle \epsilon p_+ \rangle \langle a_i p_- \rangle \Big] \\ & + \Big[\langle \kappa p_+ \rangle + \langle \kappa p_- \rangle \Big] \Big[\langle a_i p_- \rangle \langle \kappa p_+ \rangle - \langle a_i p_+ \rangle \langle \kappa p_- \rangle \Big] \Bigg) \left(B_{n_i} C_{n_i'} + C_{n_i} B_{n_i'} \right) \\ & + \frac{e}{c} a_i^2 \langle \epsilon \kappa \rangle \Big[\langle \epsilon p_+ \rangle \langle \kappa p_- \rangle + \langle \epsilon p_- \rangle \langle \kappa p_+ \rangle - \langle \epsilon \kappa \rangle \Big[\langle p_+ p_- \rangle + c^2 \Big] \Big] \left(B_{n_i} D_{n_i'} + D_{n_i} B_{n_i'} \right) \\ & + \frac{e}{c} \Bigg[a_i^2 \Bigg(\Big[\langle \kappa p_+ \rangle + \langle \kappa p_- \rangle \Big]^2 - 2 \langle \epsilon \kappa \rangle \Big[\langle \epsilon p_+ \rangle + \langle \epsilon p_- \rangle \Big] \Big[\langle \kappa p_+ \rangle + \langle \kappa p_- \rangle \Big] \Bigg) \\ & \quad - 2 \langle \epsilon \kappa \rangle^2 \left(2 \langle a_i p_+ \rangle \langle a_i p_- \rangle - a_i^2 \Big[\langle p_+ p_- \rangle + c^2 \Big] \right) \Bigg] \left(C_{n_i} C_{n_i'} \right) \\ & + \frac{e^2}{c^2} \langle \epsilon \kappa \rangle^2 \left(a_i^2 \Big[\langle a_i p_- \rangle - \langle a_i p_+ \rangle \Big] \right) \left(C_{n_i} D_{n_i'} + D_{n_i} C_{n_i'} \right) \\ & + \frac{e^3}{c^3} \langle \epsilon \kappa \rangle^2 a_i^4 \left(D_{n_i} D_{n_i'} \right) \Bigg\} \left(B_{n_j} B_{n_j'} \right) \end{aligned} \tag{2.59b}$$

$$\begin{aligned} W = \frac{1}{4c^2} \frac{2}{\langle \kappa p_+ \rangle \langle \kappa p_- \rangle} \frac{e^2}{c^2} \langle \epsilon \kappa \rangle^2 \\ \times \Bigg\{ & - 2 \Big[\langle a_1 p_+ \rangle \langle a_2 p_- \rangle + \langle a_1 p_- \rangle \langle a_2 p_+ \rangle \Big] \left(B_{n_1} C_{n_1'} C_{n_2} B_{n_2'} + C_{n_1} B_{n_1'} B_{n_2} C_{n_2'} \right) \\ & + \frac{e}{c} a_2^2 \Big[\langle a_1 p_- \rangle - \langle a_1 p_+ \rangle \Big] \left(B_{n_1} C_{n_1'} D_{n_2} B_{n_2'} + C_{n_1} B_{n_1'} B_{n_2} D_{n_2'} \right) \\ & + \frac{e}{c} a_1^2 \Big[\langle a_2 p_- \rangle - \langle a_2 p_+ \rangle \Big] \left(B_{n_1} D_{n_1'} C_{n_2} B_{n_2'} + D_{n_1} B_{n_1'} B_{n_2} C_{n_2'} \right) \\ & + \frac{e^2}{c^2} a_1^2 a_2^2 \left(B_{n_1} D_{n_1'} D_{n_2} B_{n_2'} + D_{n_1} B_{n_1'} B_{n_2} D_{n_2'} \right) \Bigg\} \end{aligned} \tag{2.59c}$$

Eq. 2.59: *Terms from the trace in Eq.* (2.55) *as defined via Eq.* (2.60) *– Each term has been gained by applying the rules presented in App.* D. *Note that U is independent of both a_i, while $V_{ij} = V_{ij}(a_i)$ only depends on one a_i and W depends on both.*

W, is in itself symmetric in a_i and the two amplitudes are interchangeable: $W = W(a_1, a_2) = W(a_2, a_1)$. In this term only products of powers of a_1 and a_2 occur.

It is worth noting that, in case one laser mode was turned off, i.e., $a_i = 0$, the terms W and V_{ij} would vanish, while U and V_{ji} would remain. This reproduces the results for a single monochromatic linearly polarized laser beam colliding with a nucleus, as obtained in Ref. [106]. Moreover, for an appropriate set of parameters, in particular by defining

$$\begin{aligned} |\mathbf{a}_1| &= |\mathbf{a}_2| = a, \\ \omega_1 &= \omega_2 = \omega, \\ \varphi_1 &= \pi/2, \\ \varphi_2 &= 0, \end{aligned} \tag{2.61}$$

the results for a circularly polarized laser wave [105] are also reproduced.

The third special case contained in the presented theory is a monochromatic laser wave of arbitrary elliptical polarization, as will be discussed in Sec. 3.2. It is achieved by setting only

$$\begin{aligned} \omega_1 &= \omega_2 = \omega, \\ \varphi_1 &= \pi/2, \\ \varphi_2 &= 0, \end{aligned} \tag{2.62}$$

and adjusting the intensities such that the desired ellipticity is reached. This way the ellipticity may be tuned continuously from the linearly polarized case (e.g., with $a_1 = a$ and $a_2 = 0$) to the circularly polarized case (as in Eq. (2.61)). Alternatively, a similar transition may be achieved with the set-up

$$\begin{aligned} |\mathbf{a}_1| &= |\mathbf{a}_2| = a, \\ \omega_1 &= \omega_2 = \omega, \end{aligned} \tag{2.63}$$

and a variation of the relative phases. For $\varphi_1 = \varphi_2 = 0$, this corresponds to a single linearly polarized laser wave with the polarization axis lying diagonally in the x-y-plane[11]. For one φ_i set to $\pi/2$ instead, one finds a circularly polarized laser wave. The continuous variation between these two extreme conditions, again, allows to tune an arbitrary ellipticity.

[11] This is in contrast to Eq. (2.62) where the linear polarization is either along the x- or y-axis.

2.3. Terminology and Parameters

In order to ease reading the results presented in the following chapters, a few short remarks on the applied notation should be made. Throughout this thesis, the notions *laser pair* and *minimal photon number* are used frequently, just as a classification of the occurring sub-processes by means of the involved number of photons. These will be introduced in the following. Furthermore, the employed intensity and nuclear beam parameters are discussed.

2.3.1. Laser Pairs and Minimal Photon Number

A pair of laser waves with frequencies ω_1 and ω_2 is denoted by $(\tilde{n}_1, \tilde{n}_2)$ when it is indistinguishable whether $\tilde{n}_1$ photons were absorbed from the first mode or $\tilde{n}_2$ from the second mode. Here, $\tilde{n}_i = \left\lceil \frac{2m_*c^2}{\omega_i} \right\rceil$ (see also App. B.4) is the minimal number of photons needed from mode i to create a pair, using no photon from the other mode. In this case, the minimal energy absorbed from mode i is $\tilde{n}_i\hbar\omega_i \gtrsim 2m_*c^2$. As long as the intensity parameter ξ_i is small, this energy is a good measure because processes involving more than the minimal number of photons (or the minimal amount of energy) are suppressed. Thus, for commensurable frequencies, i.e., frequencies with a rational ratio, where these energies are inherently equal, $\tilde{n}_1\hbar\omega_1 = \tilde{n}_2\hbar\omega_2$, they may be associated with the total photon energy E_{ph}. This energy is absorbed for every process that significantly contributes to the total rate. Particularly, processes may be possible in which photons from both modes are absorbed. Then the individual numbers n_i (or n_i', as will be discussed in the subsequent Sec. 2.3.2) may be smaller than $\tilde{n}_i$, and

$$\begin{aligned} E_{\mathrm{ph}} &= n_1\hbar\omega_1 + n_2\hbar\omega_2 \\ &= n_1'\hbar\omega_1 + n_2'\hbar\omega_2 \end{aligned} \tag{2.64}$$

$$\equiv \tilde{n}_1\hbar\omega_1 \equiv \tilde{n}_2\hbar\omega_2. \tag{2.65}$$

For incommensurable frequencies, on the other hand, the minimal photon energies are not equal and the total photon energies absorbed in the individual sub-processes may differ.

2.3.2. Term Classification

So far, no formal definition of what sub-processes may occur, has been made. In the theoretical treatment presented here, it is straightforward to use the four photon-counting indices introduced in Eq. (2.45) for this distinction. It is

Type of term	Condition ($\forall i$)	Example: $(2, 4)$
Direct	$n_i = n'_i$, only one $n_i \neq 0$	$[2, 2, 0, 0]$ or $[0, 0, 4, 4]$
Symmetrically mixed	$n_i = n'_i \neq 0$	$[1, 1, 2, 2]$
Interference (Asymmetric)	$n_i \neq n'_i$	$[0, 2, 4, 0]$ or $[2, 0, 0, 4]$

Table 2.1.: *Types, conditions, and examples of the terms $[n_1, n'_1, n_2, n'_2]$ in the summation from Eq. (2.53) – Note that, the direct and the symmetrically mixed terms are invariant under exchange of n_i and n'_i. For an interference term this leads to a different one. However, these two will contribute equally.*

particularly convenient to define different types of terms in the four-index sum of Eq. (2.53), denoted by their respective combination of indices $[n_1, n'_1, n_2, n'_2]$.

Throughout this work three classes are distinguished: *direct*, *symmetrically mixed*, and *asymmetrically mixed* terms, where the latter stem from interference (see Tab. 2.1 for the exact conditions and some examples). *Direct* terms are those originating solely from one of the two laser modes and thus would also be visible if the other mode was turned off. They can serve as contribution strength references later on, as they could be used in an experimental comparison by recording the two laser sources one at a time. The *symmetrically mixed* terms can be understood as taking a certain number of photons from the first mode and another number from the second. In these cases, no interference is involved. For the *interference* terms, on the other hand, it is, by definition, not obvious how to interpret their index combination as actual photon numbers from the two modes. These terms may only occur for commensurable frequencies as Eq. (2.49) could not be fulfilled otherwise. This can be verified by rewriting Eq. (2.49a) as either

$$(n_1 - n'_1)\,\omega_1 = (n'_2 - n_2)\,\omega_2, \tag{2.66}$$

which will only be true for arbitrary ω_i if $n_i = n'_i$, or as

$$\frac{n_1 - n'_1}{n'_2 - n_2} = \frac{\omega_2}{\omega_1}, \tag{2.67}$$

which demands commensurable ω_i for $n_i \neq n'_i$. Furthermore, as can be seen in Eq. (2.47), only interference terms are sensitive to changes of the relative phases φ_i from Eq. (2.5). For the other types of terms, where $n_i = n'_i$, the argument of the exponential therein vanishes and the whole factor becomes unity.

2.3.3. Intensity Parameters

In order to investigate interference, it is mandatory to choose a set of parameters in which contributions from the respective terms are maximal. To ensure this, the partial rates of the two direct terms with minimal photon number,

$$R_{[\tilde{n}_1,\tilde{n}_1,0,0]} = R_1, \tag{2.68}$$
$$R_{[0,0,\tilde{n}_2,\tilde{n}_2]} = R_2, \tag{2.69}$$

may be used. When these are approximately equal, the interference terms show their maximal strength, as otherwise they are limited by the smaller of the two direct terms. A straightforward way of reaching such a configuration is by introducing a common intensity parameter ζ and defining the two intensity parameters ξ_i from Eq. (2.7) via the respective other modes minimal photon number:

$$\begin{aligned} \xi_1 &\approx \zeta^{\tilde{n}_2}, \\ \xi_2 &\approx \zeta^{\tilde{n}_1}. \end{aligned} \tag{2.70}$$

The leading order of the direct rate R_i contains the square of a Bessel function with an argument that is linear in the intensity parameter ξ_i. In the multiphoton regime, i.e., for $\xi_i \ll 1$, this is the $\tilde{n}_i$th order (cf. Eq. (1.20)), and one finds

$$R_i \sim \xi_i^{2\tilde{n}_i}. \tag{2.71}$$

Combined with Eq. (2.70), this ensures

$$R_1 \approx R_2 \sim \zeta^{2\tilde{n}_1\tilde{n}_2}. \tag{2.72}$$

For a general term $[n_1, n_1', n_2, n_2']$, a scaling corresponding to Eq. (2.71) can be given and the individual ξ_i can be replaced by the newly introduced ζ:

$$R_{[n_1,n_1',n_2,n_2']} \sim \xi_1^{(n_1+n_1')}\xi_2^{(n_2+n_2')} \approx \zeta^{\tilde{n}_2(n_1+n_1')+\tilde{n}_1(n_2+n_2')}. \tag{2.73}$$

However, while these equations give the correct scaling, they do not include the proportionality factor, which differs for the two direct rates. To take this into account, a small adjustment to the ξ_i is necessary. It may be gained from the ratio of the results of the direct terms R_i^{calc} calculated for the ξ_i from Eq. (2.70), for instance a modified ξ_1 would be:

$$\xi_1 = \zeta^{\tilde{n}_2}\left(\frac{R_1^{\mathrm{calc}}}{R_2^{\mathrm{calc}}}\right)^{1/2\tilde{n}_2}. \tag{2.74}$$

Note that, due to Eq. (2.71), the ratio of the calculated rates should be approximately unity and, thus, the introduced change to ξ_1 is indeed small.

2.3.4. Nuclear Beam

For all results shown in this thesis, a proton beam target, and thus $Z = 1$, is assumed. As can be seen from Eq. (2.46), particularly from the factor C therein, for higher nuclear charges the rates would by scaled by a factor of Z^2. However, it is important to note that this is only true as long as Coulomb corrections to the first-order treatment of the nuclear field may be neglected. This is indeed the case for all parameters discussed in this work.

Coulomb corrections would include the attraction or repulsion of the created particles (electron and positron, respectively), due to the field of the nucleus [18, 74]. They have to be considered if the particles are slow enough to be deflected by the nuclear field. But even for our case of low total photon energy, the kinetic energy is sufficiently large for the particles to leave the vicinity of the nucleus without being deflected. To find a measure for the influence of the nuclear field on a nearby electron or positron, one can compare the squared modulus of the wavefunction for a Coulomb field with that of the free particle counterpart at the coordinate origin, i.e., at the position of the nucleus [88]. If no deviation is found, the assumption that the influence of the nuclear Coulomb field on the trajectory of the particles can be neglected is justified. Setting the ratio of these squared moduli, as given in formulæ (134.10) and (134.11) from Ref. [88], to unity, it can be shown that this is the case if the *Sommerfeld parameter* is small:

$$\frac{Z\alpha}{\beta_\pm} \ll 1. \tag{2.75}$$

Here $\beta_\pm = {}^{v_\pm}/_{c}$ is the velocity of the respective created particle in units of the speed of light. This quantity is indeed small for typical kinetic energies of about 40 keV, corresponding to velocities of $\beta_\pm \approx 0.4$, and small $Z < 5$. Particularly, for $Z = 1$, as considered here, one obtains

$$\frac{Z\alpha}{\beta_\pm} \approx 0.02\,. \tag{2.76}$$

Consequently, Coulomb corrections are of minor importance for the total photon energies under consideration here. However, for heavier nuclei, i.e., with $Z \gtrsim 10$, they would have to be taken into account.

In this context, it is worth mentioning that a comparison of pair-creation rates for the two projectiles currently available at the LHC [32], protons ($Z = 1$) and fully stripped lead ions ($Z = 82$), may be found in Ref. [107].

Chapter 3.

Commensurable Frequencies

In all figures of this chapter where partial rates are discussed, only those are shown that contribute to the summed-up rate significantly. Partial rates that are several orders of magnitude smaller than the leading terms (which are generally the direct terms) are neglected.

For the direct and symmetrically mixed terms, the partial contributions are invariant under exchange of n_i and n_i'. For an interference term, this exchange leads to a second term that contributes identically. In the spectral plots these two contributions overlap perfectly. Therefore, they will always be depicted by a single line, which has to be counted twice when summing up all terms.

3.1. Interference of the Two Laser Modes

In the following sections, results for commensurable frequencies are shown. The arising interference phenomena are discussed by means of angular-differential (partial) rates for various combinations of laser waves. The influence of a variation of the total photon energy and of the relative phase is studied in the nuclear rest frame and the laboratory frame. Parts of the results presented in the following sections have been published in Refs. [12, 13].

3.1.1. Variation of the Minimal Photon Number in the Nuclear Rest Frame

For the study of interference phenomena, it is mandatory to identify candidates of laser wave combinations $(\tilde{n}_1, \tilde{n}_2)$, which show strong contributions from interference terms. To do so, a fixed total photon energy in the nuclear rest frame

just above the pair-creation threshold is chosen,

$$\tilde{n}_1\hbar\omega_1 = \tilde{n}_2\hbar\omega_2 = 1.1\,\mathrm{MeV}. \tag{3.1}$$

The relative phase φ is set to zero and the intensity parameters are $\xi_i < 1$.

Experimentally, photon energies of that magnitude could be achieved, for instance, by colliding a nuclear beam with a Lorentz factor of $\gamma \approx 6000$, as the LHC provides in its current state [32], with an XUV laser beam with $\omega \sim 50\,\mathrm{eV}$. Alternatively, a much lower γ of about 50 could be used in conjunction with an X-ray laser beam of $\omega \lesssim 10\,\mathrm{keV}$.

The considerations in this section, as well as in the following two sections, are confined to the nuclear rest frame. Therefore, the Lorentz factor γ of the nucleus is only used to increase the total photon energy from the laboratory by a factor of approximately 2γ (cf. Eq. (3.8)). The further influence of different values for γ is discussed in Sec. 3.1.4, where the laboratory frame is studied.

The starting point of the presented investigation is the laser pair with lowest differing minimal photon numbers: $(1, 2)$. This corresponds to the frequencies in the nuclear rest frame

$$\omega_1 = 1.1\,\mathrm{MeV} \quad \text{and} \quad \omega_2 = 550\,\mathrm{keV}. \tag{3.2}$$

The angular-differential partial rates for the main contributions of this pair are shown in Fig. 3.1(a). The emission angle θ is measured with respect to the laser propagation direction. Due to the momentum in forward direction conveyed by the absorbed photons, the maxima of the spectra are usually below 90°. As discussed in Sec. 2.3, the intensities are chosen such that the two direct terms with minimal photon number contribute equally to the total rate. This is clearly visible in Fig. 3.1(a) where the direct term with a single photon from the first mode (long-dashed blue line) and that with two photons from the second mode (solid red line) are shown. Note that their peak positions deviate slightly. There is a further direct term using three photons of mode two (dash-dotted magenta line) visible, whose contribution is much smaller because its order in ζ is higher. Consequently, the smallest visible terms are of even higher order. These are another direct term of the first mode (dash–double-dotted cyan line) and another symmetrically mixed term (double-dashed orange line). In the latter two cases, the absorbed energy is two times that of the direct terms with minimal photon number. Therefore, the kinetic energy of the created particles is larger and they are emitted under a smaller angle.

The description so far also applies to $(1, 3)$, the laser pair with next-higher differing minimal photon numbers, as shown in Fig. 3.1(b). However, the third largest contribution, the symmetrically mixed term taking one photon from each

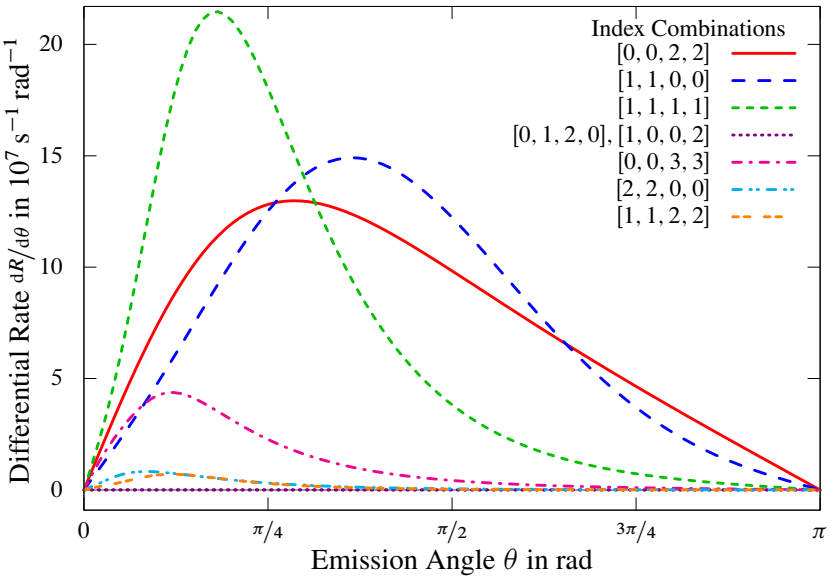

(a) Laser pair $(1, 2)$ with $\xi_1 = 1.06{\times}10^{-2}$ and $\xi_2 = 0.1$

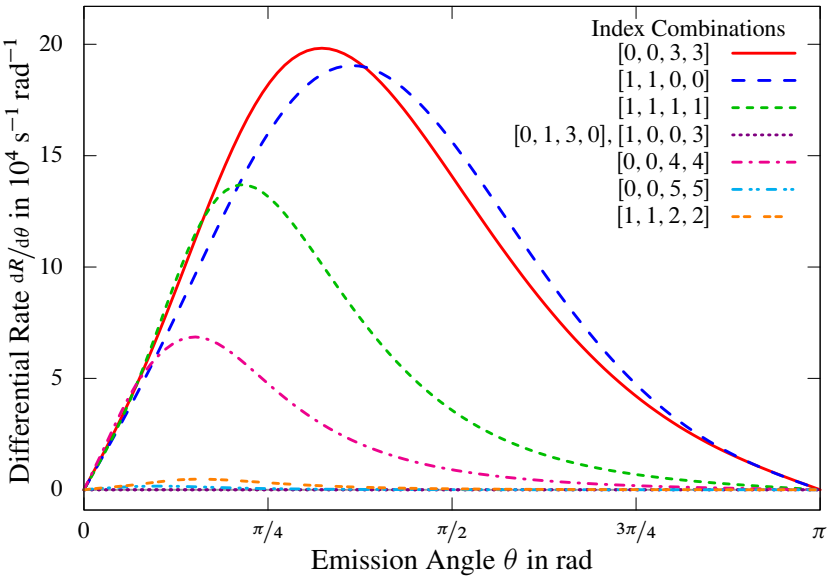

(b) Laser pair $(1, 3)$ with $\xi_1 = 3.59{\times}10^{-4}$ and $\xi_2 = 0.1$

Figure 3.1.: *Angular-differential partial rates for laser pairs* $(1, 2)$ *and* $(1, 3)$ *with total photon energy* 1.1 MeV *in the nuclear rest frame – The emission angle* θ *is measured with respect to the laser propagation direction. The frequencies are chosen such that the total photon energy is reached for* $\tilde{n}_1$ *photons from the first mode and* $\tilde{n}_2$ *photons from the second mode. The intensity parameter* ξ_1 *has been adjusted to maintain equally contributing direct terms. The relative phase is set as* $\varphi = 0$*. Both laser pairs show no significant contribution from an interference term.*

mode (short-dashed green line), shows a considerable difference: It is dominant in the first example and less pronounced in the second. Due to its higher order in ζ compared to the direct term with one photon from the first mode, this term would be expected to be suppressed in both cases. An explanation may be that the total photon energy of 1.1 MeV is just above the pair-creation threshold. It is known that the pair-creation rate vanishes at the threshold [100]. A term with total photon energy farther away from the threshold, here 1.65 MeV, has access to a substantially larger phase space for the emitted electron-positron pair. This may compensate the aforementioned suppression, however only if the intensities are not too small as the suppression gets stronger with decreasing ζ.

In these two examples interference terms (dotted violet lines) do not contribute significantly to the total rates. This will be remedied in the following. Halving the individual frequencies used in the above examples, leads to the laser pairs with doubled minimal photon numbers, $(2, 4)$ and $(2, 6)$, as depicted in Fig. 3.2. For these two laser pairs significant contribution from interference is visible. For the chosen relative phase $\varphi = 0$ this contribution is destructive for laser pair $(2, 4)$, i.e., it leads to a decreased summed-up rate, or constructive for $(2, 6)$, i.e., leads to an increased summed-up rate.

The symmetrically mixed terms expectedly contribute approximately as strong as the direct terms because they are of the same order in ζ. Instead of taking all energy from a single mode, one half is taken from the first mode, the other half from the second mode. Note that, for these two cases intensities smaller than in the examples before are used. Therefore, contributions of higher orders in ζ are negligible.

Concluding this section, a comparison to previous work on pair creation by a highly energetic photon [110] shall be made. There, interference effects were found to be strongest for a frequency ratio of 3. In the results presented here, the laser pair with the smallest photon number for this ratio, $(1, 3)$, does not show a contribution from interference terms. However, a strong contribution for the combination $(2, 6)$ is visible. Furthermore, laser pair $(2, 4)$ shows the strongest absolute contribution from an interference term, while no contribution is found for combination $(1, 2)$, with lower photon number and identical frequency ratio. These differences to the aforementioned study may be attributed to the differing laser geometries, as in Ref. [110] parallel field vectors were considered. In summary, one may note that in the results presented here interference seems to arise only when both minimal photon numbers $\tilde{n}_i$ are even.

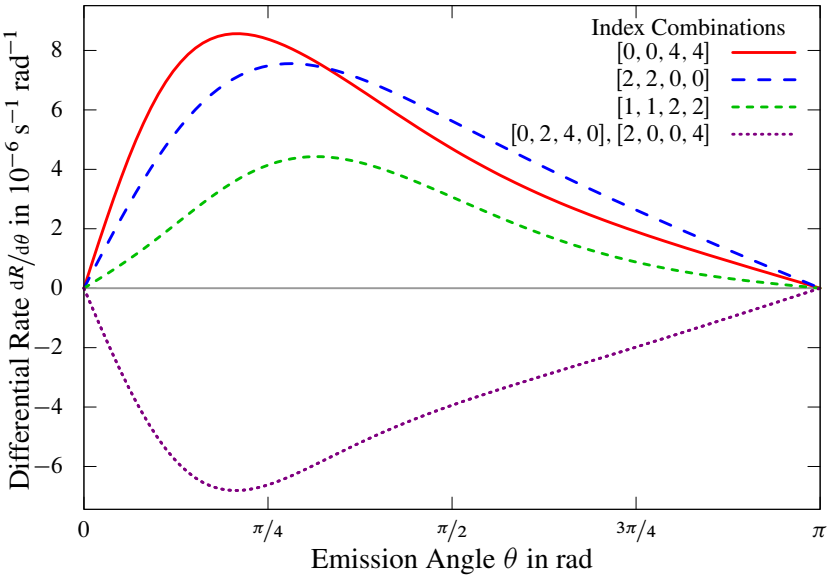

(a) Laser pair $(2, 4)$ with $\xi_1 = 4.62{\times}10^{-5}$ and $\xi_2 = 0.01$

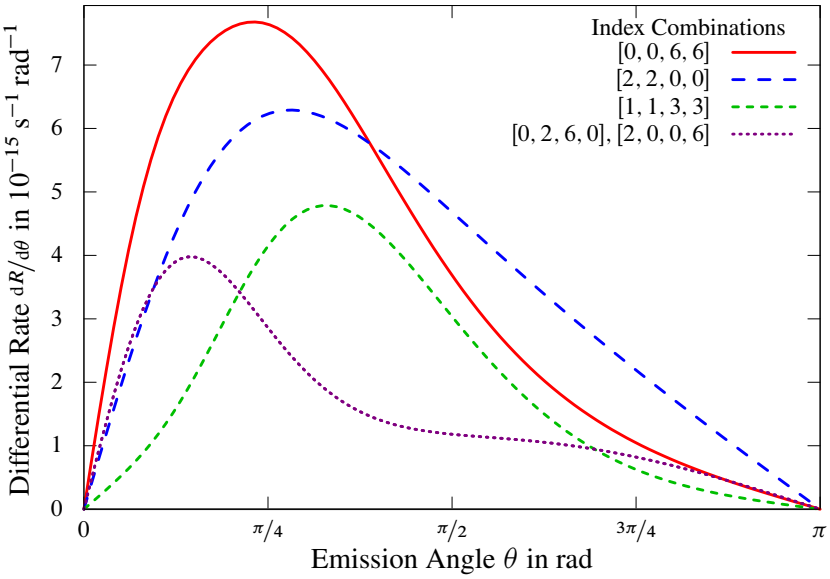

(b) Laser pair $(2, 6)$ with $\xi_1 = 2.48{\times}10^{-7}$ and $\xi_2 = 0.01$

Figure 3.2.: *Angular-differential partial rates for laser pairs* $(2, 4)$ *and* $(2, 6)$ *with total photon energy* 1.1 MeV *in the nuclear rest frame – If not indicated otherwise, the parameters are the same as in Fig.* 3.1. *These two laser pairs show a large contribution from interference terms. For the relative phase* φ *set to zero, the interference is destructive for* $(2, 4)$ *and constructive for* $(2, 6)$.

3.1.2. Variation of the Total Photon Energy in the Nuclear Rest Frame

In the previous section, laser pair $(2, 4)$ has shown the strongest absolute contribution from interference. Hence, it shall be used to investigate the influence of the variation of the total photon energy. In Fig. 3.3, the angular-differential partial rates are shown for laser pair $(2, 4)$ with total photon energies of 1.25 and 1.35 MeV. One finds that for all terms, a larger energy leads to a narrower distribution shifted to the lower part of the angular spectrum. The interference terms (violet dotted line) also show clear changes in their shape. In the 1.25 MeV case, the absolute value of the rate tends to zero for angles above 45°. For 1.35 MeV the distribution shows a zero crossing and, thus, the terms decrease the summed-up differential rate for smaller angles and increase for larger.

Besides these strong modifications for the interference terms, the relative contribution of the symmetrically mixed term (short-dashed green line) grows with rising total photon energy. It changes from the smallest non-negligible term in Fig. 3.2(a) to the dominant term in Fig. 3.3(b).

For even higher total photon energies, particularly from 1.363 MeV onwards, a new direct reaction channel, $[0, 0, 3, 3]$, opens as already three photons from the second mode are enough to create the e^-e^+ pair. This channel even dominates the total rate from 1.375 MeV onwards. This is, however, not representing laser pair $(2, 4)$ anymore, but rather $(2, 3)$. Therefore, it is not of interest for the present investigation and 1.35 MeV is the highest depicted total photon energy.

So far one can conclude that the interference is more pronounced close to the pair-creation threshold. However, the change in their curve shape for higher energies might lead to interesting effects. A direct result from the modified shape is shown in the subsequent Sec. 3.1.3 in which the influence of the relative phase is discussed.

Furthermore, the strong differences of the angular dependence of the interference terms compared to the other terms may be explained qualitatively. As discussed in Sec. 2.3.2, the interference terms are sensitive to the relative phase between both laser modes. Variations of this phase change the total field vector of the laser, leading to redistribution of the emission angles, into which the created particles are ejected. Some angular regions might become more probable, whereas others become less probable. This redistribution manifests itself in the angular dependence of the interference terms. Similar conclusions have been drawn regarding other strong-field processes, such as the two-colour multiphoton ionization of atoms [125, 138, 148].

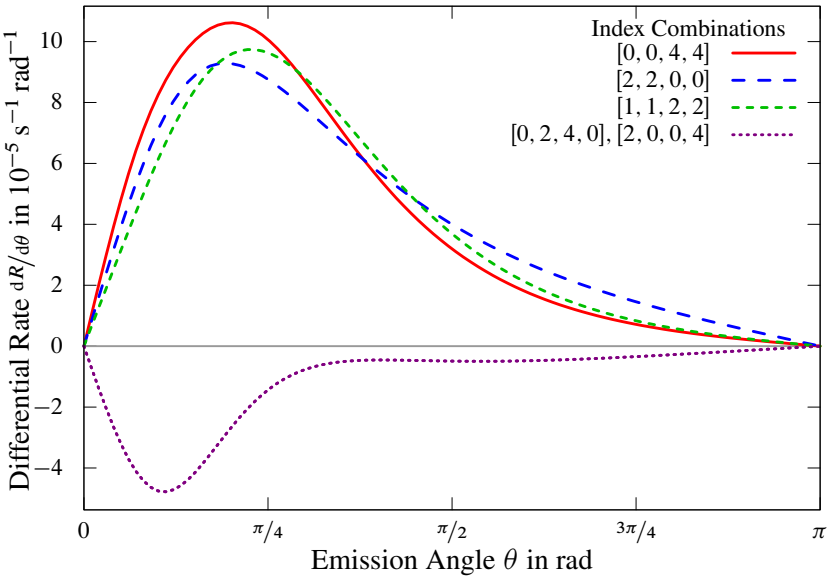

(a) Total photon energy 1.25 MeV, $\xi_1 = 5.07\times10^{-5}$, $\xi_2 = 0.01$

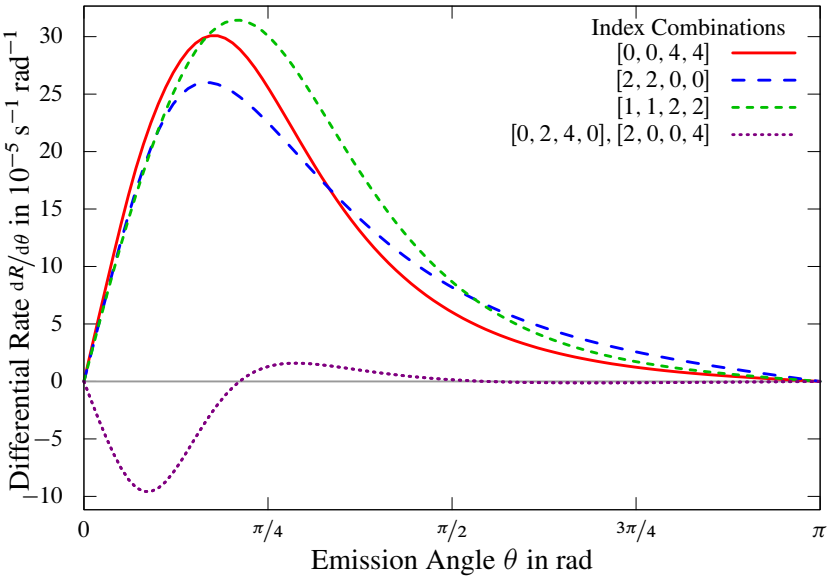

(b) Total photon energy 1.35 MeV, $\xi_1 = 5.38\times10^{-5}$, $\xi_2 = 0.01$

Figure 3.3.: *Variation of the total photon energy of the angular-differential partial rates for laser pair* $(2, 4)$ *– As the total photon energy increases, the relative contribution from interference decreases. Additionally, the shape of the interference terms changes, leading to the zero crossing in Fig.* 3.3(b).

3.1.3. Variation of the Relative Phase in the Nuclear Rest Frame

As discussed in Sec. 2.3, for terms with $n_i = n_i'$ the phase factor from Eq. (2.47) becomes unity. Therefore, only the interference terms are influenced by changes to the relative phase[12] between the two laser modes φ.

In this section, laser pair $(2, 4)$ is further studied by means of Fig. 3.4, where Fig. 3.4(a) treats an energy of 1.1 MeV, just above the threshold of $2m_*c^2$, and Fig. 3.4(b) treats 1.35 MeV, just below the energy at which the additional reaction channel opens, as discussed in the section before. The parameters are the same as in Fig. 3.2(a) and Fig. 3.3(b), respectively, except for the relative phase, which is set as $\varphi = \pi/2$. This leads to a changed sign for the interference terms, which thus become constructive.

In order to study how strong interference effects manifest themself in the sum of all terms (dash-dotted magenta line), it is useful to introduce a few sub-sums of the sum in Eq. (2.45) and compare them to the individual terms. The sum of the direct terms $[0, 0, 4, 4]$ and $[2, 2, 0, 0]$ (dash–double-dotted cyan line) shows the contribution from the two laser modes when their interaction is ignored or conversely how much their interaction enhances the pair-creation rate. The sum of the phase-independent contributions (double-dashed orange line), which are the direct terms and the symmetrically mixed term $[1, 1, 2, 2]$, shows how much change may be expected from the phase-dependent counterparts. These are shown in the sum of the two interference terms, $[0, 2, 4, 0]$ and $[2, 0, 0, 4]$ (double-dash–dotted yellow line).

The comparison shows that for the lower total photon energy (1.1 MeV), the sum of the direct terms amounts to about 50% of the summed-up rate, the symmetrically mixed term adds up to about 10%, and the sum of the interference terms contributes about 40%. For the higher energy (1.35 MeV), the interference terms are less pronounced, yielding only about 10%, with the phase-independent terms giving the other 90% (which consists of three similar shares stemming from the two direct terms and the symmetrically mixed term). This further strengthens the conclusion from Sec. 3.1.2 that the interference is more pronounced close to the pair-creation threshold.

However, the two total photon energies allow the illustration of the two distinct effects arising from changes to the relative phase by means of Fig. 3.5. There the sum of all terms (top panels) and the sum of the interference terms (bottom panels) is shown for several values for the relative phase. Additionally, the sum

[12] Recall that the second relative phase from Eq. (2.5) has been dropped, as – without loss of generality – a single relative phase is sufficient.

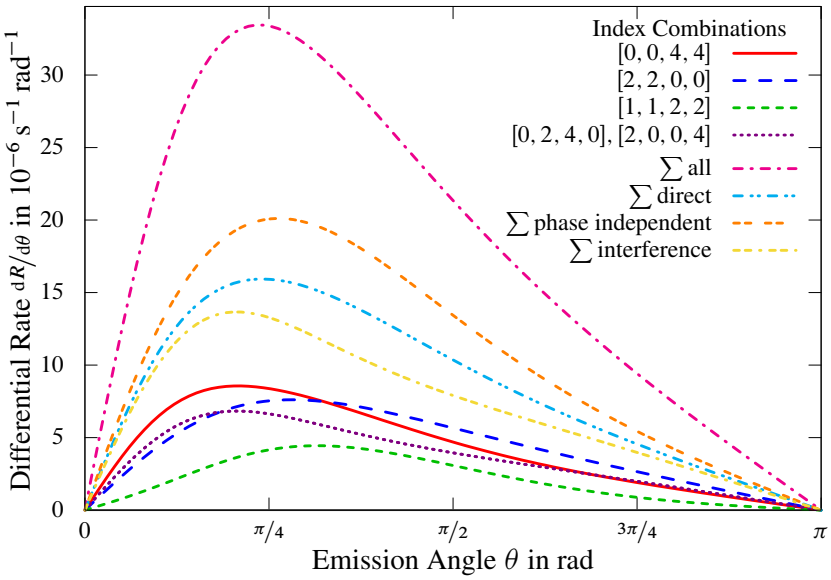

(a) Total photon energy of 1.1 MeV

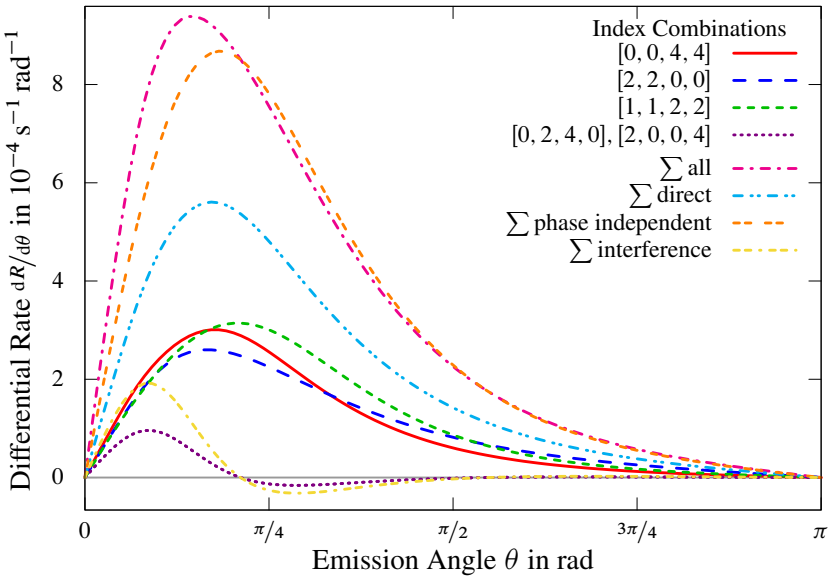

(b) Total photon energy of 1.35 MeV

Figure 3.4.: *Individual terms and several sub-sums of the angular-differential partial rates of laser pair* $(2, 4)$ *for two total photon energies – Here "*$\sum$ *all" is the sum of all individual terms, "*$\sum$ *direct" is the sum of the two terms stemming solely from the first or the second laser mode, "*$\sum$ *phase independent" is the latter plus the symmetrically mixed term, and "*$\sum$ *interference" is the sum of the two interference terms. The relative phase is set as* $\varphi = \pi/2$*. Otherwise the parameters are the same as in Fig.* 3.2(a) *and Fig.* 3.3(b)*, respectively.*

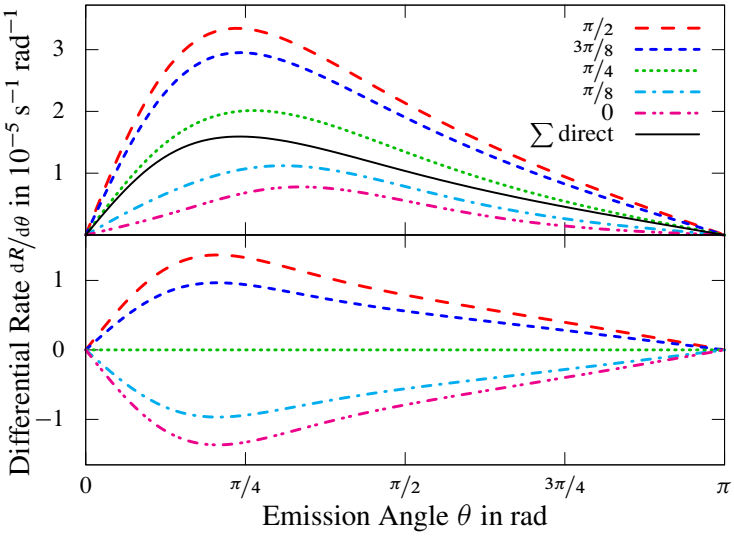

(a) Total photon energy of 1.1 MeV

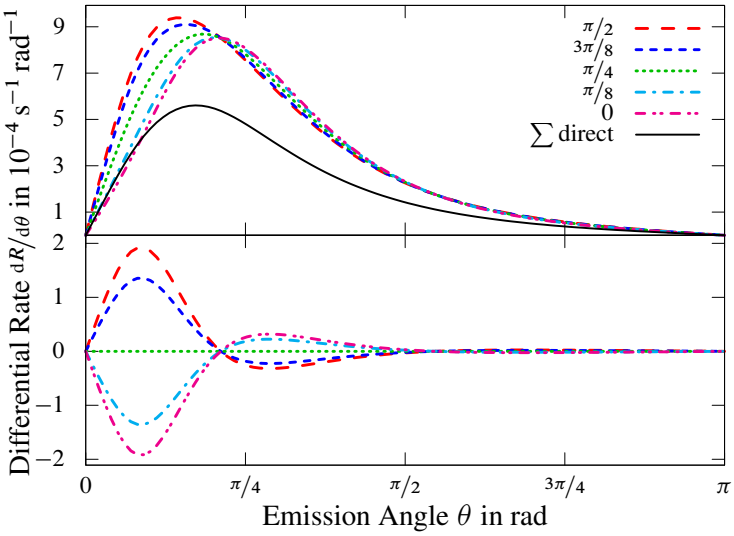

(b) Total photon energy of 1.35 MeV

Figure 3.5.: *Phase variation in the sums of all terms (top panels) and the interference contributions (bottom panels) of the angular-differential partial rates of laser pair* $(2, 4)$ *for two total photon energies – The sum of the direct terms as in Fig.* 3.4 *is given as a strength reference. For laser pair* $(2, 4)$*, the interference contribution is maximal (maximally constructive) for the relative phase* $\varphi = \pi/2$*, is minimal (maximally destructive) for* $\varphi = 0$*, and vanishes for* $\varphi = \pi/4$*. Otherwise the parameters are the same as in Fig.* 3.2(a) *and Fig.* 3.3(b)*, respectively.*

of the direct terms is given as a height reference in the top panels. For the lower energy, one finds a factor of roughly 5 between the height of the distribution for $\varphi = 0$ and $\pi/2$. This factor carries over to the result of the angular integration, which means that tuning the relative phase gives – to some extend – direct control over the total pair-creation rate. In particular, rates larger and smaller than the sum of the direct terms may be achieved. Additionally, a shift of the peak position from below to above $\pi/4$ occurs. This second effect is even better visible for the higher energy, as there the influence on the height is rather small and the aforementioned zero crossing pronounces the angular shift. Thinking about an experimental application, this may allow to steer the direction of the peak emission of the e^-e^+ pairs.

Furthermore, one finds that for laser pair $(2, 4)$ the interference terms show a sinusoidal behaviour in the relative phase φ with a periodicity of $2\pi/\tilde{n}_1 = \pi$: For vanishing φ their contribution is maximally destructive and for $\varphi = \pi/2$ it is maximally constructive. Any phase in between will lead to a decrease in the absolute interference contribution, with $\varphi = \pi/4$ removing it completely.

It should be stressed again that the choice of which relative phase to use is arbitrary. The observation for a varied φ_2 would be the same and a periodicity of $2\pi/\tilde{n}_2$ would be found. This result depends on the laser wave frequency and thus on the respective minimal number of photons $\tilde{n}_i$. For a more intuitive picture, the general periodicity

$$\Phi_i = 2\pi/\tilde{n}_i \tag{3.3}$$

may be connected to the electric fields associated with the laser waves A_i given in Eq. (2.5):

$$\mathbf{E}_i = -\frac{1}{c}\frac{\partial \mathbf{A}_i}{\partial t} = \frac{\mathbf{a}_i \omega_i}{c} \sin(\eta_i + \varphi_i) \quad (i = 1 \text{ or } 2)\,. \tag{3.4}$$

Due to the perpendicular laser-wave field-vectors $\mathbf{a}_i$, the square of the total electric field $\mathbf{E} = \mathbf{E}_1 + \mathbf{E}_2$ has the form

$$\mathscr{E}^2 = \sum_{i=1}^{2} \mathscr{E}_i^2 = \sum_{i=1}^{2} \frac{\mathbf{a}_i^2 \omega_i^2}{c^2} \sin^2(\eta_i + \varphi_i), \tag{3.5}$$

with $\mathscr{E}_{(i)} = |\mathbf{E}_{(i)}|$. From this, one can gain a measure for the phase dependence by normalizing the amplitudes

$$F^2 = \sum_{i=1}^{2} \frac{c^2}{\mathbf{a}_i^2 \omega_i^2} \mathscr{E}_i^2 = \sum_{i=1}^{2} \sin^2(\eta_i + \varphi_i), \tag{3.6}$$

and taking the modulus of the hence defined F. In Fig. 3.6, its maximum absolute value $\max(|F|)$ as a function of φ is compared to the total pair-creation rate

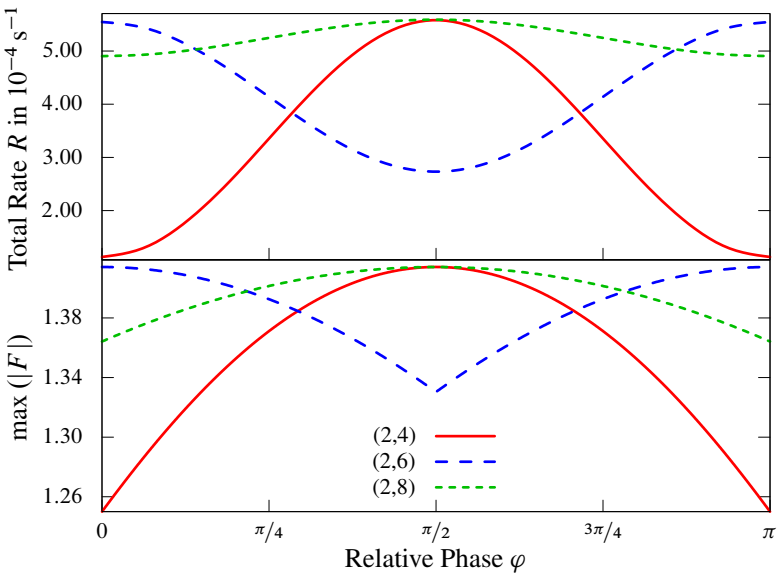

Figure 3.6.: *Comparison of the phase variation of the total pair-creation rates (top panel) and the measure derived from the combined electric field (bottom panel) for several laser pair combinations – Line types and colours are identical for both panels. As before a single relative phase φ is used. To achieve better comparability the total rates have been scaled by a factor of 1.45×10^{9} for laser pair $(2,6)$ and by 1.35×10^{18} for $(2,8)$. The measure is defined by the absolute maximum of the sum of the normalized electric fields from Eq. (3.6). The three laser pairs show qualitatively the same phase dependence in both panels.*

for laser pairs $(2,4)$, $(2,6)$, and $(2,8)$. The three laser pairs show an identical periodicity in both panels, which allows the conclusion that the phase dependence of the total rate is directly retained from the electric fields of the input laser waves. This may be contrasted with the finding that interference patterns in the spectra of created particles are connected to the phase dependence of the vector potential, as has been shown in an earlier study [86].

The connection between the phase dependence of the total pair-creation rate and that of the electric field in form of the parameter $\max(|F|)$ holds even when the contributing terms show a more complex structure. For all cases discussed so far, the interference terms had the form $[0,\tilde{n}_1,\tilde{n}_2,0]$ or $[\tilde{n}_1,0,0,\tilde{n}_2]$. However, as the only restriction on the occurring combinations of the four indices is imposed by Eq. (2.49a), terms with all indices differing from zero are possible. This may be demonstrated by means of laser pair $(4,8)$, which has the same frequency ratio as $(1,2)$ and $(2,4)$ before, but more photons are involved. Therefore, a

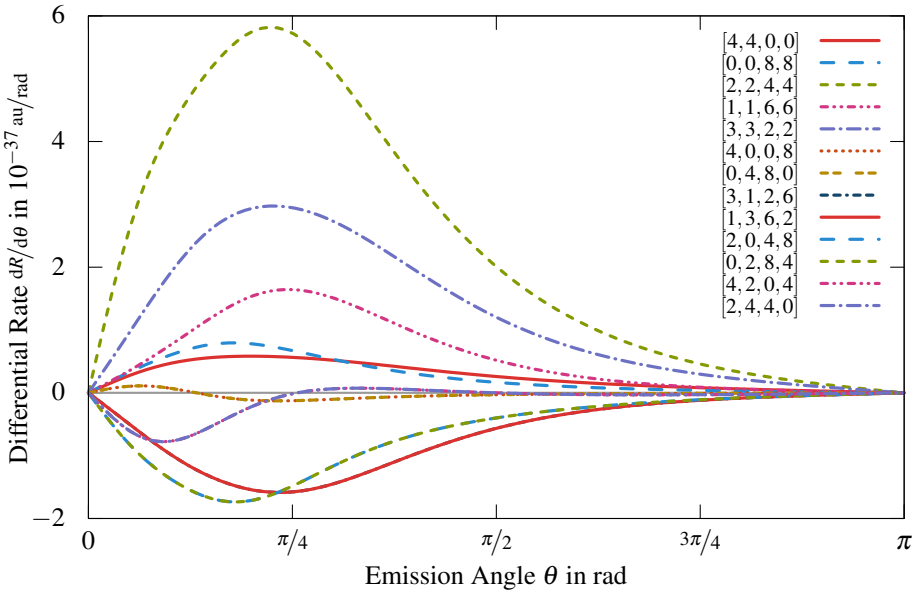

Figure 3.7.: *Angular-differential partial rates for laser pair* $(4, 8)$ *with total photon energy* 1.15 MeV *in the nuclear rest frame – The relative phase is set as* $\varphi = 0$ *and the intensity parameters as* $\xi_1 = 10^{-4}$ *and* $\xi_2 = 1.31{\times}10^{-2}$

larger set of terms contributes, as can be seen in Fig. 3.7.

Analogous to for instance Fig. 3.2(a), two direct terms, $[4, 4, 0, 0]$ and $[0, 0, 8, 8]$, taking the minimal number of photons from the individual modes are visible, as well as a symmetrically mixed term, $[2, 2, 4, 4]$, taking half the energy from each mode. However, two additional symmetrically mixed terms occur, $[1, 1, 6, 6]$ and $[3, 3, 2, 2]$, differing in how much energy is absorbed from the individual modes. The main difference between laser pair $(4, 8)$ and the earlier examples is the relative strength of the individual terms. Before, the direct terms where dominant (or at least among the dominant), while here they are much smaller than all the symmetrically mixed terms.

It is convenient to classify the terms by the sum of the indices of each mode, $n_i + n'_i$. This has been done in Tab. 3.1 together with the two parts of the exponent from Eq. (2.73), which is 64 for all cases. Therefore, all occurring terms are of the same order in ζ, despite the differing $n_i + n'_i$. However, small differences in the contribution strengths remain due to the different prefactors contained in each term (cf. Sec. 2.3.3 and Eq. (2.74), therein). Anyway, one would expect all terms to be similarly strong, which is not the case. Note that, the same line of argument is true for laser pair $(2, 4)$, where indeed all terms are of roughly equal strength.

Terms	$n_1 + n_1'$	$n_2 + n_2'$	$\tilde{n}_2(n_1 + n_1')$	$\tilde{n}_1(n_2 + n_2')$
$[0, 0, 8, 8]$	0	16	0	64
$[1, 1, 6, 6]$, $[0, 2, 8, 4]$, $[2, 0, 4, 8]$	2	12	16	48
$[2, 2, 4, 4]$, $[0, 4, 8, 0]$, $[4, 0, 0, 8]$ $[1, 3, 6, 2]$, $[3, 1, 2, 6]$	4	8	32	32
$[3, 3, 2, 2]$ $[2, 4, 4, 0]$, $[4, 2, 0, 4]$	6	4	48	16
$[4, 4, 0, 0]$	8	0	64	0

Table 3.1.: *Classification of the terms from laser pair* $(4, 8)$ *by means of the sum of the indices of each mode – Additionally, the two parts of the exponent in Eq.* (2.73) *are shown. Note that, the full exponent, i.e., the sum of the last two columns, is identical for all terms.*

Due to the classification in Tab. 3.1, the interference terms may be grouped with symmetrically mixed terms with the same $n_i + n_i'$. One notices that $[1, 1, 6, 6]$ is the weakest symmetrically mixed term, while the corresponding $[0, 2, 8, 4]$ and $[2, 0, 4, 8]$ show the strongest absolute contribution from an interference term. Conversely, the interference terms $[0, 4, 8, 0]$ and $[4, 0, 0, 8]$ show the smallest non-negligible contribution, even though the corresponding $[2, 2, 4, 4]$ is the overall strongest term.

With all terms introduced, the discussion of an analogue to Fig. 3.6 for laser pair $(4, 8)$ shall conclude this section. As can be seen in Fig. 3.8, here too, the parameter $\max(|F|)$ exhibits qualitatively the same phase dependence as the total pair-creation rate. Additionally, the phase dependence of the individual interference terms is depicted in Fig. 3.8(c), where one finds that the periodicity of the weakest terms $[4, 0, 0, 8]$ and $[0, 4, 8, 0]$ differs from that of the others. For laser pair $(2, 4)$, a periodicity of $2\pi/\tilde{n}_i$ has been found (cf. Eq. (3.3)). However, from the analytical calculation, particularly from Eq. (2.47), a more general expression for the periodicity may be extracted

$$\Phi_i = 2\pi/\Delta n_i \tag{3.7}$$

using the difference of the indices of the respective laser mode i: $\Delta n_i = |n_i - n_i'|$. The six stronger terms share $\Delta n_1 = 2$ and accordingly they all exhibit the same periodicity $\Phi_1 = \pi$, which is also the periodicity of $\max(|F|)$. In contrast, the

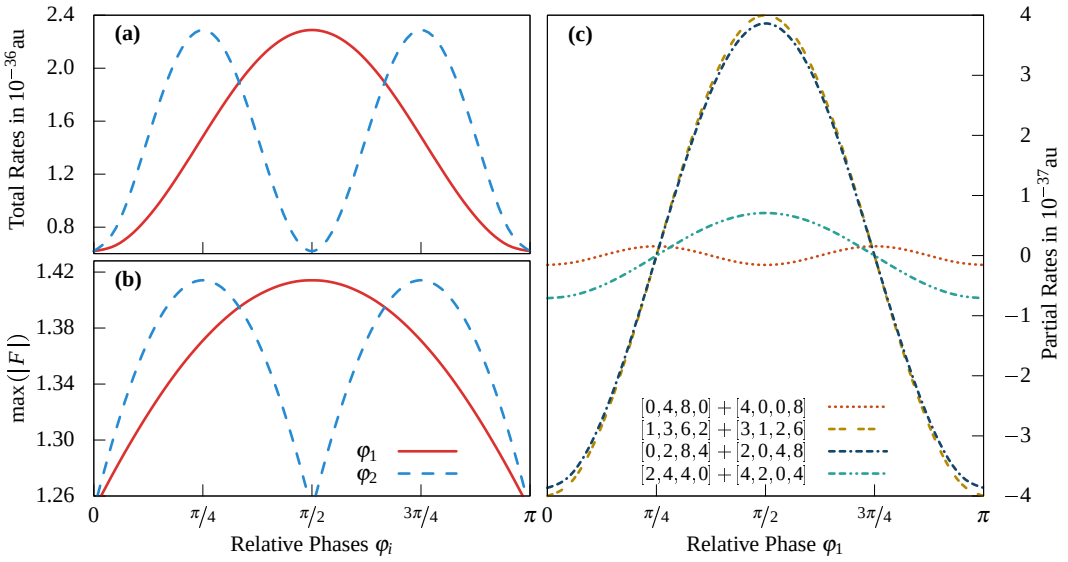

Figure 3.8.: *Variation of both relative phases φ_i for laser pair $(4, 8)$ – Parameters as in Fig. 3.7. Comparison of* (a) *the total pair-creation rate and* (b) *the measure defined via the absolute maximum of the sum of the normalized electric fields from Eq.* (3.6) *shows qualitatively the same phase dependence. Additionally, in* (c) *the relevant partial rates of the interference terms are shown for a variation of φ_1. Note the different periodicity of the terms $[4, 0, 0, 8]$ and $[0, 4, 8, 0]$.*

phase dependence of the weakest terms $[4, 0, 0, 8]$ and $[0, 4, 8, 0]$ corresponds to $\Phi_1 = \pi/2$, in accordance with $\Delta n_1 = 4$.

Thus, for laser pair $(4, 8)$, the interference terms that exhibit a different phase dependence than $\max(|F|)$ are contributing only marginally, while all strong interference terms share the periodicity of this parameter. Therefore, the periodicity is retained by the sum of all terms and, eventually, by the total rate. For laser pair $(2, 4)$, the situation is simpler as all significantly contributing interference terms satisfy $\Delta n_i = \tilde{n}_i$, in agreement with Eq. (3.3).

3.1.4. Variation of the Relative Phase in the Laboratory Frame

So far results found in the nuclear rest frame have been presented. For a comparison to a potential experimental application these results have to be transformed to the laboratory frame. As in the previous section, laser pair

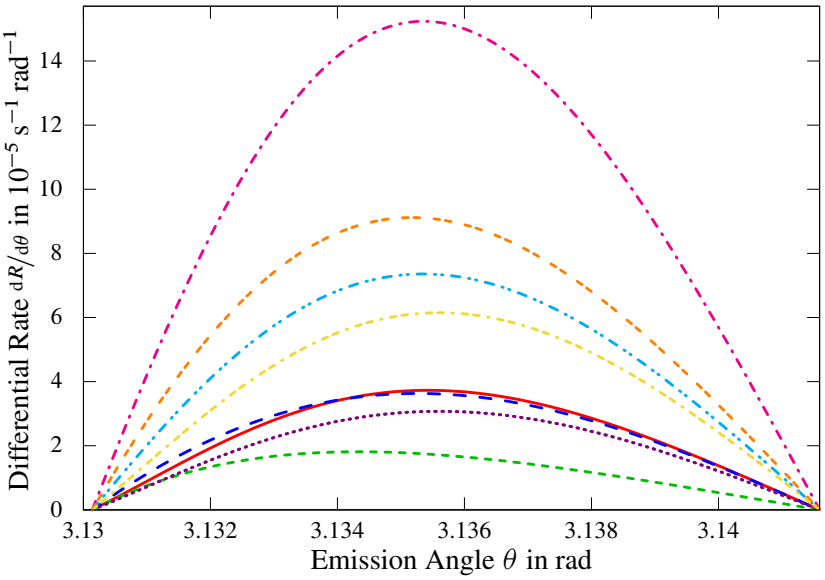

(a) Total photon energy (in nuclear rest frame) of 1.1 MeV

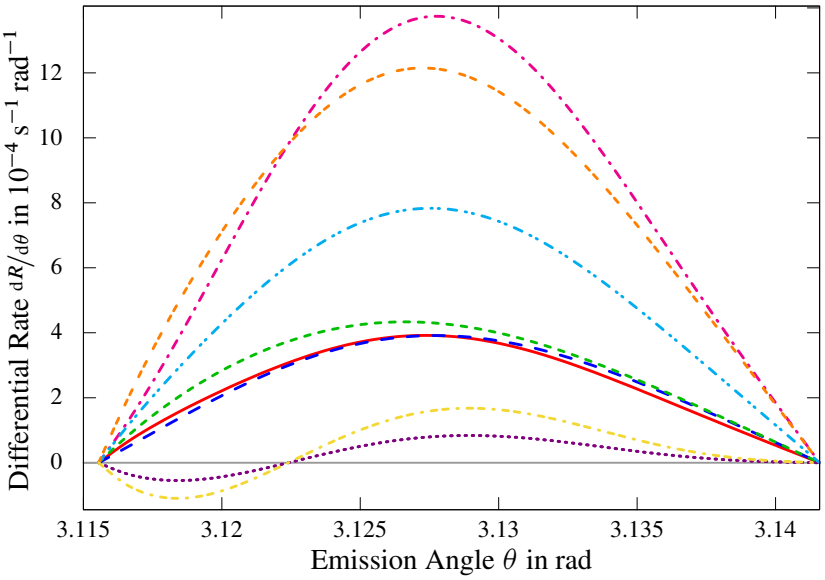

(b) Total photon energy (in nuclear rest frame) of 1.35 MeV

Figure 3.9.: *Individual terms and several sub-sums of the angular-differential partial rates of laser pair* $(2, 4)$ *for two photon energies in the laboratory frame – The Lorentz factor is set as* $\gamma = 50$*. Notation, legend, and parameters are identical to those in Fig.* 3.4.

$(2, 4)$ is studied with total photon energies of 1.1 and 1.35 MeV in the nuclear rest frame. To reach these energies, the energies supplied in the laboratory frame may be much smaller depending on the Lorentz factor γ of the nucleus. Particularly, in the nuclear rest frame the laser frequencies from the laboratory frame experience a boost:

$$\begin{aligned} \omega_i &= (1+\beta)\,\gamma\,\omega_i^{\mathrm{lab}} \\ &\approx 2\gamma\,\omega_i^{\mathrm{lab}}, \end{aligned} \tag{3.8}$$

wherein $\beta = \sqrt{1 - 1/\gamma^2} \approx 1$ for all subsequently discussed cases. The boost factor follows from the Lorentz transformation along the z-axis of an energy

$$E = \gamma \left(E^{\mathrm{lab}} + \beta p_z^{\mathrm{lab}} c \right). \tag{3.9}$$

For a photon, energy E and momentum p are given by its frequency ω. In particular, if the photon propagates along the z-axis and, thus, the absolute momentum is identical to its z-component, $p = p_z$, they are given by

$$E = p_z c = \hbar\omega. \tag{3.10}$$

It follows that $E = \gamma\,(1+\beta)\,E^{\mathrm{lab}}$, which corresponds to Eq. (3.8). Note further that, $\beta > 0.9$ is already true for $\gamma > 2.3$, just as $\beta > 0.99$ for $\gamma > 7.1$, and $\beta > 0.999$ for $\gamma > 22.4$.

The following results are obtained for $\gamma = 50$. For a total photon energy in the nuclear rest frame of 1.1 MeV this corresponds to the laboratory frequencies

$$\omega_1^{\mathrm{lab}} = 5.50\,\mathrm{keV} \quad \text{and} \quad \omega_2^{\mathrm{lab}} = 2.75\,\mathrm{keV}, \tag{3.11}$$

and for 1.35 MeV to

$$\omega_1^{\mathrm{lab}} = 6.75\,\mathrm{keV} \quad \text{and} \quad \omega_2^{\mathrm{lab}} = 3.38\,\mathrm{keV}. \tag{3.12}$$

Figure 3.9 shows the Lorentz-transformed version of Fig. 3.4. The main differences are the width and the peak position of the distribution. Note that, the emission angles shown in these two figures are only in a very small range just below 180°. This means that, the created particles are emitted in propagation direction of the nucleus, which is preferential due to the Lorentz boost. Furthermore, the shape of the individual graphs differs from the nuclear rest frame. In particular, here the two direct terms almost perfectly overlap each other, while they exhibit a crossing at $\theta \approx 1$ in the nuclear rest frame. Left of this crossing the direct term of the second mode is larger, and right of it that of the first mode dominates. The interference term for the higher energy shows a more balanced ratio of negative and positive amplitude. In the nuclear rest frame, the absolute contribution from

angles $\theta \lesssim 0.66$ is much stronger than for larger angles, while in the laboratory frame the positive and the negative part are of similar absolute height. It is also worth pointing out that in Fig. 3.4(b) the positive contribution came from small angles ($< 45°$). Due to the Lorentz boost, the small angles in the nuclear rest frame are mapped to large angles in the laboratory frame and vice versa. Therefore, the graph seems inverted in Fig. 3.9(b).

The Lorentz-transformed version of the phase variation from Fig. 3.5 is shown in Fig. 3.10. The peak height and position shift is again visible, although here, due to the aforementioned contraction of the spectrum, the latter is over a much smaller angular range. The inversion of the positive and negative contribution discussed above is mirrored in the peak position shift. In the nuclear rest frame, the shift is towards smaller emission angles for a growing relative phase φ, while this direction is reversed in the laboratory frame.

In conclusion, it should be recalled that throughout this section $\gamma = 50$ was used. However, the results for a different γ may be inferred from the presented figures, as long as the laser frequencies in the laboratory are adjusted so that the total photon energy in the nuclear rest frame stays the same. The form of the angular distribution is practically identical to that in the figures above, if γ is large enough. This is already the case for values as small as about 2. The difference would only be in the kinematically allowed range of emission angles. For higher γ, this range gets even more narrowed to the right of the spectrum, shifting the peak position even further towards 180°. For an appropriately high γ, which means larger than about 5, the width of the allowed θ-range shows a scaling of $\sim 1/\gamma$.

3.2. Monochromatic Laser Wave of Elliptical Polarization

As introduced in Sec. 2.2, particularly by means of the parameter set given in Eq. (2.62), a vector potential of the form given in Eq. (2.5) can also describe a monochromatic laser wave of arbitrary ellipticity. The study of total pair-creation rates as a function of this ellipticity presented in this section is part of the publication Ref. [13]. As $\omega_1 = \omega_2$, this represents a special case of commensurable frequencies with a ratio of 1. In the notation introduced in Sec. 2.3, this kind of set-up corresponds to laser pairs of the form $(\tilde{n}, \tilde{n})$.

The ellipticity may be adjusted in two different ways, both starting from a circularly polarized wave with $|\mathbf{a}_1| = |\mathbf{a}_2|$, $\varphi_1 = \pi/2$, and $\varphi_2 = 0$: On the one

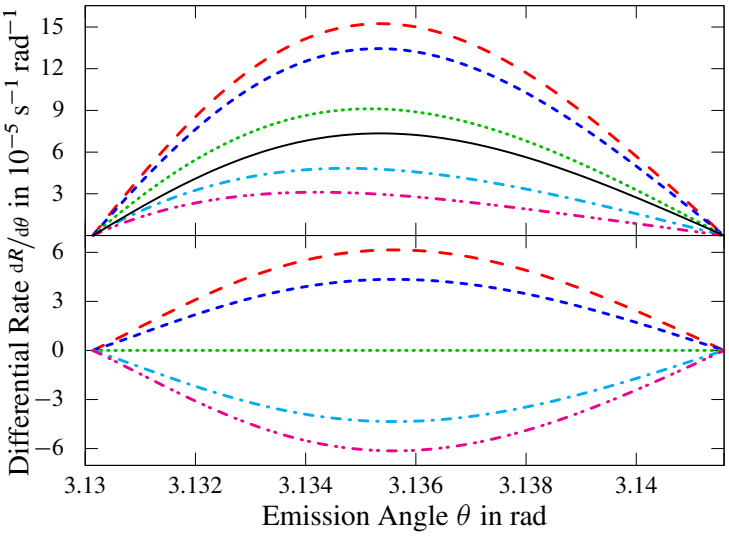

(a) Total photon energy (in nuclear rest frame) of 1.1 MeV

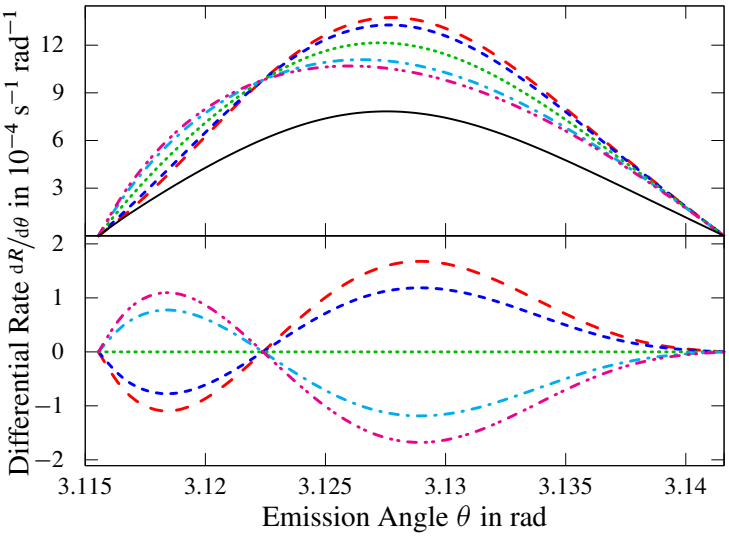

(b) Total photon energy (in nuclear rest frame) of 1.35 MeV

Figure 3.10.: *Phase variation in the sums of all terms (top panels) and the interference contributions (bottom panels) of the angular-differential partial rates of laser pair* $(2, 4)$ *for two total photon energies in the laboratory frame – The sum of the direct terms as in Fig.* 3.9 *is given as a strength reference. The Lorentz factor is set as* $\gamma = 50$*. Notation, legend, and parameters are identical to those in Fig.* 3.5.

hand, one can fix the maximum amplitude of the laser field by keeping one intensity constant and decreasing the other until it disappears, e.g,

$$\begin{aligned} \xi_1 &= \text{const.}, \\ 0 \leq \xi_2 &\leq \xi_1. \end{aligned} \tag{3.13}$$

On the other hand, one can fix the total intensity supplied to the system by decreasing one intensity while increasing the other, such that

$$I_{\text{tot}} = \xi_1^2 + \xi_2^2 = \text{const.} \tag{3.14}$$

In both cases, the ellipticity will be measured using the parameter

$$\varepsilon = \frac{|\xi_1^2 - \xi_2^2|}{\xi_1^2 + \xi_2^2} = \begin{cases} 0 & \text{for circular polarization} \\ 0 < \varepsilon < 1 & \text{for elliptical polarization} \\ 1 & \text{for linear polarization,} \end{cases} \tag{3.15}$$

which can be rewritten for the case of a fixed total intensity as

$$\varepsilon = \frac{2}{I_{\text{tot}}}\xi_1^2 - 1 = 1 - \frac{2}{I_{\text{tot}}}\xi_2^2. \tag{3.16}$$

Additionally, a third pathway has already been mentioned in Sec. 2.2 in form of the parameter set in Eq. (2.63). In this set-up, where $|\mathbf{a}_1| = |\mathbf{a}_2| = \text{const.}$, the relative phase is varied instead of the intensity parameters. However, it can be shown that this pathway corresponds[13] directly to the above case of a fixed total intensity, which is interesting because φ_i and ξ_i are independent parameters. For the variation of φ_i, the ellipticity is then given by

$$\varepsilon = |\cos \varphi_i| \,. \tag{3.17}$$

In Fig. 3.11(a), the two pathways are compared for $\tilde{n} = 2$ photons absorbed from the wave, i.e., laser pair $(2, 2)$, with a total photon energy of 1.8 MeV. For the first case of a constant maximum laser wave amplitude (bottom panel), the total pair-production rate decreases when the transition from circular to linear polarization (i.e., from left to right) is made. This can be intuitively explained by the decrease in the supplied total laser intensity as the second laser mode is gradually turned off. For the second case of a constant total intensity (top panel), the total pair-production rate increases for the same transition instead. This can be understood by means of the peak amplitude of the combined laser

[13] There is a small difference in the direction of the polarization axis, which would be rotated around the laser propagation direction by 45°. This, however, does not influence the results presented here.

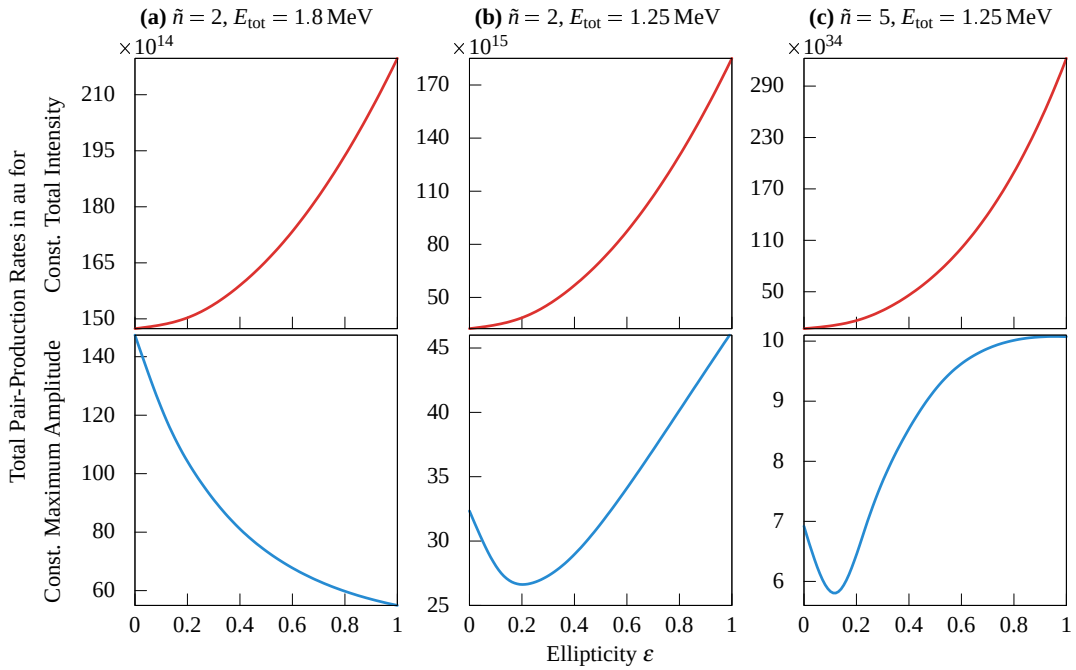

Figure 3.11.: *Variation of the ellipticity ε – Total rates for laser pair $(2, 2)$ with total photon energies in the nuclear rest frame* (a) $1.8\,\text{MeV}$ *and* (b) $1.25\,\text{MeV}$*, and for* (c) *laser pair* $(5, 5)$ *with* $1.25\,\text{MeV}$ *– Comparisons are shown between (top panels) fixed total intensity using $\xi_1^2 + \xi_2^2 = 2{\times}10^{-6}$, and (bottom panels) fixed maximum laser wave amplitude using $\xi_1^2 = 10^{-6}$ and $0 \leq \xi_2 \leq \xi_1$. For the two-photon cases* (a) *and* (b)*, where it is applicable, the fully analytical graphs obtained using the formulæ derived in Ref.* [100] *coincide perfectly with the results presented here.*

wave. In the circularly polarized case the field amplitude is constant, while only the field vector direction changes, alternately pointing along x-direction $\mathbf{e}_1$ and y-direction $\mathbf{e}_2$:

$$\mathbf{A}_{\text{circ}} = \mathbf{a}_1 \cos\eta + \mathbf{a}_2 \cos(\eta + \pi/2) = a\,(\mathbf{e}_1 \cos\eta + \mathbf{e}_2 \sin\eta)\,, \quad |\mathbf{A}_{\text{circ}}| = a. \tag{3.18}$$

In the linearly polarized case the field amplitude is subject to the sinusoidal variation of the wave, however the peak amplitude is increased by a factor of $\sqrt{2}$ due to the superposition of the two waves:

$$\mathbf{A}_{\text{lin}} = \mathbf{a}_1 \cos\eta + \mathbf{a}_2 \cos\eta \qquad = a\,(\mathbf{e}_1 + \mathbf{e}_2)\cos\eta, \qquad |\mathbf{A}_{\text{lin}}| = a\sqrt{2}\cos\eta. \tag{3.19}$$

The previous explanation for the ellipticity dependence for a fixed total field intensity also applies to lower total photon energies and higher photon orders.

Corresponding examples are shown in the top panels of Figs. 3.11(b) and (c) for a total photon energy of 1.25 MeV and $\tilde{n} = 2$ or 5 absorbed photons, respectively. However, for a fixed maximum field amplitude the argument given before does not provide an explanation for the ellipticity dependence for these parameters. As the bottom panels of Figs. 3.11(b) and (c) demonstrate, the rate exhibits a non-monotonous dependence on the ellipticity here. After passing through a minimum at about $\varepsilon \approx 0.2$ and 0.12, respectively, the rate starts growing again and reaches its maximum value for a linearly polarized wave. This strong difference might be related to the excess energy above the pair creation threshold $\Delta E = \tilde{n}\omega - 2mc^2$. Compared to Fig. 3.11(a), it is much smaller in the latter examples.

Bethe–Heitler pair creation by an elliptically polarized, monochromatic laser wave has also been studied in Ref. [100] using a polarization-operator approach. In particular, analytical expressions for the total pair-creation rate by two-photon absorption were obtained in Eqs. (15) and (26) therein. The ellipticity dependences following from these expressions coincide perfectly with numerically integrated results for the two-photon case in Figs. 3.11(a) and (b) (top and bottom panels). However, the approach presented here allows to extend these results straightforwardly to higher photon orders. For instance, the five-photon case shown in Fig. 3.11(c) where features qualitatively similar to the two-photon case are obtained. It should be noted that a non-monotonous dependence on the field ellipticity has also been obtained recently for the rate of pair creation by the non-linear Breit–Wheeler process [63].

Chapter 4.

Incommensurable Frequencies

While in Ch. 3 various examples for commensurable frequencies of the two laser modes have been discussed, this chapter shall be dedicated to incommensurable frequencies. However, it is worth discussing whether the distinction between these two cases is actually a good choice. This discussion and the accompanying direct comparison of the two cases presented in the subsequent section have been published in Ref. [13]. A publication based on the results shown in Sec. 4.2 is in preparation.

4.1. Comparison to Commensurable Frequencies

The fundamental difference between commensurable and incommensurable frequencies ω_1 and ω_2 is that in the former case the total photon energies of both modes are equal: $\tilde{n}_1\omega_1 = \tilde{n}_2\omega_2$ (cf. Sec. 2.3.1). Therefore, it is indistinguishable whether $\tilde{n}_1$ or $\tilde{n}_2$ photons were taken from mode one or two, respectively. This leads to interference of these two quantum paths, as well as all the effects connected to interference discussed in Sec. 3.1. They cannot occur in the incommensurable case.

However, due to two arguments, one physical and the other mathematical, this strict distinction may not be an ideal choice (a similar line of argument can be found in Ref. [125]): On the one hand, all physical systems inherently have finite lifetimes, thus measured energies will have a bandwidth. For instance, an experimental laser pulse with a finite pulse length will consist of a continuous range of frequencies, and physical properties should be independent of small variations therein. On the other hand, it is possible to approximate any irrational

number by a ratio of integers with arbitrary precision.[14] In the light of these two points one may conclude that commensurability is practically always fulfilled, which also means that it does not allow the intended distinction. Obviously, the question arises what alternative measure does allow it.

A physically meaningful replacement is whether the frequency ratio is comprised of two *small* integers or not. For a small-integer frequency ratio, it occurs more frequently that in the superposition of the two laser modes a maximum of one mode coincides with a maximum of the other mode. Two coinciding maxima represent the highest possible field strength of the combined field, which will – in this case – occur often and periodically. On the other hand, for those ratios with at least one large integer, two coinciding maxima are very rare. Additionally, the large integer would correspond to the number of photons[15] needed to form an interference term, and terms with high photon numbers are suppressed due to the higher order in the intensity parameter. The aforementioned approximation of an irrational number by a rational will certainly be comprised of two large integers, and interference terms will be negligible. Thus, incommensurable frequencies are indeed treated correctly by the alternative distinction.

The theoretical framework used throughout this work does not impose any limitation on the frequencies of the laser modes. Therefore, a continuous variation of the frequency ratio ω_1/ω_2 may be studied, passing by the commensurable laser pairs $(2, 4)$ and $(2, 6)$ as discussed in Sec. 3.1.1. This way, further insight into the processes leading to the aforementioned interferences may be gained. In Fig. 4.1, this variation is plotted for the total pair-production rate and several summed-up partial rates by keeping ω_1 fixed and varying ω_2. The total photon energy is chosen to be 1.05 MeV. Due to ω_1 being fixed via $\tilde{n}_1 = 2$, the direct term of the first mode with minimal photon number, $[2, 2, 0, 0]$ (long-dashed red line), is a constant offset for the sum of all terms (solid black line). In contrast, the direct terms of the second mode, $[0, 0, n, n]$ for $n = (2, 3, 4, 5, 6)$, exhibit slowly rising and falling peaks, with the maximum lying approximately at their respective $\tilde{n}_2$ value. The latter is due to two reasons: The chosen total photon energy, which is only slightly above the pair-creation threshold, and the applied scaling of the intensities. For a larger total photon energy, the peaks would be shifted to the left, as the pair-creation threshold is overcome already for smaller frequency ratios. Conversely, for a smaller total photon energy they would be

[14] A straightforward way to achieve this is the sequence $s_n(x) = \lfloor 10^n x \rfloor \cdot 10^{-n}$ for an irrational number x, for which obviously holds: $\lim_{n\to\infty} s_n(x) = x$. For instance, $x = \pi$ leads to $(s_n(\pi))_{n\in\mathbb{N}_0} = (3,\ 3.1,\ 3.14,\ 3.141, \ldots)$.

[15] To give an example: Assume $\omega_1 = 99\%\,\omega_2 = 1.2\,\text{MeV}$. The minimal photon number for both modes is obviously $\tilde{n}_1 = \tilde{n}_2 = 1$. Therefore, the direct terms with lowest number of photons are $[1, 1, 0, 0]$ and $[0, 0, 1, 1]$. However, as Eq. (2.49a) has to be fulfilled, the interference terms with lowest number of photons are $[100, 0, 0, 99]$ and $[0, 100, 99, 0]$.

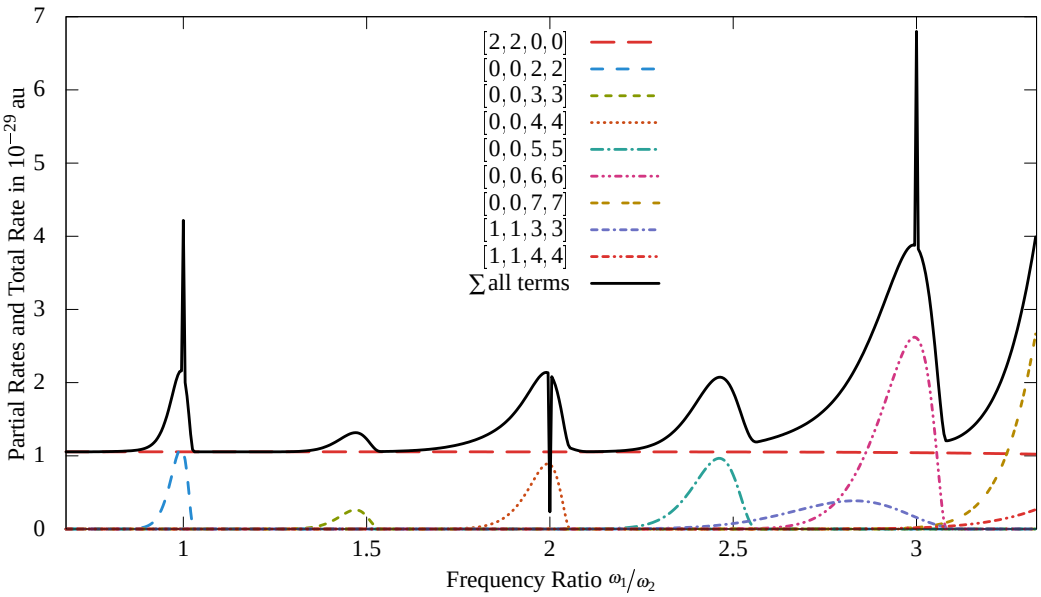

Figure 4.1.: *Variation of the frequency ratio ω_1/ω_2 – Total rate and integrated partial rates for the total photon energy $E_{ph} = 1.05\,\mathrm{MeV}$ in the nuclear rest frame with $\omega_1 = E_{ph}/2$ fixed and ω_2 varied from $E_{ph}/1.8$ to $E_{ph}/6.2$. Conversely, this means that the pair-creation threshold may be overcome by absorbing $\tilde{n}_1 = 2$ photons from the first mode or $\lceil E_{ph}/\omega_2 \rceil$ photons from the second mode. The intensity parameter ξ_2 is scaled according to Eq. (4.1) similar to Eq. (2.70), with $\zeta = \xi_1 = 10^{-6}$ and an empirically found prefactor approximating the small adjustment explained in Sec. 2.3.3. The relative phases are set as $\varphi_1 = \varphi_2 = 0$. Note that, the partial contributions of the interference terms are not shown separately as they are clearly visible as the δ-spikes for the integer frequency ratios.*

shifted to the right. The intensity parameter $\xi_1 = \zeta$ is kept constant, mirroring the fixed frequency of the first mode. In contrast,

$$\xi_2 = \sqrt{\frac{\omega_1}{\omega_2}}\,\zeta^{\omega_2/\omega_1} \tag{4.1}$$

is scaled similar to Eq. (2.70). However, an additional empirical prefactor, $\sqrt{\omega_1/\omega_2}$, approximates the necessary small adjustment discussed in Sec. 2.3.3. On top of the peaks of the direct terms, for those commensurable frequencies where the frequency ratio is an integer, interference terms are contributing sharp δ-spikes. In the presented theoretical framework, these spikes are infinitely narrow but of finite height. In the laser pair notation $(\tilde{n}_1 = 2, \tilde{n}_2)$ applied for the

commensurable results in Ch. 3, this corresponds to $\tilde{n}_2 = 2$, 4 and 6, of which the latter two have been studied in Sec. 3.1.1, as well as the first one in Sec. 3.2. Due to the chosen relative phases $\varphi_1 = \varphi_2 = 0$, the interference is constructive for $\tilde{n}_2 = 2$ or 6, and destructive for $\tilde{n}_2 = 4$. As has been discussed in Sec. 3.1.3, a variation of the relative phase only affects the δ-spikes, sinusoidally changing their height and sign.

Considering the discussion at the beginning of this section, a note on an actual experimental realization of the proposed schemes should be made: An experimental laser would not be an infinite plane wave but a finite pulse. Therefore, the δ-spikes would be expected to be smeared out and, thus, the resulting spectrum to be continuous. Nevertheless, the strong enhancement or depletion at the integer frequency ratios can be expected to remain.

4.2. γ-Assisted Tunneling Pair Creation

In Ch. 3 commensurable frequencies have been discussed, in Sec. 4.1 these have been compared to incommensurable frequencies. An important finding of the latter has been that, instead of in terms of commensurability, a pair of frequencies should be classified by whether their ratio consists of small or large integers. To complement the previously presented results, strongly differing frequencies shall be considered in this section. Furthermore, the intensity of the smaller frequency mode shall be increased compared to all results discussed before.

Similar configurations have been used recently in studies on the Schwinger effect in order to make its non-perturbative character observable with available technology. Even though the maximal intensities of modern lasers increase with every new facility, the critical electric field

$$\mathscr{E}_{\text{crit}} \simeq 1.3 \times 10^{18}\,{}^{\text{V}}/_{\text{m}}, \tag{4.2}$$

is yet to be reached. Therefore, the *dynamically assisted* Schwinger effect has been proposed [50, 140], where a slowly varying electric field (quasi-static, as in the tunneling picture introduced in Sec. 1.3) is superimposed with a rapidly oscillating one. This way a strong enhancement of the pair-creation rate is gained, while the dependence on the field strength is still exponential. Several related studies on more refined properties of this process, e.g., the momentum distribution of the created particles, have been performed since [59, 116, 119]. Furthermore, similar enhancement effects were found for the strong-field Breit–Wheeler process [71] and pair creation induced by two spatially separated electric fields periodically varying in time [72, 73].

For the strong-field Bethe–Heitler process – the subject of this section – several studies on the dynamically assisted variant [41, 42, 93] are available, also yielding Schwinger-like behaviour combined with a strong enhancement[16] over the unassisted counterpart. Specifically, the analytical formulæ obtained in Ref. [41] will be used in comparison with the results presented in this section.

4.2.1. Adapted Notation and Non-Perturbative Regime

Before specifying the subsequently employed configuration, a small remark on the notation applied in this section is necessary: In the incommensurable case, no terms with $n_i \neq n_i'$ may occur (cf. Sec. 2.3.2). Therefore, the notation used so far can be simplified. Instead of the four-index sum from Eq. (2.53), a two-index sum is sufficient:

$$\mathrm{d}^6 R = \sum_{n_1,n_2} \mathrm{d}^6 R_{[n_1,n_1,n_2,n_2]}. \tag{4.3}$$

It is convenient to introduce an alternative definition of the terms in that sum:

$$\mathrm{d}^6 R_{[n_1,n_1,n_2,n_2]} \equiv \mathrm{d}^6 R_{[n_1,n_2]}. \tag{4.4}$$

So far, for reasons discussed in Sec. 4.1, only processes where $\omega_1 \approx \omega_2$ have been discussed. In this section processes with very asymmetric frequencies are studied. As the presented theoretical framework is completely symmetric in the two modes, the choice which mode provides the assisting photons and which mode is assisted is arbitrary. The results in this section are obtained for a set-up where $\omega_2 \ll \omega_1 \lesssim 2mc^2$, and thus a single photon from the first mode in conjunction with several photons from the second mode is absorbed. More specific, the bichromatic laser field in this section is composed of a high-frequency low-intensity mode with

$$\omega_1 \lesssim 2mc^2 \quad \text{and} \quad \xi_1 \ll 1, \tag{4.5}$$

and a low-frequency high-intensity mode with

$$\omega_2 \ll 2mc^2 \quad \text{and} \quad \xi_2 \approx 1. \tag{4.6}$$

This set-up can be interpreted as a source of single γ-photons *assisting* a strong laser in the pair-creation process. Therefore, and due to the "photon-counting" nature of the theoretical framework used here, it seems more natural to speak

[16] Note that, in Ref. [42] a suppression of the rate is found when the "assisting" light source is turned on if the highly energetic photon has an energy $\hbar\omega \gg mc^2$. However, such a set-up is not considered here.

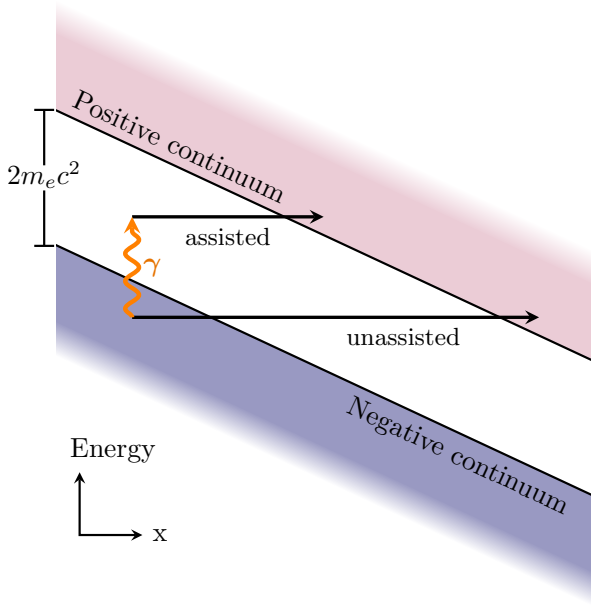

Figure 4.2.: *Illustration of γ-assisted tunneling pair creation – In the tunneling regime the continua are tilted along the x-axis by the electric field $\mathscr{E}$ (cf. also Fig. 1.2(a)). The absorption of a high energetic photon lifts an electron from the Dirac sea towards positive energies. This strongly decreases the width of the barrier through which the electron tunnels afterwards, as can be seen by the much shortened upper arrow compared to the lower one.*

of *γ-assisted tunneling pair creation* instead of the aforementioned *dynamically assisted* moniker. It is appropriate to distinguish the different occurring processes by the number of highly energetic photons n_1 involved. For each of these processes the sum over n_2 has to be performed[17]:

$$\mathrm{d}^6 R_{n_1} = \sum_{n_2} \mathrm{d}^6 R_{[n_1,n_2]}. \tag{4.7}$$

The summed-up rate from Eq. (2.53) is then given by

$$\mathrm{d}^6 R = \sum_{n_1} \mathrm{d}^6 R_{n_1}. \tag{4.8}$$

In this notation, R_1 and R_0 correspond to the rate of Bethe–Heitler pair creation in the tunneling regime with and without assisting γ-photon, respectively. The two cases are depicted schematically in Fig. 4.2, particularly illustrating how

[17] It is important to note that, R_{n_1} must not be confused with R_i, the rate of the direct terms with minimal photon number for mode i, as defined in Eq. (2.68).

the width of the barrier decreases due to the assisting γ. An expression for the barrier widths is gained as follows: For the unassisted case, the boundaries of the continua, $\pm mc^2$, tilted by the electric field $\mathscr{E}$ along the x-axis around the origin, are given by

$$C_{\pm}(x) = \pm mc^2 - e\mathscr{E}x. \tag{4.9}$$

These functions cross the abscissa, i.e., $C_{\pm}(x_{0,\pm}) \stackrel{!}{=} 0$, at

$$x_{0,\pm} = \pm\frac{mc^2}{e\mathscr{E}}. \tag{4.10}$$

The distance between the two crossing points is thus

$$l_0 = |x_{0,+}| + |x_{0,-}| = \frac{2mc^2}{e\mathscr{E}}. \tag{4.11}$$

By subtracting the energy of the γ-photon from Eq. (4.9), the respective expression for the assisted process is obtained in the same way:

$$l = \frac{2mc^2 - \hbar\omega_1}{e\mathscr{E}} = l_0 - \frac{\hbar\omega_1}{e\mathscr{E}}, \tag{4.12}$$

wherein the last term is the aforementioned decrease in the barrier width.

While the first mode should still exhibit the perturbative dependence on ξ_1 associated with the multiphoton regime ($\xi \ll 1$), a non-perturbative dependence is expected for the second mode as $\xi_2 \approx 1$. In particular, the second mode approaches the tunneling regime ($\xi \gg 1$), where a dependence similar to the Schwinger rate is expected [100] due to the characteristic length scale of the pair-creation process being much shorter than the laser wavelength.

The non-perturbative nature of the second mode can be seen in Fig. 4.3, where $R_{[0,n_2]}$ is shown as a function of n_2 for a range of ξ_2-values. One notices immediately that, the smaller ξ_2, the less steps in n_2 away from the minimal number of photons $\tilde{n}_2$ are necessary for the sum in Eq. (4.7) to converge to $R_0(\xi_2)$. For very small ξ_2, the rate shows the typical behaviour of the multiphoton regime, i.e., only the $\tilde{n}_2$-term contributes non-negligibly. In contrast, for the highest depicted value, $\xi_2 = 1.25$, more than one hundred steps, from 54 to 159, are necessary to reach an accuracy of six decimal places.

This type of plot also illustrates nicely how the assisting γ-photon alters the minimal number of photons from the strong mode necessary to overcome the pair-creation threshold, as can be seen in Fig. 4.4. The γ-assisted process is already possible for smaller n_2 and the unassisted process has an offset of steps in n_2 corresponding to the ratio of the employed frequencies. It is worth pointing out that, for the n_2-values not depicted in this figure due to their contribution

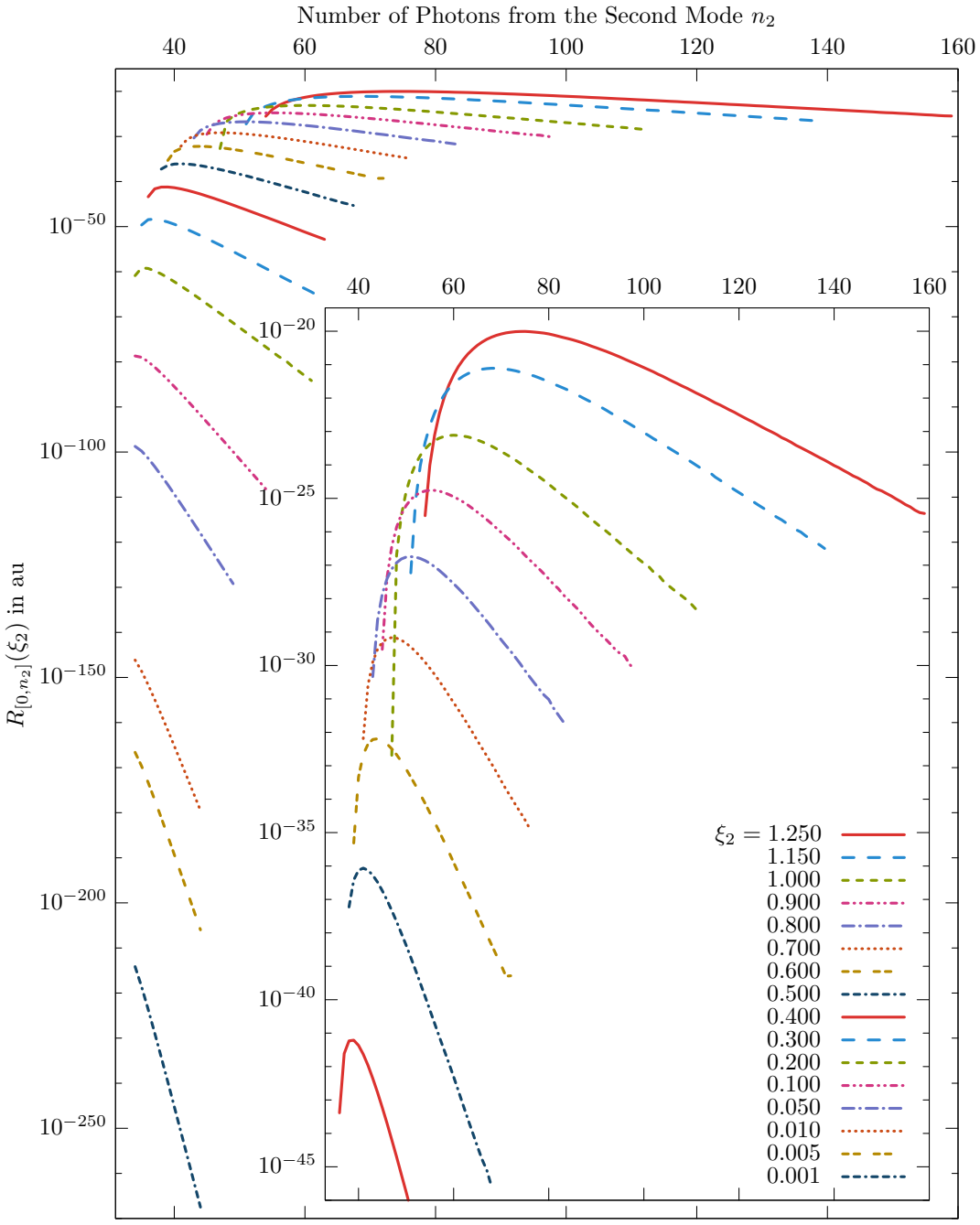

Figure 4.3.: *Comparison of the perturbative and the non-perturbative regimes of the intensity parameter ξ_2 – The summation steps $R_{[0,n_2]}$ in the photon number n_2 necessary to obtain R_0 are shown for various intensities (cf. Eq. (4.7)). The parameters are those given in Eq. (4.13b). The inset shows a zoom into the upper region of the main plot, focusing on those ξ_2-values also shown in Fig. 4.5. Particularly, the sum over the underlying points results in the unassisted curve shown in Fig. 4.5(a). Note that here, the integer steps are very dense and are therefore depicted by lines.*

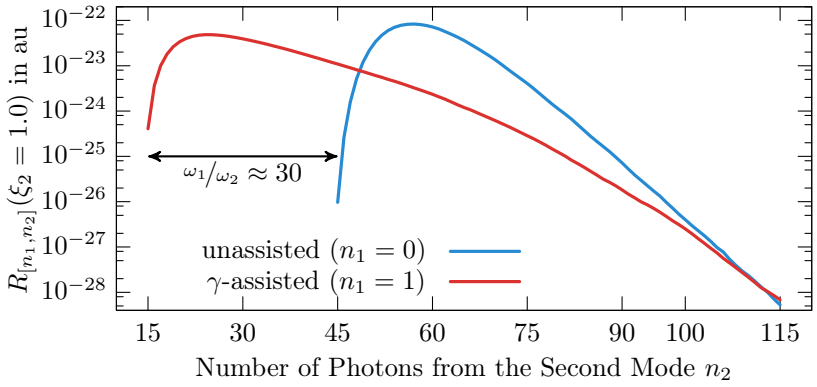

Figure 4.4.: *Example of a non-perturbative dependence on the intensity parameter ξ_2 – The summation steps $R_{[n_1,n_2]}$ in the photon number n_2 necessary to obtain R_{n_1} are shown for $\xi_2 = 1$ (cf. Eq. (4.7)). The parameters are those given in Eqs. (4.22). The sum over the underlying points results in the two points at $\xi_2 = 1$ in Fig. 4.5(b). Note that here, the integer steps are very dense and are therefore depicted by lines.*

to the overall sum being negligible, i.e., from $n_2 = 115$ onwards, the two curves converge to a single one. This can be understood as a saturation effect, in the sense that the energy provided by the photons has almost overcome 4 MeV and is, thus, so far above the pair-creation threshold that it becomes irrelevant whether or not the γ-photon assists in a specific sub-process, i.e., $R_{[n_1,n_2\geq 115]}$.

Note that, these two figures are a slight leap ahead as the parameters used to produce them are introduced and discussed in the subsequent section. However, they illustrate the underlying calculations and give context for the following results.

4.2.2. Total Rates and Intensity Dependence

In Fig. 4.5(a), the total rates $R_{n_1}(\xi_2)$ for $n_1 = 0$ and 1 are shown. Here, the process with $n_1 = 0$ corresponds to the lower arrow in Fig. 4.2, while $n_1 = 1$ is visualized as the γ-absorption followed by the upper arrow in that figure. The employed set of parameters is:

$$\omega_1 = 924\,\text{keV}, \qquad \xi_1 = 10^{-8}, \tag{4.13a}$$

$$\omega_2 = 30.76\,\text{keV}, \qquad 0.5 \leq \xi_2 \leq 1.25\,. \tag{4.13b}$$

This corresponds to a frequency ratio of $\omega_1/\omega_2 \approx 30$. In the laboratory frame, this ratio could be achieved by an XUV source for the weak field, and the IR light

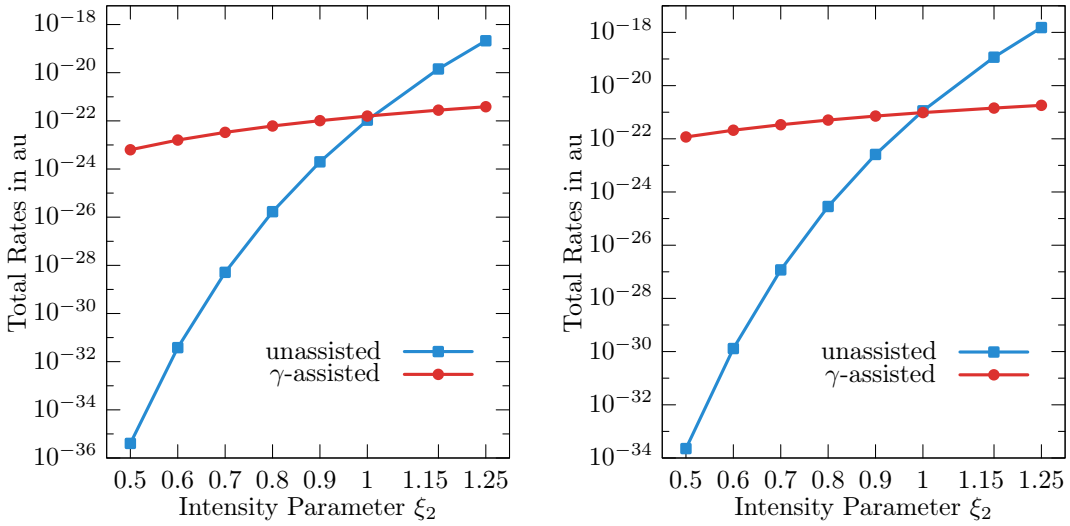

(a) $\gamma = 6600$, see also Eqs. (4.13)

(b) $\gamma = 7000$, see also Eqs. (4.22)

Figure 4.5.: *Comparison of total pair-creation rates of the γ-assisted and the unassisted process – The assisted process is much stronger for smaller intensities of the second mode. This reverses at $\xi_2 \approx 1$, where the two curves cross. It is interesting to point out that, here the results for the two values of γ are very similar. In contrast, they differ strongly for the analytical counterpart shown in Fig. 4.6.*

(1064 nm) emitted by an Nd:YAG laser[18] combined with a frequency doubler (532 nm) [120] for the strong field:

$$\omega_1^{\text{lab}} = 70\,\text{eV} \quad \text{and} \quad \omega_2^{\text{lab}} = 2.33\,\text{eV}. \tag{4.14}$$

The parameters in the nuclear rest frame given in Eq. (4.13) are reached with a laboratory-frame intensity of the strong mode of roughly $(10^{19}\text{–}10^{20})\,{}^{\text{W}}/_{\text{cm}^2}$ (cf. Eqs. (A.13) and (A.10)) and a Lorentz factor of $\gamma = 6600$. The latter is well within the current limits of the LHC of $\gamma \lesssim 7460$ [32]. The XUV photon may be provided be an FEL or a source based on HHG, making a set-up of technology available today feasible. Moreover, a HHG-based set-up would allow the bichromatic laser field to be generated by transportable "table-top" devices.

Even though the depicted intensity range of the strong mode is $\xi_2 \approx 1$, the total

[18] A neodymium-doped yttrium aluminium garnet (Nd:$Y_3\,Al_5\,O_{12}$) laser is a common solid-state laser delivering high output power in the IR regime [15].

rates of both processes show a Schwinger-like dependence on this parameter:

$$R_{n_1} \sim \exp\left(-\frac{C_{n_1}}{\xi_2}\right). \tag{4.15}$$

However, the coefficient C_{n_1} differs for the two cases. In the assisted process it is smaller, leading to an almost flat curve, while in the unassisted case a steep increase is visible and saturation will occur only for larger intensities.

The influence of the assisting γ-photon can be deduced from the absolute height of the two curves: For $\xi_2 < 1$, the assisted process shows a strong enhancement over its unassisted counterpart. The situation inverses for $\xi_2 > 1$, where the unassisted process dominates. Here, the two curves cross at $\xi_2 \approx 1$. The value for which this crossing occurs may be influenced by adjusting the intensity of the weak field ξ_1. The unassisted process is obviously independent of this parameter. In contrast, the assisted process depends quadratically on it (cf. Eq. (1.20)). Therefore, ξ_1 allows for a relative scaling of the two curves.

A further point should be stressed here, the R_0-curve could be measured experimentally by turning off the assisting γ-source. In contrast, the R_1-curve is not accessible independently, instead the sum over n_1, and thus $R = R_0 + R_1$, would be measured in an experimental realization of the assisted process (cf. Eq. (4.8)). However, for the discussion and comparison of the occurring processes, it is more illustrative which of the two curves, $R_0(\xi_2)$ or $R_1(\xi_2)$, contributes stronger to the total rate. Therefore, the above representation of separated R_{n_1} has been chosen.

As mentioned above, total rates of dynamically-assisted tunneling pair creation have been investigated fully analytically in Ref. [41] in a scheme very similar to the one presented here, however, under the assumption that $\xi_2 \gg 1$. Specifically, Eq. (9) therein (here not quoted verbatim, but with adapted naming convention),

$$R \sim \exp\left(-\frac{2\sqrt{2}}{3\zeta}\right), \tag{4.16}$$

with the parameters

$$\zeta = \frac{\chi}{\delta^{3/2}}, \quad \text{where} \quad \chi = \frac{1}{\sqrt{2}}\frac{\omega_2}{\omega_1}\xi_2, \tag{4.17a}$$

$$\delta = \left(\frac{2mc^2}{\omega_1}\right)^2 - 1 \approx \frac{2mc^2 - \omega_1}{mc^2}, \tag{4.17b}$$

can be employed for a comparison of the dependences on the strong field intensity ξ_2 with the results presented here. With the parameter ζ inserted, Eq. (4.16)

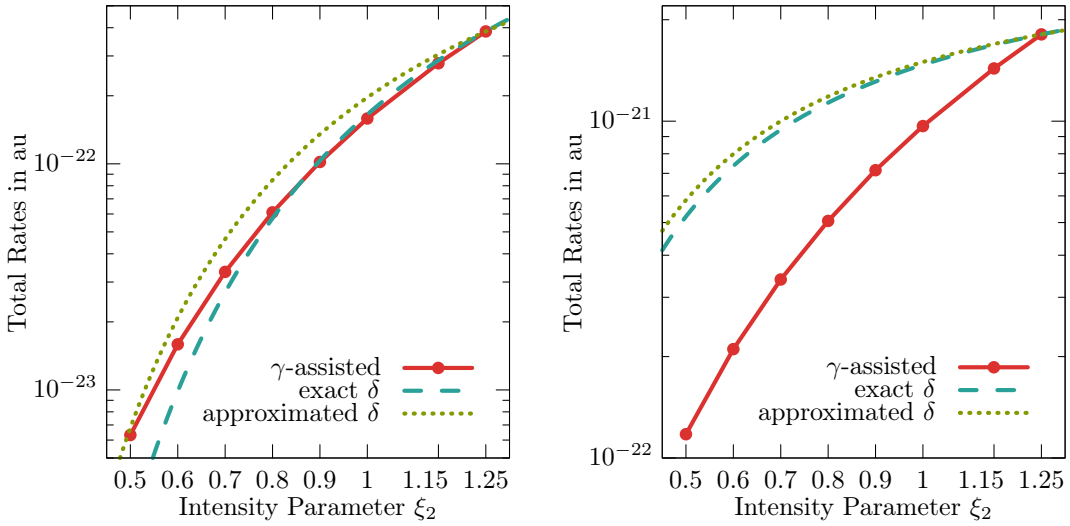

(a) $\gamma = 6600$, see also Eqs. (4.13)

(b) $\gamma = 7000$, see also Eqs. (4.22)

Figure 4.6.: *Comparison of total pair-creation rates of the γ-assisted process obtained from the theoretical framework presented here and the analytical counterpart extracted from Ref. [41] – The red curve is identical to that in Fig. 4.5. The two additional curves are for the exact and the approximated δ given in Eq. (4.17b). The latter two are scaled to the value of the former at $\xi_2 = 1.25$. The three curves coincide very well for $\gamma = 6600$. In contrast, a strong deviation is visible for $\gamma = 7000$.*

reads

$$R \sim \exp\left(-\frac{4}{3}\frac{1}{\omega_2}\,\omega_1\,\delta^{3/2}\,\frac{1}{\xi_2}\right). \tag{4.18}$$

For the comparison, this exponential is scaled by a proportionality factor such that the value at $\xi_2 = 1.25$ coincides with the result obtained from the calculation presented here. Even though the requirement of $\xi_2 \gg 1$ is not met in the latter, the two additional graphs – one for the exact and one for the approximated δ from Eq. (4.17b) – in Fig. 4.6(a) coincide very well with it. Moreover, to some surprise, the approximated δ shows the better agreement.

Besides the requirement of very large intensities, two constraints are imposed for the applicability of Eq. (4.18): The two parameters from Eqs. (4.17) should both be very small:

$$\zeta \ll 1 \quad \text{and} \quad \delta \ll 1. \tag{4.19}$$

For the parameter set from Eqs. (4.13), their respective values are indeed relatively

small, namely

$$\zeta \approx \delta \approx 0.2\,. \tag{4.20}$$

However, for the same laser combination in the laboratory as in Eq. (4.14), an increase in γ to 7000 and the accompanying increase in the photon energies in the nuclear rest frame leads to a larger value for one of the parameters:

$$\zeta \approx 0.9\,. \tag{4.21}$$

For the resulting set of laser field parameters,

$$\omega_1 = 980\,\mathrm{keV}, \qquad \xi_1 = 10^{-8}, \tag{4.22a}$$
$$\omega_2 = 32.62\,\mathrm{keV}, \qquad 0.5 \leq \xi_2 \leq 1.25, \tag{4.22b}$$

a significant deviation between the results presented here and those obtained from Eq. (4.18) can be seen in Fig. 4.6(b). For a reduced γ, a similar deviation occurs, as then the parameter δ (cf. Eq. (4.17b)) grows to and eventually surpasses unity (cf. Sec. 4.2.4).

Nevertheless, the found results show a strongly non-perturbative dependence on the intensity parameter ξ_2 that is similar to the analytical expression given in Eq. (4.18). Therefore, a survey of a wider range of parameters, where the requirements of Eq. (4.19) are not fulfilled, might show if and how an empirical extension to Eq. (4.18) can be gained. As can be seen from the definition of the two parameters in Eqs. (4.17), for $\xi_2 \approx 1$, as considered here, this would mean for relatively small ω_1 and relatively large ω_2. Here, this is done by calculating total rates for various combinations of laser frequencies in the nuclear rest frame within the bounds

$$800\,\mathrm{keV} \leq \omega_1 \leq 1\,\mathrm{MeV}, \tag{4.23a}$$
$$10\,\mathrm{keV} \leq \omega_2 \leq 100\,\mathrm{keV}, \tag{4.23b}$$

and the considered intensity range $0.5 \leq \xi_2 \leq 1.25$. Indeed, one finds that the results for all tested combinations can be reproduced by introducing an additional degree of freedom d into Eq. (4.18) with the approximated δ,

$$R \sim \exp\!\left(-\frac{4}{3}\frac{1}{\omega_2}\,\omega_1\left(2-\frac{\omega_1}{mc^2}\right)^{3/2}\frac{1}{\xi_2^d}\right), \tag{4.24}$$

such that the two equations are identical for $d = 1$. Then, the found results have been successively fitted with functions extracted from Eq. (4.24), in order to remove the dependence on the individual ω_i. In the first step, a function of the form

$$\mathcal{R}_{[\omega_2,\,\xi_2]}(\omega_1) = -\mathcal{A}\,\omega_1\left(2-\frac{\omega_1}{mc^2}\right)^{3/2} + \mathcal{B}, \tag{4.25}$$

is fitted to the logarithm of the results, separately for fixed ω_2 and ξ_2. Note that, this is almost a straight line in the considered ω_1-range given in Eq. (4.23a). The fit-parameter $\mathcal{B}$ corresponds to the proportionality factor of Eq. (4.24) and is not further taken into account. In contrast, the obtained values for the fit-parameter $\mathcal{A}$ are then examined for fixed ω_2. By fitting a function of the form

$$\mathcal{A}_{\omega_2}(\xi_2) = \mathcal{C}\,\frac{1}{\xi_2^d}, \tag{4.26}$$

one finds that for

$$d \approx 0.8, \tag{4.27}$$

the results for the whole tested parameter range given in Eqs. (4.23) are very well reproduced. Thus, with only a small modification to the analytical expression and, consequently, only a small deviation from the Schwinger-like dependence therein, an empirical extension to Eq. (4.18) is obtained, which works well for a large range of parameters outside the original requirements.

4.2.3. Momentum, Energy, and Emission-Angle Spectra

So far, the total pair-creation rates of the γ-assisted and the unassisted case have been compared. Further insight can be gained from analysis of the underlying differential spectra.

The first two comparisons of differential spectra of pair-creation rates of both processes are shown in Fig. 4.7. The parameters from Eqs. (4.22) are examined at $\xi_2 = 1$, the approximate crossing point found in Fig. 4.5(b). For this intensity, both processes show an approximately equal total rate. Figures 4.7(a) and 4.7(b) depict the radial momentum distribution and the energy distribution, respectively. The both abscissæ correspond directly to each other by means of the relativistic energy-momentum relation given in Eq. (1.6). However, they are not linearly mapped to each other, which leads to the slight alteration of the curve shapes. Furthermore, the energy distribution is not given in atomic units, but in seconds and electronvolt. One notices that the distribution obtained for the assisted process is wider than that of the unassisted counterpart.

The total energy of the created particles is identical to the total energy of the incoming photons. In this sense the distributions depicted here are closely related to Fig. 4.3, where the summation steps in the photon number n_2 are depicted for the unassisted process. With each step in n_2 the total photon energy is increased by ω_2, making the n_2-axis in said figure a quantized energy axis. Moreover, the peaking curve therein maps to the energy distribution of the created particles. Conversely, the curves for the γ-assisted process corresponding to those in Fig. 4.3

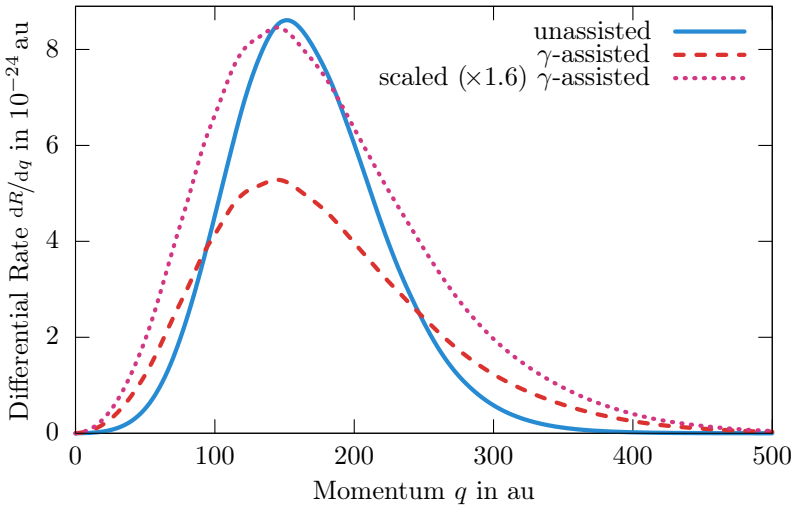

(a) Momentum distribution

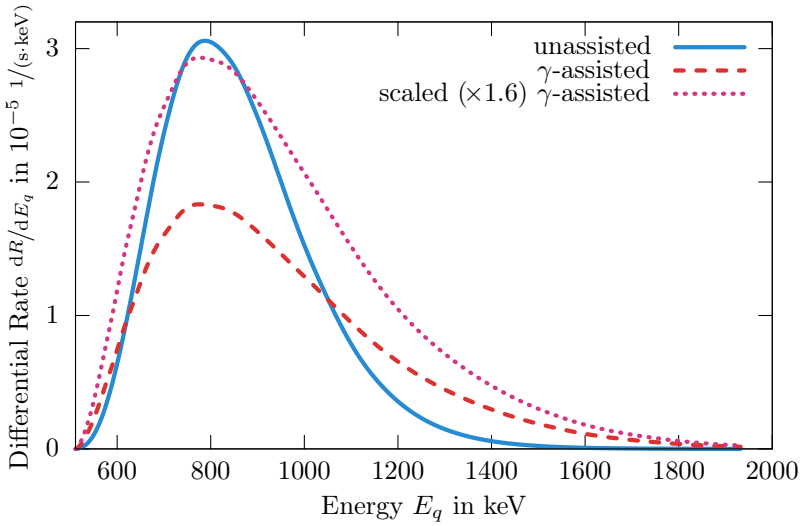

(b) Energy distribution (note the converted units)

Figure 4.7.: *Comparison of momentum- and energy-differential pair-creation rates of the γ-assisted and the unassisted process in the nuclear rest frame – Both spectra are obtained for the parameters in Eqs.* (4.22) *at* $\xi_2 = 1$*, the approximate crossing of the curves in Fig.* 4.5(b)*. A scaled version of the γ-assisted spectrum has been added for better comparability. Momentum and energy are connected according to Eq.* (1.6)*. Since this is not a linear mapping, slight differences in the curve shapes occur. However, in both figures the distribution obtained for the γ-assisted process is wider than the unassisted process.*

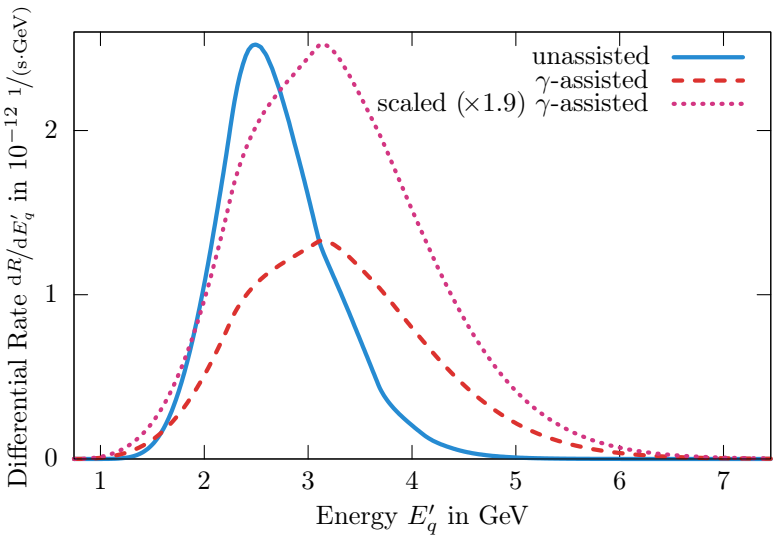

Figure 4.8.: *Comparison of energy-differential pair-creation rates of the γ-assisted and the unassisted process in the laboratory frame – The same parameters as in Fig. 4.7 have been used. Besides the widened distribution also found in the nuclear rest frame, the peak position is shifted towards larger energies. Note that, the distribution is converted to second and electronvolt, instead of the respective atomic units.*

are also much wider. This can be seen in Fig. 4.4, for the same parameters as in Fig. 4.7.

Furthermore, in Fig. 4.8 the results from Fig. 4.7(b) have been transformed to the laboratory frame. The widened distribution for the assisted process is again clearly visible. Moreover, the effect is enhanced by the Lorentz transformation and the width of the distribution of the assisted process is almost doubled compared to the unassisted process. Additionally, the peak position is shifted towards larger energies. Both effects can be understood from the subsequently shown emission angle distributions since the Lorentz transformation mixes the temporal component of the four-momentum, i.e., the energy, with its spatial component along the nuclear propagation direction, i.e, the z-component of the momentum three-vector. The latter is given by the cosine of the emission angle ϑ (cf. also Eq. (E.6)). Note that, the laboratory frame counterpart of the momentum distribution in Fig. 4.7(a) is not shown as the differences of the curve shapes compared to the energy distribution in Fig. 4.7(b) vanishes when the transformation to the laboratory frame is performed.

In Fig. 4.9, the pair-creation rate differential in the emission angle ϑ is shown for

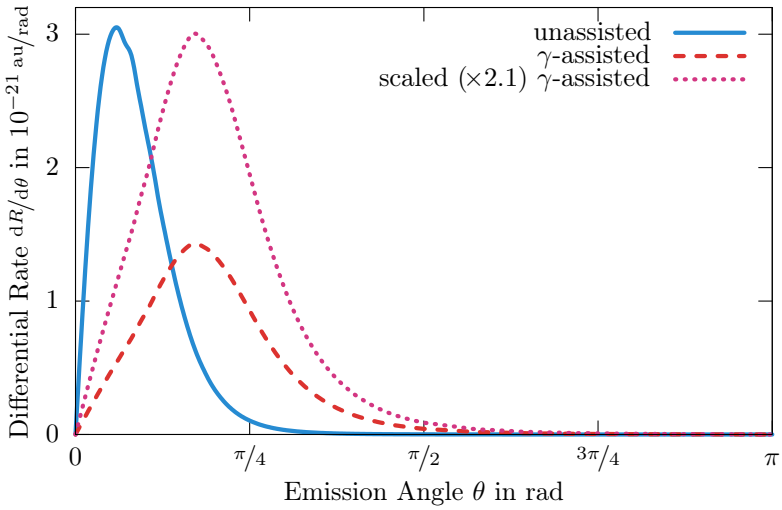

(a) Nuclear rest frame

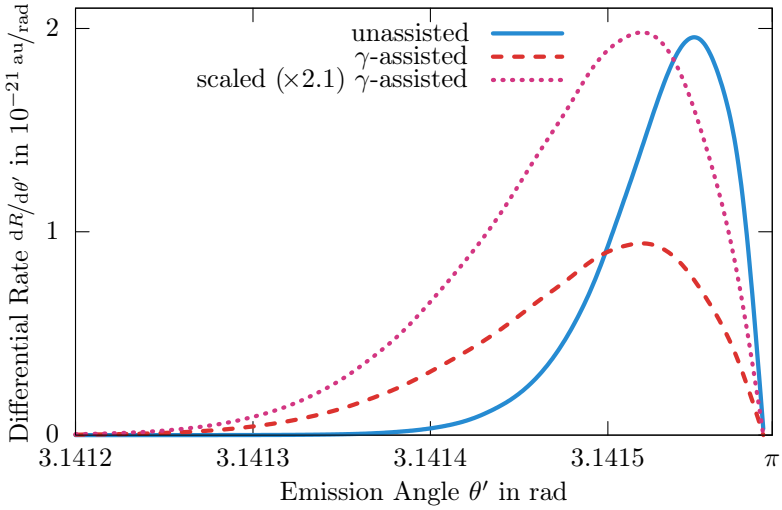

(b) Laboratory frame (note the narrow range of angles)

Figure 4.9.: *Comparison of angular-differential pair-creation rates of the γ-assisted and the unassisted process in the nuclear rest frame and the laboratory frame – Both spectra are obtained for the parameters in Eqs. (4.22) at $\xi_2 = 1$, the approximate crossing of the curves in Fig. 4.5(b). A scaled version of the γ-assisted spectrum has been added for better comparability. In both frames of reference, the distribution obtained for the γ-assisted process is widened compared to the unassisted process. Furthermore, the peak position is shifted towards larger (smaller) angles in the nuclear rest frame (laboratory frame).*

both processes for the same parameters as above. Figures 4.9(a) and 4.9(b) depict the results in the nuclear rest frame and the laboratory frame, respectively. In both frames of reference, the distribution obtained for the γ-assisted process has an approximately doubled width compared to the unassisted process. Besides the strong contraction of the allowed range of emission angles, the Lorentz transformation maps small angles to large ones, and vice versa. Therefore, the shift of the emission peak position towards larger angles in the nuclear rest frame results in a slight shift towards smaller angles in the laboratory frame. Note that, while in the nuclear rest frame the e^-e^+ pairs are mainly emitted into a small cone in laser propagation direction, in the laboratory frame they are mainly emitted into a very small cone in propagation direction of the nucleus. This is a general observation imparted by the Lorentz transformation.

4.2.4. Higher-Order γ-Assisted Tunneling Pair Creation

In the theoretical framework employed throughout this thesis, the results presented in Secs. 4.2.2 and 4.2.3 can be straightforwardly extended to higher-order γ-assisted processes. In this section, the case of two assisting γ-photons is discussed and compared to the singly γ-assisted and the unassisted processes (the latter obviously remains unchanged). To this end, the photon energy of the highly intense mode is kept as in Eqs. (4.22), while that of the assisting mode is halved. The intensity of the latter is increased to ensure better comparability of the three processes of interest. Thus, the employed parameters are:

$$\omega_1 = 490\,\mathrm{keV}, \qquad \xi_1 = 5{\times}10^{-5}, \tag{4.28a}$$

$$\omega_2 = 32.62\,\mathrm{keV}, \qquad 0.5 \leq \xi_2 \leq 1.25\,. \tag{4.28b}$$

This corresponds to a frequency ratio of $\omega_1/\omega_2 \approx 15$. It is worth pointing out that here, the process with a single assisting photon represents the aforementioned case where the parameter δ from Eq. (4.17b) is larger than unity since $\delta \approx 3.4$.

Analogously to Fig. 4.5, the comparison of total pair-creation rates of the three processes as a function of the intensity parameter ξ_2 is shown in Fig. 4.10. Here, a result consistent with that of Sec. 4.2.2 is found: For the smallest depicted intensities, $\xi_2 < 0.85$, the doubly assisted process is dominant, then it is overcome by the singly assisted process. For $\xi_2 > 1.02$, the unassisted process is strongest. Here it is important to stress again that, these crossing points may be modified by means of the intensity of the first mode, as the three processes depend differently on the parameter ξ_1. The unassisted case is independent of it, while the singly assisted case depends on its square and the doubly assisted on its fourth power.

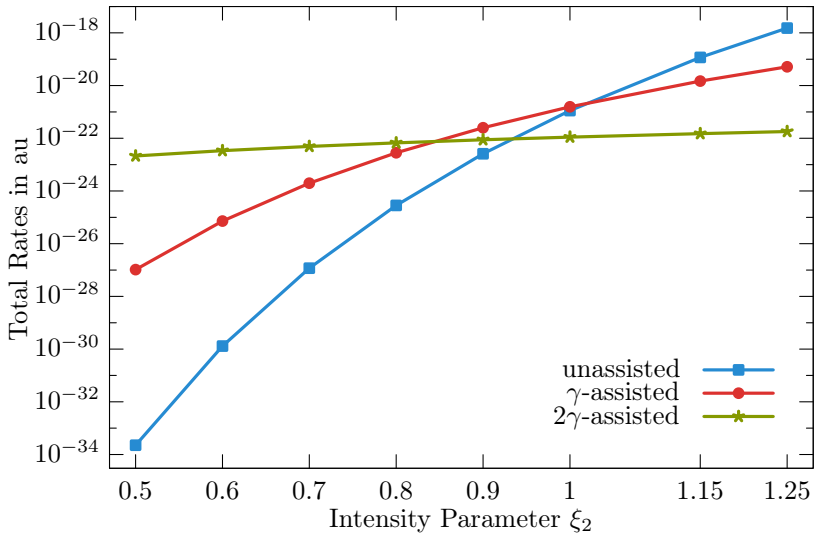

Figure 4.10.: *Comparison of total pair-creation rates of the singly or doubly γ-assisted and the unassisted process – This figure should be understood as higher-order version of Fig. 4.5 obtained for the parameters in Eqs. (4.28). The doubly-assisted process is much stronger for smaller intensities of the second mode, while the unassisted process dominates for the largest depicted intensities. In an intermediate range, $0.85 \lesssim \xi_2 \lesssim 1.02$, the singly-assisted process is strongest.*

As in Sec. 4.2.3, the differential pair-creation rates of the higher-order assisted process depicted in Figs. 4.11 and 4.12 shall be discussed in the following for both frames of reference.

The angular-differential pair-creation rates of the unassisted, the singly and the doubly γ-assisted process are compared in Fig. 4.11(a) for the nuclear rest frame at the intensity parameter $\xi_2 = 1$. As can be seen in Fig. 4.10, for this intensity the unassisted and the singly assisted rates are of approximately equal strength, while the doubly assisted process is slightly suppressed. Therefore, a scaled version of its curve has been added to the figure. Just as in Fig. 4.9(a), the more assisting γ-photons participate in the process, the wider the distribution and the larger the emission angle to which the peak position is shifted.

In analogue to Fig. 4.9(b), the angular spectrum is transformed to the laboratory frame in Fig. 4.11(b). Due to the Lorentz transformation, the unassisted process experiences a slight widening and, consequently, a decrease of the peak height. Therefore, an additional scaled version of its curve has been added to this figure. The broadening of the distribution is also found in this frame of reference. However, the shift of the peak position is less pronounced. Particularly, the main emission direction of the two assisted processes is almost identical.

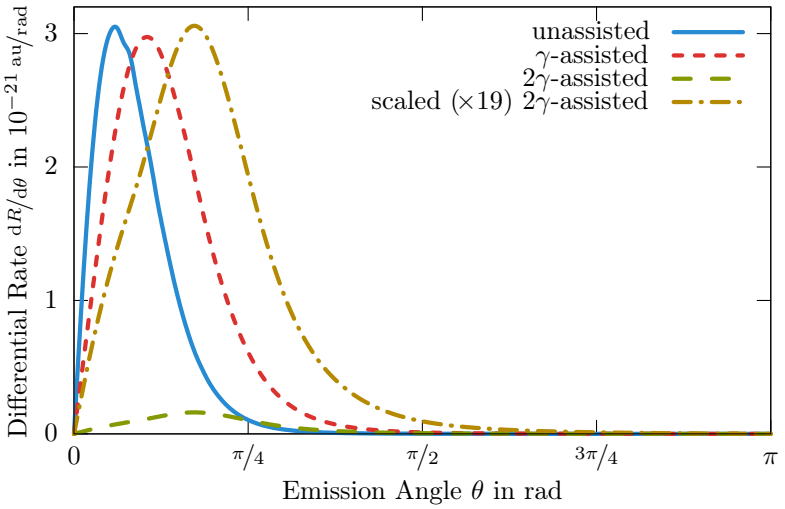

(a) Nuclear rest frame (cf. Fig. 4.9(a))

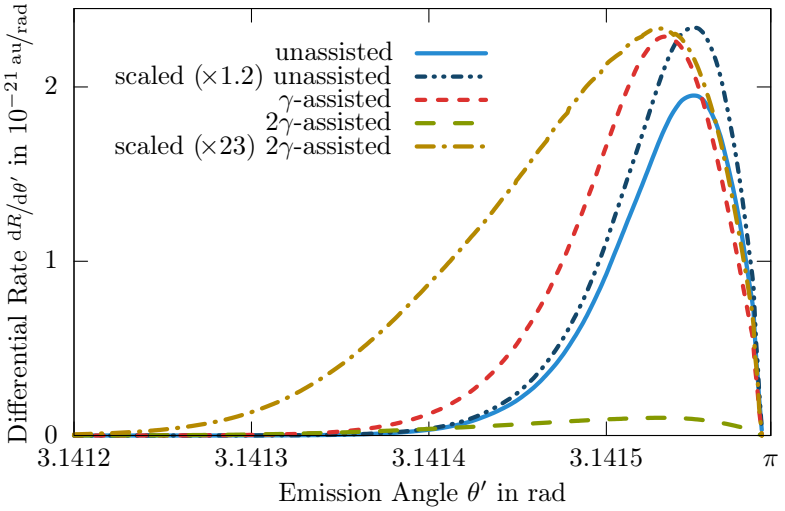

(b) Laboratory frame (cf. Fig. 4.9(b))

Figure 4.11.: *Comparison of angular-differential pair-creation rates of the unassisted, the singly and the doubly γ-assisted process in the nuclear rest frame and the laboratory frame – These figures should be understood as higher-order versions of those indicated in their respective caption (cf. Fig. 4.9). They are obtained for the parameters in Eqs. (4.28) at the intensity parameter $\xi_2 = 1$. Scaled versions of the unassisted and the doubly assisted spectrum have been added for better comparability. In both frames of reference, the more assisting photons participate, the wider the respective distribution becomes and the more the peak position is shifted towards larger (smaller) angles in the nuclear rest frame (laboratory frame).*

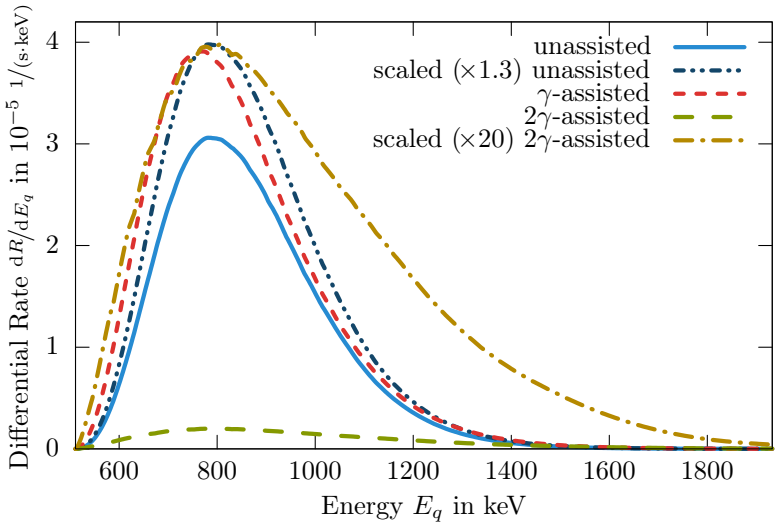

(a) Nuclear rest frame (cf. Fig. 4.7(b))

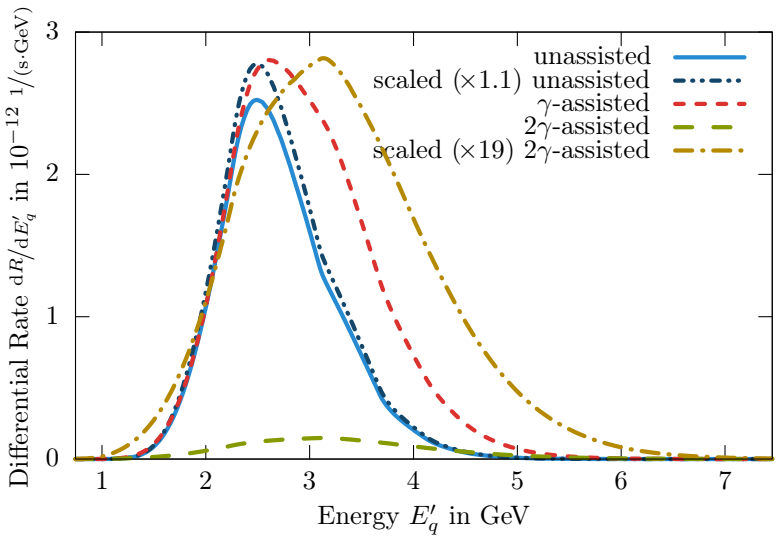

(b) Laboratory frame (cf. Fig. 4.8)

Figure 4.12.: *Comparison of energy-differential pair-creation rates of the unassisted, the singly and the doubly γ-assisted process in the nuclear rest frame and the laboratory frame – These figures should be understood as higher-order versions of those indicated in their respective caption. They are obtained for the parameters in Eqs. (4.28) at the intensity parameter $\xi_2 = 1$. Scaled versions of the unassisted and the doubly assisted spectrum have been added for better comparability. In both frames of reference, the more assisting photons participate, the wider the respective distribution becomes. Furthermore, in the laboratory frame, the more the peak position is shifted towards larger energies.*

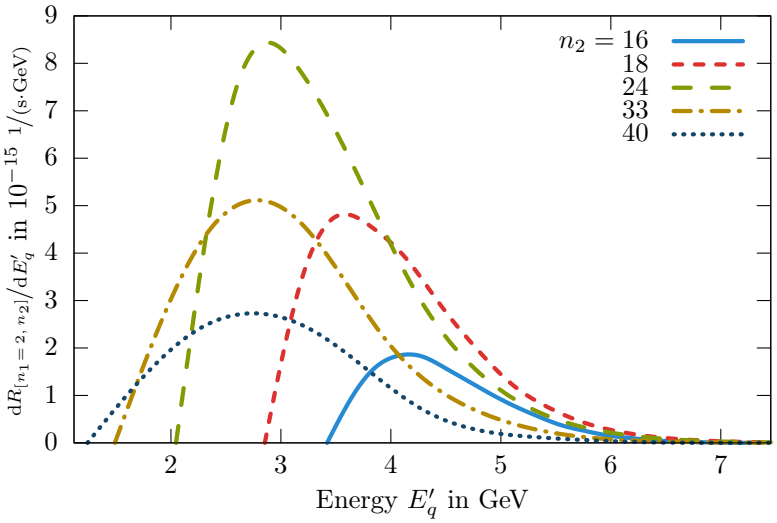

Figure 4.13.: *Comparison of exemplary energy-differential partial pair-creation rates of the doubly γ-assisted process in the laboratory frame – The individual contributions to the total rate (cf. Eq. (4.7)) cover differing energy ranges since the total energy involved depends on the number of absorbed photons. Note that, the more photons are absorbed, the lower the peak energy of the emitted particle. This may be unexpected at first, but is due to the nature of the Lorentz transformation. In the nuclear rest frame the order is reversed.*

The energy-differential pair-creation rates of the three processes are compared in Fig. 4.12 for both frames of reference. In the nuclear rest frame, the broadening found above is again visible for the doubly assisted process. However, the difference betweens the widths of the unassisted and the singly assisted process is almost negligible. This might be explained by the fact that even with a single highly energetic photon of 490 keV assisting the process there are still 30 photons from the low-energetic mode needed to overcome the pair-creation threshold. In the laboratory frame both effects, the peak position shift and the broadening of the distribution, are again clearly visible. This stronger pronunciation of the modifications may again be attributed to the mix of the energy and the momentum z-coordinate by the Lorentz transformation, which imparts the effects on the angular spectrum onto the energy distribution.

Concluding this section it is worth pointing out that in the laboratory frame shown in Fig. 4.12(b), the energetic spectra of the three processes exhibit prominent differences in their curve shapes. These are also visible in Fig. 4.8, the corresponding figure for the first-order assisted process. They may be attributed

to the underlying sub-processes $[n_1, n_2]$, which all have a different allowed radial momentum and, thus, energy range (cf. App. E). The total photon energy, as given in Eq. (2.64), differs for each sub-process leading to a relative shift on the energy axis in the laboratory frame. In the sum over n_2 (cf. Eq. (4.7)) the structure of the curve shapes appears. The partial rates $R_{[n_1,n_2]}$ of the doubly assisted process ($n_1 = 2$) are shown for five exemplary values of n_2 in Fig. 4.13.

Chapter 5.

Conclusion

In the scope of this thesis, $e^- e^+$ pair creation in the vicinity of a nucleus induced by bichromatic or bimodular laser fields has been studied. In the subsequent sections, the results for the two studied cases, laser pairs with commensurable and incommensurable frequencies, are summarized. Furthermore, an the prospects of an experimental realization of the proposed pair-creation schemes is given, as well as an outlook on the continuation of the theoretical investigation.

5.1. Commensurable Frequencies

In the first part of the presented results, the influence of quantum interference between two commensurable laser modes, with both intensity parameters $\xi_i \ll 1$, on the non-linear Bethe–Heitler effect has been investigated. Particularly, total and differential rates of electron-positron pair creation in the multiphoton regime have been studied under variation of various parameters.

To allow the distinction between different types of contributing sub-processes for a given set of parameters, individual terms in a four-index sum were discussed in form of differential partial rates. This sum has been introduced via a Fourier expansion of all periodic functions in the squared pair-creation amplitude. The actual physical observables are gained by performing these four sums and an appropriate number of integrations in momentum space. This leads to differential rates and total rates, which are also studied for interference effects.

In a variation of the energy of a single photon and thus the number of photons needed to provide the energy to overcome the pair-creation threshold, only laser pairs with even minimal photon numbers for both modes were found to show contributions from interference terms. Of those, laser pair $(2, 4)$ yields the strongest interference contribution and has thus been used as the prime example for the subsequent considerations. Here it is worth noting that, laser

combination $(1, 2)$ with lower photon number but identical frequency ratio does not feature interference.

The next step, a variation of the total photon energy for a fixed number of photons, corresponds to a variation of the excess energy available as kinetic energy for the created particles. Here, the interference has been found to be strongest near the pair-creation threshold. However, strong modifications of the curve shape of the angular distribution occur for higher energies.

The different curve shapes for the various energies lead to differing behaviour once the variation of the relative phase between the two laser modes, i.e., the lateral offset between the peaks of the two laser wave amplitudes, is considered. For the lower energies, phase variation mainly manifests itself in a raised (lowered) summed-up differential rate and thus eventually in an increase (decrease) in the total rate. For the altered shape of the angular distribution found for higher energies, the peak position shift along the emission angle axis is more emphasized. The latter effects have been explained within an intuitive picture based on the phase dependence of the peak amplitude of the electric field. The found connection is – with a slight modification – also applicable for laser pairs with higher number of involved photons, in particular laser pair $(4, 8)$. However, for these laser pairs the number of contributing terms increases significantly, making the results less intuitive.

Furthermore, some results have been transferred to the laboratory frame, where both interference effects – peak height and position change – are found as well. However, the shift of the main emission angle is over a much narrower region, as the whole angular spectrum is Lorentz contracted.

Finally, for two modes with identical frequency, the dependence of the pair-production rate on the ellipticity of the combined laser wave has been studied. This dependence shows the expected behaviour when the total field intensity is held constant, i.e., when the intensity of one mode is decreased, while that of the other is increased. Thus, in the linearly polarized case the peak amplitude is higher than in the respective case of circular polarization, leading to an increasing pair-creation rate when traversing from the former to the latter. In contrast, interesting features arise when the maximum field amplitude is kept fixed instead. In this case the intensity of one mode is kept constant and the other mode is gradually turned off. The field amplitude in the circularly polarized case is constant, while it varies sinusoidally in the linear case. Thus, the rate would be expected to decrease monotonously in a variation from the former to the latter. However, for some parameter sets – instead of such a simple ellipticity dependence – a minimum is found in this variation. Beyond this ellipticity where the rate is lowest, the rate rises again towards linear polarization.

5.2. Incommensurable Frequencies

The second part of the presented results begins with a comparison of commensurable and incommensurable frequencies by continuously varying the frequency ratio of the two laser modes. This further solidifies the extraordinary role of commensurable frequencies with even minimal photon numbers, as these show strong enhancement or decrease due to the interference contribution.

Additionally, it is discussed that instead of the differentiation between commensurable and incommensurable frequencies one should distinguish whether the frequency ratio is comprised of small or large integers. Therefore, to complement the first part, the focus of this part lies on largely differing frequencies. Particularly, the influence of an assisting highly energetic photon, with an energy just below the pair-creation threshold, on the non-linear Bethe–Heitler process by a highly intense laser in the non-perturbative regime is studied.

The two studied cases are chosen such that for a fixed laser combination in the laboratory the adjustment of the Lorentz factor of the nucleus switches from a regime where the parameters of a previous fully analytical study [41], which are required to be small therein, vary from being relatively small to being approximately unity. The results found for the total pair-creation rate coincide very well in the former and deviate in the latter case. Nevertheless, a Schwinger-like dependence of the pair-creation rate on the intensity of the laser is found in both cases. By studying a wide range of parameters, an empirical extension to the aforementioned analytical expression for the total pair-creation rate is obtained, which is applicable when the respective parameters of the analytical theory are not very small.

When the assisted and the unassisted process are compared, one finds that the total pair-creation rate is dominated by the assisted case for lower intensities of the strong laser. For higher intensities the opposite is found and the unassisted case becomes the stronger of the two. Furthermore, the employed theoretical framework allows to examine the underlying differential spectra. This is done for the emission angle and the energy of the created particles, where the latter is linked to the radial momentum coordinate. One finds that, for both coordinates the distribution is broadened for the assisted case. Additionally, the main emission direction is shifted from just above 0° to approximately 45° in the nuclear rest frame. In the laboratory frame, this shift is from angles just below 180° to slightly smaller angles, due to the contraction of the spectrum and the reversal of the propagation direction of the created particles imparted by the Lorentz transform.

Finally, the assisted process of next-higher order is studied. For two assisting highly energetic photons, results consistent with those for the single assisting photon are found. For lower intensities of the assisted mode one finds that, the more assisting photons are involved, the stronger the contribution to the total rate from the respective process is. Conversely, for the highest examined intensities, the unassisted case dominates. Again, the energetic and the angular distributions show a broadening for the processes with assisting photon(s), just as the latter shows the shift towards larger angles. Both effects get stronger, as the number of involved assisting photons rises.

5.3. Experimental Realization

In principle, an experimental realization of the proposed pair-creation schemes would rely on two counterpropagating components: a laser providing an intense beam of high-energetic photons, and a relativistic nuclear beam. The LHC, today's prime example for a source of the latter, has already been mentioned. The main objectives of this machine are the search for the Higgs boson [55, 62, 66, 67] and for physics beyond the Standard Model (e.g., supersymmetrie [1] and strings [94]). However, once its primary tasks have been accomplished, other research domains – such as pair-creation – might become interesting for the LHC. Even more so, now that the Higgs boson has been discovered [10, 39]. Nevertheless, it should be noted that there exist several other particle accelerators (an overview may be found in Ref. [21]) that, while not providing Lorentz factors as high as the LHC, would still be well suited for pair-creation experiments. Particularly, when combined with an X-ray laser source – such as an FEL – a relativistic proton beam with a Lorentz factor of $\gamma \sim 50$ would be sufficient. The main problem for the realization of these pairings of FELs and ion accelerator facilities is that they both are large in size and located at different places. The HERA (*Hadron-Elektron-Ring-Anlage*) proton accelerator, which is unfortunately defunct since 2007, is a noteworthy example since it shared the site with FLASH at DESY (*Deutsches Elektronen-Synchrotron*).

Pair-creation schemes like the γ-assisted process proposed in Sec. 4.2 are particularly aimed at counter-acting the aforementioned problem by making pair-creation accessible via table-top laser devices. These could in principle be transported to or built at CERN. In this context it should be mentioned that, intensities up to $6 \times 10^{13}\,\mathrm{W/cm^2}$ have been reported for HHG-based light sources [97]. However, that magnitude is not yet commonly reached.

In Sec. 1.4, various laser sources have already been discussed with an emphasis on bichromatic fields. Besides the FELs mentioned there, FLASH with $10^{16}\,\mathrm{W/cm^2}$

[147], LCLS with $10^{18}\,\mathrm{W/cm^2}$ [28], and FERMI, two further FELs situated at RIKEN should be mentioned: SCSS[19] in the XUV regime and SACLA[20] in the X-ray regime. Two hard-X-ray FELs, the SwissFEL at the *Paul Scherrer Institut* in Villigen [122] and the European XFEL (X-ray FEL) at DESY in Hamburg [61], are currently planned and built. Future X-ray FELs are expected to reach up to $10^{21}\,\mathrm{W/cm^2}$ [150].

The most intense laser light sources available today are petawatt-class infrared lasers with an intensity of $\sim 10^{21}\,\mathrm{W/cm^2}$ [16]. For instance, HERCULES[21], PHELIX[22], the Texas Petawatt Laser[23], and the Vulcan laser[24]. Two further light sources currently in planning, ELI[25] and HiPER[26], aim for even higher intensities of $\sim 10^{23}\,\mathrm{W/cm^2}$.

5.4. Outlook

To conclude this thesis, a few remarks on potential expansions and enhancements of the presented theoretical approach are expedient. Furthermore, its applicability to different processes should be briefly discussed.

A natural continuation of the study presented here would be to replace the idealized picture of a laser field as a plane wave of infinite extent with finite laser pulses. The Volkov solutions are usually employed for the former case. However, in the original publication Volkov has already discussed the corresponding solutions for a superposition of many plane waves with differing frequencies [153]. These could be employed to describe a wave packet and, thus, to realize a pulsed laser beam. Furthermore, there exist closed-form expressions for a specific form of an ultra-short single-cycle laser pulse [114].

Another potential area of further development has already been mentioned in Sec. 2.3.4, where the influence of the nuclear charge Z is briefly discussed. Since the Coulomb field of the nucleus is only treated in the lowest order of perturbation theory, the found Z^2-scaling of the pair-creation rate is only valid

[19] SPring-8 (Super Photon Ring – 8 GeV) Compact SASE Source [144]
[20] SPring-8 Angstrom Compact Free-Electron Laser [69]
[21] High Energy Repetitive CUOS (Center for Ultrafast Optical Science) Laser System, at the University of Michigan in Ann Arbor [155].
[22] Petawatt High Energy Laser for Heavy Ion Experiments, at the GSI (*Gesellschaft für Schwerionenforschung*) *Helmholtzzentrum für Schwerionenforschung* in Darmstadt [159].
[23] At the University of Texas in Austin [164].
[24] At Rutherford Appleton Lab in Didcot [161].
[25] Extreme Light Infrastructure [158].
[26] High Power Laser Energy Research [160].

for relatively small nuclear charges. For larger values, the presented treatment has to be extended. One possibility would be to take the next-higher orders of perturbation theory of the interaction between the nucleus and the created particles into account. However, this may not be the best choice as the numerical effort can be expected to grow immensely.

The methods developed in this thesis could also be applied to other relativistic quantum processes in bichromatic laser fields. For instance, laser-induced atomic ionization and e^-e^+ pair creation are well known to exhibit similar characteristics, which is explicable by the fact that the latter may be interpreted as "ionization from the Dirac sea" [106]. With some modifications, the theoretical approach presented here could also be used to examine ionization of (hydrogen-like) atoms in bichromatic fields of high intensity. Atomic ionization in the relativistic regime is currently studied both theoretically [79, 80] and experimentally [44, 45] complementing the available comprehensive knowledge about non-relativistic laser-induced ionization [99]. As the previous studies have been restricted to monochromatic laser fields, the question arises how processes of relativistic ionization are modified by the presence of a second laser mode. Based on the results presented in this thesis, characteristic quantum-interference and rate-enhancement effects are to be expected for ionization processes in bichromatic laser fields, as well. Moreover, these could be probed by modern experimental techniques.

Appendix A.

Units

Throughout this thesis, several systems of measurement are used. The first is the *International System of Units* (abbreviated SI from French: *Le Système international d'unités*). The second is the system of *atomic units* (au), which is defined in terms of several universal physical constants such that quantities on the atomic scale a represented in terms of properties of nature. Therefore, au are a set of *natural units*. Furthermore, they are based on the *Gaussian unit system* commonly used in electrodynamics. In contrast to SI, which is based on the units[27] metre, kilogram, second, and ampere (MKSA), Gaussian units are a CGS (centimetre-gram-second) system. As they are the most commonly used variant of a CGS system, Gaussian units are often referred to as *the* CGS system. The main difference between SI and Gaussian units is the "lack" of a base unit associated with electrical phenomena in the latter. While SI allows the ampere the same defining status as metre, kilogram, and second, the unit of the electric current, the franklin, is a derived unit in CGS.

A.1. Atomic Units

The defining constants are chosen to represent the dimensions of the electronic motion in an atom. This is emphasized by the strong connection between au and the ground state of hydrogen as described by the Bohr model. There exist two commonly used variants of au[28]: Rydberg[29] and Hartree units. They differ in their respective unit of mass and charge, and are named after their respective

[27] Actually, SI is based on seven units. The remaining ones are candela, kelvin, and mole.

[28] Besides, the abbreviation au might lead to confusion with *astronomical* or *arbitrary units*. Particularly, the latter are therefore not used in this work.

[29] Rydberg units are gained by setting $2m_e = {}^{e^2}/_2 = \hbar = {}^1/_{4\pi\epsilon_0} \stackrel{!}{=} 1$. The resulting set of units is sometimes abbreviated aru (*atomic Rydberg units*) instead of au. The eponymous unit of energy, $\mathrm{Ry} = {}^H/_2 \simeq 13.6\,\mathrm{eV}$, corresponds to the energy required to ionize atomic hydrogen.

Constant	Symbol	Dimension	SI value [103]
Electron rest mass	m_e	mass	$9.109 \times 10^{-31}\,\mathrm{kg}$
Elementary charge	e	charge	$1.602 \times 10^{-19}\,\mathrm{C}$
Reduced Planck constant	$\hbar = {}^{h}/_{2\pi}$	action	$1.054 \times 10^{-34}\,\mathrm{J\,s}$
Electrostatic constant	${}^{1}/_{4\pi\epsilon_0}$	inverse ϵ_0	$8.987 \times 10^{9}\,{}^{\mathrm{V\,m}}/_{\mathrm{A\,s}}$

Table A.1.: *Numerical values of the four fundamental atomic units in SI units – Here, the vacuum permittivity* $\epsilon_0 = 8.854 \times 10^{-12}\,{}^{\mathrm{A\,s}}/_{\mathrm{V\,m}}$ *is used.*

unit of energy. In this work, Hartree units are used, which are gained by setting the electron mass, the elementary charge, the reduced Planck constant and the electrostatic constant to unity:

$$m_e = e = \hbar = \frac{1}{4\pi\epsilon_0} \stackrel{!}{=} 1. \tag{A.1}$$

An overview of the numerical values of these constants in SI units is given in Tab. A.1. Note that, in this convention the speed of light c has a value different from unity. It can be inferred from the dimensionless fine-structure constant

$$\alpha = \frac{e^2}{4\pi\epsilon_0\,\hbar c} \simeq \frac{1}{137.036}. \tag{A.2}$$

Dimensionless constants retain their value independent of the unit system. Therefore, one finds:

$$c = \frac{1}{\alpha} \approx 137. \tag{A.3}$$

To be more precise, one may write $c \approx 137\,\mathrm{au}$. However, the au suffix is often dropped if all quantities are given in atomic units. A full set of units may be derived from the fundamental atomic units above, a subset of which is given in Tab. A.2. The au of time is of particular importance, as the results presented herein are usually pair-creation rates with the dimension particles per time.

A.2. Intensity

A particularly important unit is that of the intensity I. It has the dimension of a radiative flux, which is ${}^{\mathrm{W}}/_{\mathrm{m}^2}$ in SI units. However, as focus sizes of lasers are usually rather small the more commonly used unit is ${}^{\mathrm{W}}/_{\mathrm{cm}^2}$. The corresponding unit in atomic units is gained from that of the electric field strength via the Poynting vector

$$\mathbf{S} = \epsilon_0 c\,(\mathbf{E} \times \mathbf{B})\,, \tag{A.4}$$

Constant	Symbol	Dimension	SI value [103]	Alternative
Hartree	$H = m_e\alpha^2c^2$	energy	4.360×10^{-18} J	27.211 eV
Bohr radius	$a_0 = \hbar/m_e\alpha c$	length	5.292×10^{-11} m	0.529 Å
	$\hbar/H$	time	2.419×10^{-17} s	
	$\mathscr{E}_0 = H/ea_0$	electric field	5.142×10^{11} V/m	

Table A.2.: *Numerical values of some derived atomic units – For two values a commonly used alternative representation is given. Note that, the atomic unit of time corresponds to the time an electron needs for one revolution on the ground-state orbit of hydrogen according to the Bohr model. Similarly, the atomic unit of the electric field strength is felt by such an electron.*

where $\mathbf{E} = -\frac{1}{c}\frac{\partial \mathbf{A}}{\partial t}$ is the electric field and $\mathbf{B} = \nabla \times \mathbf{A}$ is the magnetic field associated with the plane wave potential $\mathbf{A}$ as in Eq. (2.5). For the directions holds $\mathbf{A} \parallel \mathbf{E} \perp \mathbf{B}$ and $\boldsymbol{\kappa} = \frac{c}{\omega}\mathbf{k} = \mathbf{E} \times \mathbf{B}$, therefore it is sufficient to consider only the absolute values:

$$A = a\cos(\omega t - \mathbf{k}\cdot\mathbf{r}), \tag{A.5}$$

$$\mathscr{E} = \mathscr{E}_0\sin(\omega t - \mathbf{k}\cdot\mathbf{r}), \tag{A.6}$$

$$\mathscr{B} = \mathscr{B}_0\sin(\omega t - \mathbf{k}\cdot\mathbf{r}), \tag{A.7}$$

with $\mathscr{B}_0 = \mathscr{E}_0 = -a\frac{\omega}{c}$. The intensity is then given by the averaged absolute value of the Poynting vector:

$$I = \overline{|\mathbf{S}|} = \frac{\epsilon_0 c}{2}\mathscr{E}_0^2, \tag{A.8}$$

where the factor $1/2$ stems from the average of the squared sine. Employing $[\mathscr{E}_0]$ from Tab. A.2 the SI value can be given:

$$[I] \simeq 3.509 \times 10^{16}\ \mathrm{W/cm^2}. \tag{A.9}$$

In atomic units, where $\epsilon_0 = 1/4\pi$, the conversion formula

$$[I] = \frac{c}{8\pi}[\mathscr{E}_0]^2 \tag{A.10}$$

can be used. Here it is worth pointing out that, $[I]$ is not unity when the definitions from Eq. (A.1) are inserted. Therefore, it is not an atomic unit in the formal sense.

In the theoretical framework applied in this work, the intensity is usually given by means of the intensity parameter ξ defined in Eq. (2.7), which can be rewritten as

$$\xi = \frac{e}{mc}\frac{1}{\sqrt{2}}\frac{\mathscr{E}_0}{\omega}. \tag{A.11}$$

This allows to give a conversion formula similar to Eq. (A.8) for the intensity parameter:

$$I = \frac{m^2}{e^2}\epsilon_0 c^3 \omega^2 \xi^2 \tag{A.12}$$

$$= \frac{1}{4\pi} c^3 \omega^2 \xi^2. \tag{A.13}$$

A.3. Electronvolt

As for most physical quantities, for those with the dimension energy several representations are available. Besides the SI unit Joule (J) and the atomic unit Hartree (H), the electronvolt (eV) is commonly used. It is defined as the amount of energy gained by moving an elementary charge e across an electric potential difference of 1 V:

$$e \cdot 1\,\mathrm{V} = 1\,\mathrm{eV} \simeq 1.602 \times 10^{-19}\,\mathrm{J}. \tag{A.14}$$

Furthermore, quantities that are not energies are regularly expressed in eV by applying the mass-energy equivalence

$$E = mc^2, \tag{A.15}$$

with the relativistic mass $m = \gamma m_0$, the rest mass m_0, the Lorentz factor $\gamma = 1/\sqrt{1-\beta^2}$, and the velocity in units of the speed of light in vacuum $\beta = v/c$. For instance, the electron rest mass m_e is often expressed as $m_e = 511\,\mathrm{keV}/c^2$, in which the factor $1/c^2$ is sometimes dropped.

Similarly, from the relation between the frequency ω and the energy of a photon

$$E = \hbar\omega \tag{A.16}$$

the reduced Planck constant $\hbar$ is often dropped, leading to frequencies given in electronvolt.

Finally, for the wavelength λ and the energy of a photon

$$E = \hbar\omega = \frac{hc}{\lambda}, \tag{A.17}$$

with the Planck constant $h = 2\pi\hbar = 6.626 \times 10^{-34}\,\mathrm{J\,s}$, the convenient conversion formula

$$E[\mathrm{eV}] \approx \frac{1240}{\lambda[\mathrm{nm}]} \tag{A.18}$$

can be found.

A.4. Ångström

The atomic unit of length, the Bohr radius a_0, provides a measure for lengths on the atomic scale. However, another unit is also commonly employed, the Ångström (Å):

$$1\,\text{Å} = 10^{-10}\,\text{m} \approx 2a_0. \tag{A.19}$$

While a_0 describes the radius of lowest orbit in hydrogen, 1 Å may be understood as the corresponding diameter.

Appendix B.

Notation

In this appendix a few short remarks on the notation applied throughout this thesis shall be made. In particular, the employed conventions of the Einstein summation, the inner products of three- and four-vectors, the Dirac matrices, and the rounding functions floor and ceiling are introduced.

B.1. Einstein Summation

For brevity, the summation over indices appearing twice in a product is implied. The standard convention is followed, which means that Latin letters count only spatial dimensions, e.g.,

$$i = (1, 2, 3), \tag{B.1}$$

while Greek letters also count time as the zeroth coordinate, e.g.,

$$\mu = (0, 1, 2, 3). \tag{B.2}$$

B.2. Inner Products

Inner products are written either as Einstein summation, as scalar product (in the three-dimensional case), or as bilinear form (in the four-dimensional case):

$$a_i b^i = \sum_i a_i b_i = \mathbf{a}\cdot\mathbf{b}, \tag{B.3}$$

$$a_\mu b^\mu = \sum_\mu a_\mu b^\mu = a_0 b_0 - \mathbf{a}\cdot\mathbf{b} = \langle ab \rangle , \tag{B.4}$$

with the four-vectors $a = (a_0, \mathbf{a})$ and $b = (b_0, \mathbf{b})$ and the (three-)vectors $\mathbf{a} = (a_1, a_2, a_3)$ and $\mathbf{b} = (b_1, b_2, b_3)$

Note that, here covariant four-vectors $a_\mu = (a_0, a_1, a_2, a_3)$ and contravariant four-vectors $a^\mu = (a^0, a^1, a^2, a^3) = (a_0, -a_1, -a_2, -a_3)$ are used. They are connected by the metric tensor with the signature $(+,-,-,-)$,

$$g_{\mu\nu} = g^{\mu\nu} = \begin{pmatrix} 1 & 0 & 0 & 0 \\ 0 & -1 & 0 & 0 \\ 0 & 0 & -1 & 0 \\ 0 & 0 & 0 & -1 \end{pmatrix}, \tag{B.5}$$

via the relation

$$a_\mu = g_{\mu\nu} a^\nu. \tag{B.6}$$

B.3. Dirac Matrices

The Dirac γ-matrices are defined via the anticommutator

$$\{\gamma_\mu, \gamma_\nu\} = \gamma_\mu\gamma_\nu + \gamma_\nu\gamma_\mu = 2g_{\mu\nu}. \tag{B.7}$$

They are connected to the Pauli matrices

$$\sigma_1 = \begin{pmatrix} 0 & 1 \\ 1 & 0 \end{pmatrix},\ \sigma_2 = \begin{pmatrix} 0 & -\mathrm{i} \\ -\mathrm{i} & 0 \end{pmatrix},\ \text{and}\ \ \sigma_3 = \begin{pmatrix} 1 & 0 \\ 0 & -1 \end{pmatrix}, \tag{B.8}$$

via the $\boldsymbol{\alpha} = (\alpha_i)$ and β matrices

$$\alpha_i = \begin{pmatrix} 0 & \sigma_i \\ \sigma_i & 0 \end{pmatrix}\ \text{and}\ \ \beta = \begin{pmatrix} \mathbb{1} & 0 \\ 0 & -\mathbb{1} \end{pmatrix}, \tag{B.9}$$

by $\gamma_0 = \beta$ and $\gamma_i = \beta\alpha_i$. The four resulting matrices are usually collected in an object of the form of a four-vector: $\gamma = (\gamma_\mu)$. Products of four-vectors a with this γ are then treated as inner products. Furthermore, a convenient notation for these particular inner products is the *Feynman slash notation*:

$$\not{a} = \langle \gamma a \rangle = \gamma_\mu a^\mu. \tag{B.10}$$

B.4. Floor and Ceiling

Due to the quantized nature of photons, it is often convenient to employ rounding functions to obtain integer photon numbers from energy ratios.

The floor and ceiling functions map a real number to the largest previous or the smallest following integer, respectively. They are commonly denoted by symbols derived from the older *Gaussian bracket*, a notation for the floor function using square brackets.

Formally, for a real number x, $\text{floor}(x) = \lfloor x \rfloor$ is the largest integer not greater than x, while $\text{ceiling}(x) = \lceil x \rceil$ is the smallest integer not less than x:

$$\lfloor x \rfloor = \max\{k \in \mathbb{Z} \mid k \leq x\}, \tag{B.11}$$

$$\lceil x \rceil = \min\{k \in \mathbb{Z} \mid k \geq x\}. \tag{B.12}$$

Appendix C.

Volkov Wave Functions

For an electron (or a positron) interacting with the field of an electromagnetic plane wave in vacuum the Dirac equation may be solved exactly. This leads to the so-called Volkov solutions, which were first derived in 1935 [153]. A brief overview of this derivation is given in the following (cf. also Ref. [30]).

Instead of Eq. (2.1), the corresponding second-order equation

$$\left(\mathrm{i}\hbar\not{\partial} + \frac{e}{c}\not{A} + mc\right)\left(\mathrm{i}\hbar\not{\partial} + \frac{e}{c}\not{A} - mc\right)\Psi = 0 \tag{C.1}$$

may be used as starting point. Here, the four-potential is only required to fulfil $A = A(\eta)$ and $\langle kA\rangle = 0$. A specific potential can be found in Eq. (2.5). With the abbreviation $A' = \frac{\partial A}{\partial \eta}$, this can be rewritten as

$$\left(-\hbar^2\partial^2 + 2\mathrm{i}\hbar\frac{e}{c}\langle A\partial\rangle + \mathrm{i}\hbar\frac{e}{c}\not{k}\not{A}' + \frac{e^2}{c^2}A^2 - m^2c^2\right)\Psi = 0. \tag{C.2}$$

In the wave function, the dependence on the product $\langle px\rangle$ may be separated from the remaining wave function $\psi_p(\eta)$, which depends on the space-time coordinate x only in form of the phase coordinate $\eta = \langle kx\rangle$. This is achieved by employing the ansatz

$$\Psi = \mathrm{e}^{-\frac{\mathrm{i}}{\hbar}\langle px\rangle}\psi(\eta), \tag{C.3}$$

wherein p is the four-momentum with $p^2 = m^2c^2$. Upon insertion of this ansatz into Eq. (C.2), one finds

$$2\mathrm{i}\hbar\langle kp\rangle\,\psi' + \left(2\frac{e}{c}\langle pA\rangle + \mathrm{i}\hbar\frac{e}{c}\not{k}\not{A}' + \frac{e^2}{c^2}A^2\right)\psi = 0, \tag{C.4}$$

which can be integrated employing *separation of variables*[30] leading to

$$\psi = N\exp\left(\frac{\mathrm{i}e}{\hbar c\langle kp\rangle}\int^{\eta}\left[\langle pA(\tilde\eta)\rangle + \frac{e}{2c}A^2(\tilde\eta)\right]\mathrm{d}\tilde\eta\right)\exp\left(-\frac{e}{2c\langle kp\rangle}\not{k}\not{A}\right)w, \tag{C.5}$$

[30] A differential equation of the form $\dot x = \lambda x$ is written as $\frac{\mathrm{d}x}{x} = \lambda\,\mathrm{d}t$, such that both sides may be integrated independently, leading to $\ln(x) = \lambda t + c$. After applying the exponential, the integration constant c turns into a normalizer $x_0 = \exp(c)$ such that $x = x_0\exp(\lambda t)$.

with the normalizer N and the spinor w. Note that, the lower limit of the integral is not necessary, as it would only contribute a constant offset to the phase coordinate. The second exponential is independent of η. Any term of its series expansion with an order of two or higher vanishes due to $\langle kA\rangle = k^2 = 0$:

$$(\not{k}\not{A})^2 = 2\langle kA\rangle \not{k}\not{A} - \not{k}^2\not{A}^2 = -k^2A^2 = 0, \tag{C.6}$$

employing the rules from App. D. Therefore, one can simplify:

$$\exp\left(-\frac{e}{2c\langle kp\rangle}\not{k}\not{A}\right) = \mathbb{1} - \frac{e}{2c\langle kp\rangle}\not{k}\not{A}. \tag{C.7}$$

The spinor w is identified with the free Dirac spinor $u_{p,s}$ by the requirement that the solution found here has to correspond to that of a free electron with momentum p and spin s once the external field is turned off ($A \to 0$).

In the final expression for the Volkov solution

$$\Psi^{(-)}_{p_-,s_-} = N_- \left(\mathbb{1} - \frac{e\not{k}\not{A}}{2c\langle kp_-\rangle}\right) \exp\left(\frac{\mathrm{i}}{\hbar}S^{(-)}\right) u^{(-)}_{p_-,s_-} \tag{C.8}$$

with the action

$$S^{(-)} = -\langle xp_-\rangle + \frac{e}{c\langle kp_-\rangle}\int^{\eta}\left[\langle A(\tilde{\eta})p_-\rangle + \frac{e}{2c}A^2(\tilde{\eta})\right]\mathrm{d}\tilde{\eta} \tag{C.9}$$

it is indicated by the superscript $(-)$ that this result describes an electron. Note that, this distinction extends to several other quantities as denoted by the subscripted particle charge. The complementary Volkov solution for the positron is gained by replacing

$$p_- \to -p_+ \tag{C.10}$$

and all other subscripts $-$ with $+$, as well as all superscripts $(-)$ with $(+)$. The two solutions can be combined into the compact expression given in Eq. (2.3).

Finally, it should be noted that the requirement of the transition to the solution of a free particle for vanishing external field is fulfilled as

$$\lim_{A\to 0}\Psi^{(\pm)}_{p_\pm,s_\pm} = N_\pm \exp\left(\pm\frac{\mathrm{i}}{\hbar}\langle xp_\pm\rangle\right) u^{(\pm)}_{p_\pm,s_\pm} \tag{C.11}$$

corresponds to $u^{(\pm)}$ in momentum space.

Appendix D.

Spin Sum and Traces of Slashed Quantities

The spin sum from Eq. (2.55), which occurs when a rate is calculated from the squared transition amplitude, may be rewritten as a trace of a product of slashed quantities. This is possible due to the two relations [24]

$$\sum_{s_\pm} u_\mu^{(\pm)} \bar{u}_\nu^{(\pm)} = \left(\frac{\not{p}_\pm \mp c}{2c} \right)_{\mu\nu}, \tag{D.1}$$

with $\bar{u} = u^\dagger \gamma_0$.

The aforementioned spin sum is a double sum over a 4×4 matrix Γ containing the slashed quantities. Using Eq. (D.1) in the first two steps, together with the abbreviation $\bar{\Gamma} = \gamma_0 \Gamma^\dagger \gamma_0$, it may be transformed as follows:

$$\begin{aligned}
\sum_{s_+,s_-} \left| \bar{u}^{(-)} \, \Gamma \, u^{(+)} \right|^2 &= \sum_{s_+,s_-} \bar{u}_\mu^{(-)} \, \Gamma_{\mu\nu} \, u_\nu^{(+)} \; \bar{u}_{\nu'}^{(+)} \, \bar{\Gamma}_{\nu'\mu'} \, u_{\mu'}^{(-)} \\
&= \sum_{s_-} \bar{u}_\mu^{(-)} \underbrace{\Gamma_{\mu\nu} \left(\frac{\not{p}_+ - c}{2c} \right)_{\nu\nu'} \bar{\Gamma}_{\nu'\mu'}}_{= \left(\Gamma \frac{\not{p}_+ - c}{2c} \bar{\Gamma} \right)_{\mu\mu'}} u_{\mu'}^{(-)} \\
&= \left(\Gamma \, \frac{\not{p}_+ - c}{2c} \, \bar{\Gamma} \right)_{\mu\mu'} \left(\frac{\not{p}_- + c}{2c} \right)_{\mu'\mu} \\
&= \mathrm{tr} \left(\Gamma \, \frac{\not{p}_+ - c}{2c} \, \bar{\Gamma} \, \frac{\not{p}_- + c}{2c} \right),
\end{aligned} \tag{D.2}$$

where $\mathrm{tr}(A) = \sum_i A_{ii}$ denotes the trace of a matrix A. The trace is a linear mapping, which means that additivity and homogenity are fulfilled:

$$\mathrm{tr}(A + B) = \mathrm{tr}(A) + \mathrm{tr}(B) \tag{D.3a}$$

$$\mathrm{tr}(cA) = c \, \mathrm{tr}(A) \tag{D.3b}$$

for the matrices A and B, and the scalar c.

Traces of slashed quantities may then be evaluated by applying a few rules derived from the defining properties of the γ-matrices (cf. Eq. (B.7)):

$$\{\not{a}, \not{b}\} = \not{a}\not{b} + \not{b}\not{a} = 2\, a_\mu b^\mu \tag{D.4a}$$

$$\not{a}\not{a} = a_\mu a^\mu = a^2 \tag{D.4b}$$

$$\mathrm{tr}(\not{a}\not{b}) = 4\, a_\mu b^\mu \tag{D.4c}$$

$$\mathrm{tr}(\not{a}\not{b}\not{c}\not{d}) = 4\,[(a\cdot b)(c\cdot d) - (a\cdot c)(b\cdot d) + (a\cdot d)(b\cdot c)] \tag{D.4d}$$

The occurring factors of 4 stem from the trace of the identity matrix.

The trace is invariant under cyclic permutation or reversal of the order of the matrices. The latter is of interest as the complex conjugate of a product of slashed quantities is reversing the order of the product, thus

$$\mathrm{tr}(\underbrace{\not{a}_1\not{a}_2\ldots\not{a}_n}_{\overline{\not{a}_n\ldots\not{a}_2\not{a}_1}}) = \mathrm{tr}(\not{a}_n\ldots\not{a}_2\not{a}_1) = \mathrm{tr}(\overline{\not{a}_1\not{a}_2\ldots\not{a}_n}), \tag{D.5}$$

wherein $\overline{\not{a}} = \not{a}^\dagger$. Furthermore, the trace of an odd number of slashed quantities vanishes.

Appendix E.

Integration Bounds

The fully differential rate from Eq. (2.44) contains six integrations in momentum space, three spherical coordinates for each of the two created particles. Of these six, one can be performed analytically employing the δ-function introduced in Eq. (2.43), which has the zeroth component of the momentum transfer to the nucleus, as defined in Eq. (2.40), as argument. Thus, it is straightforward to express the radial momentum coordinate of one particle via that of the other, leaving four angular and one radial integration. In order to obtain total rates or rates differential in only one coordinate, the remaining integrations are performed numerically. Therefore, the bounds of the integrations have to be known.

Note that, in the following the symbols m and p will be used for the electron mass and the momentum. In an actual implementation of the theoretical framework employed throughout this thesis, the effective counterparts, m_* and q, have to be used instead (cf. Eqs. (2.16) and (2.11), respectively).

E.1. Nuclear Rest Frame

In the nuclear rest frame, the angular integrations simply cover the full 4π solid angle for each created particle (indicated by the subscript $\pm$):

$$0 \leq \phi_{\pm} < 2\pi, \tag{E.1a}$$

$$0 \leq \vartheta_{\pm} \leq \pi. \tag{E.1b}$$

The remaining radial component, however, must not be integrated until infinity, instead it has a finite upper bound $p_{\max}$:

$$0 \leq p \leq p_{\max}. \tag{E.1c}$$

This upper bound is obtained as follows: The total energy provided by the involved photons E_{ph} has been introduced in Eq. (2.64). Under the assumption that one particle is created at rest, the other particle has the maximum energy

$$E_{\max} = E_{\mathrm{ph}} - mc^2. \tag{E.2}$$

By means of the energy-momentum relation from Eq. (1.6),

$$E_{\max}^2 = (\mathbf{p}_{\max} c)^2 + \left(mc^2\right)^2, \tag{E.3}$$

this can be converted to

$$\begin{aligned} p_{\max} &= |\mathbf{p}_{\max}| \\ &= \frac{1}{c}\sqrt{E_{\max}^2 - \left(mc^2\right)^2} = \frac{E_{\mathrm{ph}}}{c}\sqrt{1 - \frac{2mc^2}{E_{\mathrm{ph}}}}. \end{aligned} \tag{E.4}$$

Furthermore, from this derivation the necessity of the upper momentum limit becomes clear: For one particle with $p_{\max}$, the other particle is created at rest. Thus, for momenta higher than $p_{\max}$, the second particle would have to have less than its rest energy. This obviously must not occur.

E.2. Laboratory Frame

The propagation direction of both, the laser wave and the nucleus, are along the z-axis. Therefore, the Lorentz transformation does not affect the angle measured perpendicular to that axis, and its bounds are unchanged in the laboratory frame, where all coordinates are primed:

$$0 \leq \phi'_{\pm} < 2\pi. \tag{E.5a}$$

The emission angle, on the other hand, is measured with respect to the laser propagation direction and is thus influenced by the Lorentz transformation, just as the radial coordinate:

$$\vartheta'_{\pm,\min} \leq \vartheta'_{\pm} \leq \vartheta'_{\pm,\max}, \tag{E.5b}$$

$$p'_{\min} \leq p' \leq p'_{\max}. \tag{E.5c}$$

In the following derivation of these bounds the subscript $\pm$ for ϑ' is dropped, as the result is applicable for both particles. From the Lorentz transformation

of a four-momentum $p_\mu = (E/c, \mathbf{p})$ with $\mathbf{p} = (p_x, p_y, p_z)$ and $|\mathbf{p}| = p$ along the z-axis,

$$p'_\mu = \begin{pmatrix} E'/c \\ p'_x \\ p'_y \\ p'_z \end{pmatrix} = \begin{pmatrix} \gamma & 0 & 0 & -\beta\gamma \\ 0 & 1 & 0 & 0 \\ 0 & 0 & 1 & 0 \\ -\beta\gamma & 0 & 0 & \gamma \end{pmatrix} p_\mu = \gamma \begin{pmatrix} E/c - \beta p_z \\ p_x \\ p_y \\ -\beta E/c + p_z \end{pmatrix}, \tag{E.6}$$

the maximum energy in the laboratory frame, corresponding to Eq. (E.2),

$$E'_{\mathrm{max}} = \gamma E_{\mathrm{ph}} \left(1 - \frac{mc^2}{E_{\mathrm{ph}}} - \beta \sqrt{1 - \frac{2mc^2}{E_{\mathrm{ph}}}} \right), \tag{E.7}$$

can be calculated. Here, Eqs. (E.2) and (E.4), the Lorentz factor $\gamma = 1/\sqrt{1-\beta^2}$, the velocity in units of the speed of light $\beta = v/c$, and

$$p_z = p \cos(\vartheta) \tag{E.8}$$

have been used, where the latter is maximized for $\cos(\vartheta) = 1$. The minimal energy in any frame is obviously mc^2.

In between this minimal and maximal energy, the momentum in the laboratory frame $\mathbf{p}' = (p'_x, p'_y, p'_z)$, with $p'_z = p' \cos(\vartheta')$ and $p' = |\mathbf{p}'|$, has to be calculated for all potential ϑ' by means of the energy-momentum relation. The corresponding four-momentum is then transformed back to the nuclear rest frame analogously to Eq. (E.6), however with the sign of β switched. This way, the corresponding energy

$$E(p', \vartheta') = \gamma \left(E' + \beta c\, p' \cos(\vartheta') \right) \tag{E.9}$$

is obtained. The allowed p'- and ϑ'-ranges are then found by employing the same condition as in Sec. E.1, i.e.,

$$E(p', \vartheta') \leq E_{\mathrm{max}}, \tag{E.10}$$

with the maximum energy in the nuclear rest frame E_{max} as in Eq. (E.2). Depending on the order of integration, Eq. (E.10) is either evaluated for a given value of ϑ' and the respective allowed p'-range is obtained or vice-versa. Herein, one has to allow for the range to be empty and, consequently, assume a vanishing integral.

In the actual implementation of the integrations used to obtain the results presented throughout this thesis, the variations of E', p', and ϑ' are not performed linearly. Instead of testing the combinations of coordinates stepwise, a *binary*

search[31] is used to reduce the runtime without losing accuracy. However, this is only possible due to the allowed ranges being continuous. That this is indeed the case, can be seen immediately from the nature of the Lorentz transformation, which is only contracting space instead of introducing any subdivision.

[31] Also known as *bisection method* or *interval halving*. Binary search is a search algorithm applicable for sorted data. By testing the middle of an interval, the half of the data in which the result cannot lie is eliminated. This is repeated until the result is found. Instead of a $O(n)$ complexity like the linear approach, a binary search takes $O(\log n)$ steps.[32] Here, this is particularly useful as each step is not a mere lookup in an existing array of data, instead $E(p', \vartheta')$ is only calculated when needed.

[32] The complexity is given in the so-called *Big O* notation, which can be read as "order of". More formally, it is a member of a family of notations called *Bachmann–Landau symbols*.

List of Figures

List of Tables

Bibliography

[1] S. A. Abel *et al.* – "Will the LHC Look into the Fate of the Universe?" in *arXiv e-prints* (2008) ⚭ (see p. 78)

[2] W. Ackermann *et al.* – "Operation of a free-electron laser from the extreme ultraviolet to the water window" in *Nat. Photon.* **1** 6 (2007) on pp. 336–342 ⚭ (see p. 10)

[3] G. D. Adams – "The Absorption of High Energy Quanta. I." in *Phys. Rev.* **74** 11 (1948) on pp. 1707–1711 ⚭ (see p. 4)

[4] E. Akkermans and G. V. Dunne – "Ramsey Fringes and Time-Domain Multiple-Slit Interference from Vacuum" in *Phys. Rev. Lett.* **108** 3 (2012) on p. 030401 ⚭ (see p. 9)

[5] G. Alexander *et al.* – "Observation of Polarized Positrons from an Undulator-Based Source" in *Phys. Rev. Lett.* **100** 21 (2008) on p. 210801 ⚭ (see p. 4)

[6] E. Allaria *et al.* – "Highly coherent and stable pulses from the FERMI seeded free-electron laser in the extreme ultraviolet" in *Nat. Photon.* **6** 10 (2012) on pp. 699–704 ⚭ (see p. 10)

[7] E. Allaria *et al.* – "Two-colour pump–probe experiments with a twin-pulse-seed extreme ultraviolet free-electron laser" in *Nat. Commun.* **4** (2013) ⚭ (see p. 10)

[8] J. Amann *et al.* – "Demonstration of self-seeding in a hard-X-ray free-electron laser" in *Nat. Photonics* **6** 10 (2012) on pp. 693–698 ⚭ (see p. 10)

[9] C. D. Anderson – "The apparent existence of easily deflectable positives" in *Science* **76** 1967 (1932) on pp. 238–239 ⚭ (see p. 4)

[10] ATLAS Collaboration – "Observation of a new particle in the search for the Standard Model Higgs boson with the ATLAS detector at the LHC" in *Phys. Lett. B* **716** 1 (2012) on pp. 1 –29 ⚭ (see p. 78)

[11] S. Augst *et al.* – "Laser ionization of noble gases by Coulomb-barrier suppression" in *J. Opt. Soc. Am. B* **8** 4 (1991) on pp. 858–867 ⚭ (see p. 6)

[12] S. Augustin and C. Müller – "Interference Effects in Bethe–Heitler Pair Creation in a Bichromatic Laser Field" in *Phys. Rev. A* **88** 2 (2013) on p. 022109 ⚮ (see pp. 12, 29)

[13] S. Augustin and C. Müller – "Nonlinear Bethe–Heitler Pair Creation in an Intense Two-Mode Laser Field" in *J. Phys. Conf. Ser.* **497** 1 (2014) on p. 012020 ⚮ (see pp. 12, 29, 46, 51)

[14] H. K. Avetissian *et al.* – "X-ray free electron laser for electron-positron pair production on the nuclei" in *Nucl. Instrum. Methods Phys. Res. Sect. A* **507** 1 - 2 (2003) on pp. 582 –586 ⚮ (see p. 8)

[15] T. Baer and M. Keirstead – *Nd-YAG laser* US Patent 4,653,056 1987 ⚮ (see p. 60)

[16] S.-W. Bahk *et al.* – "Generation and characterization of the highest laser intensities (10^{22} W/cm^2)" in *Opt. Lett.* **29** 24 (2004) on pp. 2837–2839 ⚮ (see p. 79)

[17] C. Bamber *et al.* – "Studies of nonlinear QED in collisions of 46.6 GeV electrons with intense laser pulses" in *Phys. Rev. D* **60** 9 (1999) on p. 092004 ⚮ (see p. 7)

[18] S. Basile, F. Trombetta and G. Ferrante – "Twofold Symmetric Angular Distributions in Multiphoton Ionization with Elliptically Polarized Light" in *Phys. Rev. Lett.* **61** 21 (1988) on pp. 2435–2437 ⚮ (see p. 28)

[19] A. R. Bell and J. G. Kirk – "Possibility of Prolific Pair Production with High-Power Lasers" in *Phys. Rev. Lett.* **101** 20 (2008) on p. 200403 ⚮ (see p. 6)

[20] V. B. Berestetskii, E. M. Lifshitz and L. P. Pitaevskii – *Course of Theoretical Physics* vol. 4: *Relativistic Quantum Theory* First Edition (in Sec. §40) Oxford: Pergamon Press, 1971 (see p. 15)

[21] J. Beringer *et al.* – "Review of Particle Physics" in *Phys. Rev. D* **86** 1 (2012) on p. 010001 ⚮ (see p. 78)

[22] H. A. Bethe and W. Heitler – "On the Stopping of Fast Particles and on the Creation of Positive Electrons" in *Proc. R. Soc. London, Ser. A* **146** 856 (1934) on pp. 83–112 ⚮ (see p. 3)

[23] K. J. Betsch, D. W. Pinkham and R. R. Jones – "Directional Emission of Multiply Charged Ions During Dissociative Ionization in Asymmetric Two-Color Laser Fields" in *Phys. Rev. Lett.* **105** 22 (2010) on p. 223002 ⚮ (see p. 10)

[24] J. D. Bjorken and S. D. Drell – *Relativistic Quantum Mechanics* (in Sec. 7.1) New York: McGraw-Hill, 1964 (see pp. 20, 21, 93)

[25] P. M. S. Blackett and G. P. S. Occhialini – "Some Photographs of the Tracks of Penetrating Radiation" in *Proc. R. Soc. London, Ser. A* **139** 839 (1933) on pp. 699–726 ⌀ (see p. 4)

[26] J. van Bladel – "Lorenz or Lorentz?" in *IEEE Antennas & Propagation Magazine* **33** 2 (1991) on p. 69 ⌀ (see p. 14)

[27] R. Bonifacio, C. Pellegrini and L. Narducci – "Collective instabilities and high-gain regime in a free electron laser" in *Opt. Commun.* **50** 6 (1984) on pp. 373–378 ⌀ (see p. 10)

[28] J. D. Bozek – "AMO instrumentation for the LCLS X-ray FEL" in *Eur. Phys. J. Spec. Top.* **169** 1 (2009) on pp. 129–132 ⌀ (see p. 79)

[29] G. Breit and J. A. Wheeler – "Collision of Two Light Quanta" in *Phys. Rev.* **46** 12 (1934) on pp. 1087–1091 ⌀ (see p. 3)

[30] L. S. Brown and T. W. B. Kibble – "Interaction of Intense Laser Beams with Electrons" in *Phys. Rev.* **133** 3A (1964) on A705–A719 ⌀ (see p. 91)

[31] L. Brugnera *et al.* – "Trajectory Selection in High Harmonic Generation by Controlling the Phase between Orthogonal Two-Color Fields" in *Phys. Rev. Lett.* **107** 15 (2011) on p. 153902 ⌀ (see p. 11)

[32] O. S. Brüning *et al.* – "The LHC Main Ring" in *LHC Design Report* **I** (2004) ⌀ (see pp. 8, 28, 30, 60)

[33] C. Bula and K. T. McDonald – "E-144: The Weizsäcker–Williams Approximation to Trident Production in Electron-Photon Collisions" in *E-144 Internal Notes* **970114** (1997) ⌀ (see p. 8)

[34] S. S. Bulanov *et al.* – "Electron-positron pair production by electromagnetic pulses" in *JETP* **102** 1 (2006) on pp. 9–23 ⌀ (see p. 6)

[35] S. S. Bulanov *et al.* – "Multiple Colliding Electromagnetic Pulses: A Way to Lower the Threshold of e^+ e^- Pair Production from Vacuum" in *Phys. Rev. Lett.* **104** 22 (2010) on p. 220404 ⌀ (see p. 6)

[36] D. L. Burke *et al.* – "Positron Production in Multiphoton Light-by-Light Scattering" in *Phys. Rev. Lett.* **79** 9 (1997) on pp. 1626–1629 ⌀ (see p. 7)

[37] J. Chadwick, P. M. S. Blackett and G. P. S. Occhialini – "Some Experiments on the Production of Positive Electrons" in *Proc. R. Soc. London, Ser. A* **144** 851 (1934) on pp. 235–249 ⌀ (see p. 4)

[38] T. Cheng *et al.* – "Interference in electron-positron creation" in *Laser Phys.* **18** 3 (2008) on pp. 190–196 ⌀ (see p. 9)

[39] CMS Collaboration – "Observation of a new boson at a mass of 125 GeV with the CMS experiment at the LHC" in *Phys. Lett. B* **716** 1 (2012) on pp. 30 –61 ⌀ (see p. 78)

[40] A. Di Piazza, A. I. Milstein and C. Müller – "Polarization of the electron and positron produced in combined Coulomb and strong laser fields" in *Phys. Rev. A* **82** 6 (2010) on p. 062110 ⚮ (see p. 8)

[41] A. Di Piazza *et al.* – "Barrier control in tunneling e^+-e^- photoproduction" in *Phys. Rev. Lett.* **103** 17 (2009) on p. 170403 ⚮ (see pp. 10, 55, 61, 62, 77)

[42] A. Di Piazza *et al.* – "Effect of a strong laser field on electron-positron photoproduction by relativistic nuclei" in *Phys. Rev. A* **81** 6 (2010) on p. 062122 ⚮ (see pp. 10, 55)

[43] A. Di Piazza *et al.* – "Extremely high-intensity laser interactions with fundamental quantum systems" in *Rev. Mod. Phys.* **84** 3 (2012) on pp. 1177–1228 ⚮ (see p. 6)

[44] A. D. DiChiara *et al.* – "Photoionization by an ultraintense laser field: Response of atomic xenon" in *Phys. Rev. A* **81** 4 (2010) on p. 043417 ⚮ (see p. 80)

[45] A. D. DiChiara *et al.* – "Relativistic MeV Photoelectrons from the Single Atom Response of Argon to a 10^{19} W/cm^2 Laser Field" in *Phys. Rev. Lett.* **101** 17 (2008) on p. 173002 ⚮ (see p. 80)

[46] P. A. M. Dirac – "The Quantum Theory of the Electron" in *Proc. R. Soc. London, Ser. A* **117** 778 (1928) on pp. 610–624 ⚮ (see p. 13)

[47] M. Drescher *et al.* – "Time-resolved atomic inner-shell spectroscopy" in *Nature* **419** 6909 (2002) on pp. 803–807 ⚮ (see p. 10)

[48] C. K. Dumlu and G. V. Dunne – "Interference effects in Schwinger vacuum pair production for time-dependent laser pulses" in *Phys. Rev. D* **83** 6 (2011) on p. 065028 ⚮ (see p. 9)

[49] C. K. Dumlu and G. V. Dunne – "Stokes Phenomenon and Schwinger Vacuum Pair Production in Time-Dependent Laser Pulses" in *Phys. Rev. Lett.* **104** 25 (2010) on p. 250402 ⚮ (see p. 6)

[50] G. V. Dunne, H. Gies and R. Schützhold – "Catalysis of Schwinger vacuum pair production" in *Phys. Rev. D* **80** 11 (2009) on p. 111301 ⚮ (see pp. 10, 54)

[51] F. Ehlotzky, K. Krajewska and J. Z. Kamiński – "Fundamental processes of quantum electrodynamics in laser fields of relativistic power" in *Rep. Prog. Phys.* **72** 4 (2009) on p. 046401 ⚮ (see p. 6)

[52] F. Ehlotzky – "Atomic phenomena in bichromatic laser fields" in *Phys. Rep.* **345** 4 (2001) on pp. 175 –264 ⚮ (see p. 9)

[53] A. Einstein – "Ist die Trägheit eines Körpers von seinem Energieinhalt abhängig?" in *Ann. Phys.* **323** 13 (1905) on pp. 639–641 ⚮ (see p. 1)

[54] P. Emma *et al.* – "First lasing and operation of an angstrom-wavelength free-electron laser" in *Nat. Photon.* **4** 9 (2010) on pp. 641–647 ⚮ (see p. 10)

[55] F. Englert and R. Brout – "Broken Symmetry and the Mass of Gauge Vector Mesons" in *Phys. Rev. Lett.* **13** 9 (1964) on pp. 321–323 ⚮ (see p. 78)

[56] L. Euler – "Découverte dun nouveau principe de mécanique" in *Mémoires de l'académie des sciences de Berlin* 6 (1752) on pp. 185–217 ⚮ (see p. 1)

[57] M. V. Fedorov, M. A. Efremov and P. A. Volkov – "Double- and multi-photon pair production and electron-positron entanglement" in *Opt. Commun.* **264** 2 (2006) on pp. 413 –418 ⚮ (see p. 9)

[58] J. Feldhaus – "Flash – the first soft x-ray free electron laser (FEL) user facility" in *J. Phys. B* **43** 19 (2010) on p. 194002 ⚮ (see p. 10)

[59] C. Fey and R. Schützhold – "Momentum dependence in the dynamically assisted Sauter–Schwinger effect" in *Phys. Rev. D* **85** 2 (2012) on p. 025004 ⚮ (see p. 54)

[60] F. Fillion-Gourdeau, E. Lorin and A. D. Bandrauk – "Resonantly Enhanced Pair Production in a Simple Diatomic Model" in *Phys. Rev. Lett.* **110** 1 (2013) on p. 013002 ⚮ (see p. 8)

[61] G. Geloni *et al.* – "Coherence properties of the european XFEL" in *New J. Phys.* **12** 3 (2010) on p. 035021 ⚮ (see p. 79)

[62] G. S. Guralnik, C. R. Hagen and T. W. B. Kibble – "Global Conservation Laws and Massless Particles" in *Phys. Rev. Lett.* **13** 20 (1964) on pp. 585–587 ⚮ (see p. 78)

[63] L.-Y. He *et al.* – "Electron-Positron Pair Production in an Arbitrary Polarized Ultrastrong Laser Field" in *Commun. Theor. Phys.* **58** 6 (2012) on p. 863 ⚮ (see p. 50)

[64] F. Hebenstreit, R. Alkofer and H. Gies – "Particle Self-Bunching in the Schwinger Effect in Spacetime-Dependent Electric Fields" in *Phys. Rev. Lett.* **107** 18 (2011) on p. 180403 ⚮ (see p. 6)

[65] W. Heisenberg and H. Euler – "Folgerungen aus der Diracschen Theorie des Positrons" in *Z. Physik* **98** 11–12 (1936) on pp. 714–732 ⚮ (see p. 3)

[66] P. W. Higgs – "Broken Symmetries and the Masses of Gauge Bosons" in *Phys. Rev. Lett.* **13** 16 (1964) on pp. 508–509 ⚮ (see p. 78)

[67] P. Higgs – "Broken symmetries, massless particles and gauge fields" in *Phys. Lett.* **12** 2 (1964) on pp. 132 –133 ⚮ (see p. 78)

[68] H. Hu, C. Müller and C. H. Keitel – "Complete QED Theory of Multiphoton Trident Pair Production in Strong Laser Fields" in *Phys. Rev. Lett.* **105** 8 (2010) on p. 080401 ⚭ (see p. 8)

[69] Z. Huang and I. Lindau – "Free-electron lasers: SACLA hard-X-ray compact FEL" in *Nat. Photon.* **6** 8 (2012) on pp. 505–506 ⚭ (see p. 79)

[70] A. Ilderton – "Trident Pair Production in Strong Laser Pulses" in *Phys. Rev. Lett.* **106** 2 (2011) on p. 020404 ⚭ (see p. 8)

[71] M. J. A. Jansen and C. Müller – "Strongly enhanced pair production in combined high- and low-frequency laser fields" in *Phys. Rev. A* **88** 5 (2013) on p. 052125 ⚭ (see pp. 10, 54)

[72] M. Jiang *et al.* – "Enhancement of electron-positron pair creation due to transient excitation of field-induced bound states" in *Phys. Rev. A* **87** 4 (2013) on p. 042503 ⚭ (see p. 54)

[73] M. Jiang *et al.* – "Pair creation enhancement due to combined external fields" in *Phys. Rev. A* **85** 3 (2012) on p. 033408 ⚭ (see pp. 9, 54)

[74] L. V. Keldysh – "Ionization in the Field of a Strong Electromagnetic Wave" in *Sov. Phys. JETP* **20** 5 (1965) on pp. 1307–1314 ⚭ (see pp. 6, 7, 28)

[75] R. Kienberger *et al.* – "Atomic transient recorder" in *Nature* **427** 6977 (2004) on pp. 817–821 ⚭ (see p. 10)

[76] B. King, H. Gies and A. Di Piazza – "Pair production in a plane wave by thermal background photons" in *Phys. Rev. D* **86** 12 (2012) on p. 125007 ⚭ (see p. 5)

[77] B. King and H. Ruhl – "Trident pair production in a constant crossed field" in *Phys. Rev. D* **88** 1 (2013) on p. 013005 ⚭ (see pp. 8, 9)

[78] M. Kitzler and M. Lezius – "Spatial Control of Recollision Wave Packets with Attosecond Precision" in *Phys. Rev. Lett.* **95** 25 (2005) on p. 253001 ⚭ (see p. 11)

[79] M. Klaiber, K. Z. Hatsagortsyan and C. H. Keitel – "Fully relativistic laser-induced ionization and recollision processes" in *Phys. Rev. A* **75** 6 (2007) on p. 063413 ⚭ (see p. 80)

[80] M. Klaiber, E. Yakaboylu and K. Z. Hatsagortsyan – "Above-threshold ionization with highly charged ions in superstrong laser fields. II. Relativistic Coulomb-corrected strong-field approximation" in *Phys. Rev. A* **87** 2 (2013) on p. 023418 ⚭ (see p. 80)

[81] O. Klein – "Die Reflexion von Elektronen an einem Potentialsprung nach der relativistischen Dynamik von Dirac" in *Z. Physik* **53** 3–4 (1929) on pp. 157–165 ⚭ (see p. 3)

[82] T. Koffas and A. C. Melissinos – "On the Trident Calculation for E-144" in *E-144 Internal Notes* **980410** (1998) ⚭ (see p. 8)

[83] C. Kohlfürst *et al.* – "Optimizing the pulse shape for Schwinger pair production" in *Phys. Rev. D* **88** 4 (2013) on p. 045028 ⚭ (see p. 6)

[84] K. Krajewska and J. Z. Kamiński – "Correlations in laser-induced electron-positron pair creation" in *Phys. Rev. A* **84** 3 (2011) on p. 033416 ⚭ (see p. 8)

[85] K. Krajewska and J. Z. Kamiński – "Phase effects in laser-induced electron-positron pair creation" in *Phys. Rev. A* **85** 4 (2012) on p. 043404 ⚭ (see p. 9)

[86] K. Krajewska and J. Z. Kamiński – "Symmetries in the nonlinear Bethe–Heitler process" in *Phys. Rev. A* **86** 2 (2012) on p. 021402 ⚭ (see pp. 9, 40)

[87] M. Y. Kuchiev and D. J. Robinson – "Electron-positron pair creation by Coulomb and laser fields in the tunneling regime" in *Phys. Rev. A* **76** 1 (2007) on p. 012107 ⚭ (see p. 8)

[88] L. D. Landau and E. M. Lifshitz – *Course of Theoretical Physics* vol. 3: *Quantum Mechanics: Non-relativistic Theory* Second Edition (in Sec. §134) Oxford: Pergamon Press, 1965 ⚭ (see p. 28)

[89] J. L. Lawson – "88-MeV Gamma-Ray Cross Sections" in *Phys. Rev.* **75** 3 (1949) on pp. 433–444 ⚭ (see p. 4)

[90] S. Lebedev and V. I. Ritus – "Virial representation of the imaginary part of the Lagrange function of the electromagnetic field" in *Sov. Phys. JETP* **59** 2 (1984) on p. 237 ⚭ (see p. 16)

[91] M. Lewenstein *et al.* – "Theory of high-harmonic generation by low-frequency laser fields" in *Phys. Rev. A* **49** 3 (1994) on pp. 2117–2132 ⚭ (see p. 10)

[92] L. Lorenz – "On the Identity of the Vibrations of Light with Electrical Currents" in *Philos. Mag. Ser. 4* **34** 230 (1867) on pp. 287–301 ⚭ (see p. 14)

[93] E. Lötstedt, U. D. Jentschura and C. H. Keitel – "Coulomb-field-induced conversion of a high-energy photon into a pair assisted by a counterpropagating laser beam" in *New J. Phys.* **11** 1 (2009) on p. 013054 ⚭ (see pp. 10, 55)

[94] D. Lüst, S. Stieberger and T. R. Taylor – "The LHC string Hunter's companion" in *Nucl. Phys. B* **808** 1–2 (2009) on pp. 1–52 ⚭ (see p. 78)

[95] A. A. Lutman *et al.* – "Experimental Demonstration of Femtosecond Two-Color X-Ray Free-Electron Lasers" in *Phys. Rev. Lett.* **110** 13 (2013) on p. 134801 ⚭ (see p. 10)

[96] T. H. Maiman – "Stimulated Optical Radiation in Ruby" in *Nature* **187** 4736 (1960) on pp. 493–494 ⚭ (see p. 4)

[97] H. Mashiko, A. Suda and K. Midorikawa – "Focusing multiple high-order harmonics in the extreme-ultraviolet and soft-x-ray regions by a platinum-coated ellipsoidal mirror" in *Appl. Opt.* **45** 3 (2006) on pp. 573–577 ⚭ (see p. 78)

[98] M. Meyer *et al.* – "Angle-Resolved Electron Spectroscopy of Laser-Assisted Auger Decay Induced by a Few-Femtosecond X-Ray Pulse" in *Phys. Rev. Lett.* **108** 6 (2012) on p. 063007 ⚭ (see p. 10)

[99] D. B. Milošević *et al.* – "Above-threshold ionization by few-cycle pulses" in *J. Phys. B* **39** 14 (2006) on R203 ⚭ (see p. 80)

[100] A. I. Milstein *et al.* – "Polarization-operator approach to electron-positron pair production in combined laser and Coulomb fields" in *Phys. Rev. A* **73** 6 (2006) on p. 062106 ⚭ (see pp. 32, 49, 50, 57)

[101] M. H. Mittleman – "Multiphoton pair creation" in *Phys. Rev. A* **35** 11 (1987) on pp. 4624–4628 ⚭ (see p. 7)

[102] G. R. Mocken *et al.* – "Nonperturbative multiphoton electron-positron-pair creation in laser fields" in *Phys. Rev. A* **81** 2 (2010) on p. 022122 ⚭ (see p. 6)

[103] P. J. Mohr, B. N. Taylor and D. B. Newell – "CODATA recommended values of the fundamental physical constants: 2010" in *Rev. Mod. Phys.* **84** 4 (2012) on pp. 1527–1605 ⚭ (see pp. 82, 83)

[104] R. Moshammer *et al.* – "Second-order autocorrelation of XUV FEL pulses via time resolved two-photon single ionization of He" in *Opt. Express* **19** 22 (2011) on pp. 21698–21706 ⚭ (see p. 10)

[105] C. Müller, A. B. Voitkiv and N. Grün – "Differential rates for multiphoton pair production by an ultrarelativistic nucleus colliding with an intense laser beam" in *Phys. Rev. A* **67** 6 (2003) on p. 063407 ⚭ (see pp. 7, 8, 24)

[106] C. Müller, A. B. Voitkiv and N. Grün – "Few-photon electron-positron pair creation in the collision of a relativistic nucleus and an intense x-ray laser beam" in *Phys. Rev. A* **70** 2 (2004) on p. 023412 ⚭ (see pp. 8, 24, 80)

[107] C. Müller – "Nonlinear Bethe–Heitler pair creation with attosecond laser pulses at the LHC" in *Phys. Lett. B* **672** 1 (2009) on pp. 56–60 ⚮ (see p. 28)

[108] S. J. Müller and C. Müller – "Few-photon electron-positron pair creation by relativistic muon impact on intense laser beams" in *Phys. Rev. D* **80** 5 (2009) on p. 053014 ⚮ (see p. 8)

[109] T.-O. Müller and C. Müller – "Longitudinal spin polarization in multiphoton Bethe–Heitler pair production" in *Phys. Rev. A* **86** 2 (2012) on p. 022109 ⚮ (see p. 8)

[110] N. B. Narozhny and M. S. Fofanov – "Quantum processes in a two-mode laser field" in *JETP* **90** 3 (2000) on pp. 415–427 ⚮ (see pp. 9, 32)

[111] N. B. Narozhny, A. I. Nikishov and V. I. Ritus – "Quantum Processes in the Field of a Circularly Polarized Electromagnetic Wave" in *Sov. Phys. JETP* **20** (1965) on p. 622 (see p. 6)

[112] R. Nevels and C.-S. Shin – "Lorenz, Lorentz, and the gauge" in *IEEE Antennas & Propagation Magazine* **43** 3 (2001) on pp. 70–71 ⚮ (see p. 14)

[113] I. Newton – *Philosophiæ Naturalis Principia Mathematica* The Royal Society, 1687 ⚮ (see p. 1)

[114] A. I. Nikishov – "Problems of intense external-field intensity in quantum electrodynamics" in *J. Sov. Laser Res.* **6** 6 (1985) on pp. 619–717 ⚮ (see p. 79)

[115] A. I. Nikishov and V. I. Ritus – "Quantum Processes in the Field of a Plane Electromagnetic Wave and in a Constant Field 1" in *Sov. Phys. JETP* **19** (1964) on pp. 529–541 ⚮ (see p. 6)

[116] A. Nuriman *et al.* – "Enhanced electron-positron pair creation by dynamically assisted combinational fields" in *Phys. Lett. B* **717** 4–5 (2012) on pp. 465–469 ⚮ (see p. 54)

[117] H. Ohmura, N. Saito and M. Tachiya – "Selective Ionization of Oriented Nonpolar Molecules with Asymmetric Structure by Phase-Controlled Two-Color Laser Fields" in *Phys. Rev. Lett.* **96** 17 (2006) on p. 173001 ⚮ (see p. 10)

[118] T. Omori *et al.* – "Efficient Propagation of Polarization from Laser Photons to Positrons through Compton Scattering and Electron-Positron Pair Creation" in *Phys. Rev. Lett.* **96** 11 (2006) on p. 114801 ⚮ (see p. 4)

[119] M. Orthaber, F. Hebenstreit and R. Alkofer – "Momentum spectra for dynamically assisted Schwinger pair production" in *Phys. Lett. B* **698** 1 (2011) on pp. 80–85 ⚮ (see p. 54)

[120] U. Österberg and W. Margulis – "Dye laser pumped by Nd:YAG laser pulses frequency doubled in a glass optical fiber" in *Opt. Lett.* **11** 8 (1986) on pp. 516–518 ⚭ (see p. 60)

[121] G. D. Palazzi – "High-Energy Bremsstrahlung and Electron Pair Production in Thin Crystals" in *Rev. Mod. Phys.* **40** 3 (1968) on pp. 611–631 ⚭ (see p. 9)

[122] B. D. Patterson *et al.* – "Coherent science at the SwissFEL x-ray laser" in *New J. Phys.* **12** 3 (2010) on p. 035012 ⚭ (see p. 79)

[123] T. Pfeifer *et al.* – "Partial-coherence method to model experimental free-electron laser pulse statistics" in *Opt. Lett.* **35** 20 (2010) on pp. 3441–3443 ⚭ (see p. 10)

[124] V. Popov – "Schwinger mechanism of electron-positron pair production by the field of optical and X-ray lasers in vacuum" in *JETP Lett.* **74** 3 (2001) on pp. 133–138 ⚭ (see p. 7)

[125] R. M. Potvliege and P. H. G. Smith – "Two-colour multiphoton ionization of hydrogen by an intense laser field and one of its harmonics" in *J. Phys. B* **25** 11 (1992) on p. 2501 ⚭ (see pp. 34, 51)

[126] J. Proriol and G. Roche – "Molecular-coherence effect in pair production" in *Lett. Nuovo Cimento* **3** 15 (1972) on pp. 642–644 ⚭ (see p. 9)

[127] D. Ray *et al.* – "Ion-energy dependence of asymmetric dissociation of D_2 by a two-color laser field" in *Phys. Rev. Lett.* **103** 22 (2009) on p. 223201 ⚭ (see p. 10)

[128] H. R. Reiss – "Absorption of Light by Light" in *J. Math. Phys.* **3** 1 (1962) on pp. 59–67 ⚭ (see p. 6)

[129] H. R. Reiss – "Effect of an intense electromagnetic field on a weakly bound system" in *Phys. Rev. A* **22** 5 (1980) on pp. 1786–1813 ⚭ (see p. 19)

[130] H. R. Reiss – "Limits on Tunneling Theories of Strong-Field Ionization" in *Phys. Rev. Lett.* **101** 4 (2008) on p. 043002 ⚭ (see p. 7)

[131] H. R. Reiss – "Unsuitability of the Keldysh parameter for laser fields" in *Phys. Rev. A* **82** 2 (2010) on p. 023418 ⚭ (see p. 7)

[132] A. Ringwald – "Pair production from vacuum at the focus of an x-ray free electron laser" in *Phys. Lett. B* **510** 1–4 (2001) on pp. 107–116 ⚭ (see p. 6)

[133] I. Robinson, G. Gruebel and S. Mochrie – "Focus on X-ray Beams with High Coherence" in *New J. Phys.* **12** 3 (2010) on p. 035002 ⚭ (see p. 10)

[134] S. P. Roshchupkin – "Interference effect in the photoproduction of electron-positron pairs on a nucleus in the field of two light waves" in *Phys. At. Nucl.* **64** 2 (2001) on pp. 243–252 ⚮ (see p. 9)

[135] M. Ruf *et al.* – "Pair Production in Laser Fields Oscillating in Space and Time" in *Phys. Rev. Lett.* **102** 8 (2009) on p. 080402 ⚮ (see p. 6)

[136] R. Ruffini, L. Vitagliano and S.-S. Xue – "On plasma oscillations in strong electric fields" in *Phys. Lett. B* **559** 1–2 (2003) on pp. 12–19 ⚮ (see p. 6)

[137] F. Sauter – "Über das Verhalten eines Elektrons im homogenen elektrischen Feld nach der relativistischen Theorie Diracs" in *Z. Physik* **69** 11–12 (1931) on pp. 742–764 ⚮ (see p. 3)

[138] K. J. Schafer and K. C. Kulander – "Phase-dependent effects in multiphoton ionization induced by a laser field and its second harmonic" in *Phys. Rev. A* **45** 11 (1992) on pp. 8026–8033 ⚮ (see p. 34)

[139] K. Schnorr *et al.* – "FD 171: Multiple ionization and fragmentation dynamics of molecular iodine studied in IR-XUV pump-probe experiments" in *Faraday Discuss.* (2014) ⚮ (see p. 10)

[140] R. Schützhold, H. Gies and G. Dunne – "Dynamically Assisted Schwinger Mechanism" in *Phys. Rev. Lett.* **101** 13 (2008) on p. 130404 ⚮ (see pp. 10, 54)

[141] J. Schwinger – "On Gauge Invariance and Vacuum Polarization" in *Phys. Rev.* **82** 5 (1951) on pp. 664–679 ⚮ (see pp. 3, 5)

[142] M. Shapiro and P. Brumer – "Coherent control of atomic, molecular, and electronic processes" in *Adv. Atom. Mol. Opt. Phys.* **42** (2000) ed. by B. Bederson and H. Walther on pp. 287 –345 ⚮ (see p. 9)

[143] B. Sheehy, B. Walker and L. F. DiMauro – "Phase control in the two-color photodissociation of HD^+" in *Phys. Rev. Lett.* **74** 24 (1995) on pp. 4799–4802 ⚮ (see p. 10)

[144] T. Shintake *et al.* – "A compact free-electron laser for generating coherent radiation in the extreme ultraviolet region" in *Nat. Photon.* **2** 9 (2008) on pp. 555–559 ⚮ (see p. 79)

[145] P. Sieczka *et al.* – "Electron-positron pair creation by powerful laser-ion impact" in *Phys. Rev. A* **73** 5 (2006) on p. 053409 ⚮ (see p. 8)

[146] A. Sihvola – "Lorenz-Lorentz or Lorentz-Lorenz?" in *IEEE Antennas & Propagation Magazine* **33** 4 (1991) on p. 56 ⚮ (see p. 14)

[147] A. A. Sorokin *et al.* – "Photoelectric Effect at Ultrahigh Intensities" in *Phys. Rev. Lett.* **99** 21 (2007) on p. 213002 ⚮ (see p. 79)

[148] D. A. Telnov, J. Wang and S.-I. Chu – "Above-threshold multiphoton detachment of H^- by two-color laser fields: Angular distributions and partial rates" in *Phys. Rev. A* **51** 6 (1995) on pp. 4797–4808 ⚭ (see p. 34)

[149] U. I. Uggerhøj – "The interaction of relativistic particles with strong crystalline fields" in *Rev. Mod. Phys.* **77** 4 (2005) on pp. 1131–1171 ⚭ (see p. 9)

[150] J. Ullrich, A. Rudenko and R. Moshammer – "Free-Electron Lasers: New Avenues in Molecular Physics and Photochemistry" in *Annu. Rev. Phys. Chem.* **63** 1 (2012) on pp. 635–660 ⚭ (see p. 79)

[151] A. B. Voitkiv and B. Najjari – "Interference effects in bound-free pair production in relativistic collisions of nuclei with molecules" in *Phys. Rev. A* **84** 4 (2011) on p. 042708 ⚭ (see p. 9)

[152] R. L. Walker – "Absorption of 17.6 Mev Gamma-Rays in C, Al, Cu, Sn, and Pb" in *Phys. Rev.* **76** 4 (1949) on pp. 527–530 ⚭ (see p. 4)

[153] D. M. Wolkow – "Über eine Klasse von Lösungen der Diracschen Gleichung" in *Z. Phys.* **94** 3-4 (1935) on pp. 250–260 ⚭ (see pp. 14, 79, 91)

[154] V. P. Yakovlev – "Electron-Positron Pair Production By A Strong Electromagnetic Wave In Field Of A Nucleus" in *Sov. Phys. JETP* **22** 1 (1966) on p. 223 (see p. 6)

[155] Website – *CUOS: HERCULES* ⚭ (see p. 79)

[156] Website – *DESY: FLASH* ⚭ (see p. 10)

[157] Website – *Elettra: FERMI* ⚭ (see p. 10)

[158] Website – *ELI* ⚭ (see p. 79)

[159] Website – *GSI: PHELIX* ⚭ (see p. 79)

[160] Website – *HiPER* ⚭ (see p. 79)

[161] Website – *Rutherford Appleton Laboratory: Vulcan* ⚭ (see p. 79)

[162] Website – *SLAC: LCLS* ⚭ (see p. 10)

[163] Website – *SLAC: MEC* ⚭ (see p. 10)

[164] Website – *TCHILS: Texas Peta Watt Laser* ⚭ (see p. 79)